

INVESTIGATION OF POWER SWING PHENOMENON IN A
NETWORK INTEGRATED WITH PHOTOVOLTAIC GENERATION

MUTHU KUMARAN GUNASEGARAN

DISSERTATION SUBMITTED IN FULFILMENT
OF THE REQUIREMENT FOR THE DEGREE OF
MASTER OF PHILOSOPHY

INSTITUTE OF GRADUATE STUDIES
UNIVERSITY OF MALAYA
KUALA LUMPUR

2016

UNIVERSITI MALAYA

ORIGINAL LITERARY WORK DECLARATION

Name of Candidate: **Muthu Kumaran A/L Gunasegaran**

Registration/Matric No: **HGF 130002**

Name of Degree: **Master of Philosophy**

Title of Project Paper/Research Report/Dissertation/Thesis (“this Work”):
Investigation of Power Swing Phenomenon in a Network Integrated With Photovoltaic Generation

Field of Study: **Energy and Electricity**

I do solemnly and sincerely declare that:

- (1) I am the sole author/writer of this Work;
- (2) This Work is original;
- (3) Any use of any work in which copyright exists was done by way of fair dealing and for permitted purposes and any excerpt or extract from, or reference to or reproduction of any copyright work has been disclosed expressly and sufficiently and the title of the Work and its authorship have been acknowledged in this Work;
- (4) I do not have any actual knowledge nor do I ought reasonably to know that the making of this work constitutes an infringement of any copyright work;
- (5) I hereby assign all and every rights in the copyright to this Work to the University of Malaya (“UM”), who henceforth shall be owner of the copyright in this Work and that any reproduction or use in any form or by any means whatsoever is prohibited without the written consent of UM having been first had and obtained;
- (6) I am fully aware that if in the course of making this Work I have infringed any copyright whether intentionally or otherwise, I may be subject to legal action or any other action as may be determined by UM.

Candidate’s Signature

Date:

Subscribed and solemnly declared before,

Witness’s Signature

Date:

Name:

Designation:

ABSTRACT

Power swings are known to occur due to the presence of sudden disturbances in the power network. The oscillation of power results in impedance swaying and causes the impedance trajectory to swing back and forth within the distance relay operating characteristics which may lead to unintended relay operation. Ideally, the distance relays in transmission system should not trip unexpectedly during dynamic system conditions such as stable power swings. Commonly, the relay settings are customized to prevent the impedance swing in order to avoid nuisance tripping. However, as the electrical system evolves, its complexity increases in line with the increasing risk of swing severity which may trigger unwanted relay operations. In recent times, the integration of inverter driven generation has been increasing. The penetration of large scale renewable generation into transmission network and its impact to the power swing characteristics has yet to be established. Therefore, this research will investigate the severity of power swing, critical clearing time of synchronous generator and the risk of distance relay mal-operation in the presence of large solar PV generator in transmission system. It is demonstrated in this research that the severity of swing increases and the critical clearing time of the synchronous machine decreases in the presence of inverter driven generation (solar PV generator) when compared to an equivalent synchronous machine. Various sensitivity studies have been conducted and a suitable preventive measure has been proposed to reduce the risk of distance relay mal-operation during power swing. These studies are important to reduce the risk of distance relay malfunction so that the security of the future grid can be strengthened.

ABSTRAK

Ayunan kuasa berlaku akibat kehadiran gangguan secara tiba-tiba dalam rangkaian sistem kuasa. Akibatnya, perubahan pada galangan menyebabkan trajektori galangan untuk mengayun ke dalam dan keluar geganti jarak yang boleh mendorong kepada operasi geganti jarak yang tidak diingini. Sebaik-baiknya, geganti jarak pada sistem penghantaran tidak patut beroperasi dalam keadaan sistem yang dinamik seperti perubahan kuasa stabil. Dalam keadaan biasa, tetapan geganti jarak disesuaikan agar menahan ayunan kuasa untuk mengelakkan operasi yang tidak diingini. Walau bagaimanapun, kerumitan ayunan meningkat selaras dengan risiko yang semakin tinggi apabila sistem elektrik semakin berkembang. Sejak kebelakangan ini, integrasi tenaga boleh diperbaharui telah meningkat. Penembusan sistem jana kuasa yang boleh diperbaharui dan berkapasiti besar ke dalam rangkaian penghantaran utama dan kesan kepada ciri-ciri ayunan kuasa masih dalam pembangunan. Justeru itu, kajian ini mengkaji tahap ayunan kuasa, masa operasi kritikal bagi penjana segerak, dan risiko operasi geganti jarak yang tidak diingini dengan kehadiran penjana solar PV yang berkapasiti besar. Kajian ini menunjukkan bahawa ayunan kuasa bertambah teruk dan masa operasi kritikal penjana segerak berkurang dengan kehadiran penjana kuasa didorong inverter (penjana solar PV) berbanding dengan mesin segerak yang mempunyai kuasa keluaran yang sama. Pelbagai kajian sensitiviti telah dijalankan dan pencegahan yang sesuai telah dicadangkan untuk mengurangkan risiko mal - operasi geganti jarak semasa ayunan kuasa. Kajian ini adalah penting bagi mengurangkan risiko operasi geganti jarak yang tidak diingini supaya keselamatan grid pada masa hadapan boleh diperkukuhkan.

ACKNOWLEDGEMENTS

It is a privilege to acknowledge the contribution of individuals who had assisted in the successful completion of this project whether directly or indirectly.

I am, especially very grateful to my supervisors Ir. Dr. Ab Halim Abu Bakar and Dr. Tan Chia Kwang for providing guidance on this research and giving valuable suggestions for improvement especially during the case study of this project. I feel fortunate to have them as my advisor as their constant stimulation, keen vision and full support had deeply affected my thought on power swing research. In spite of their tight schedule, they had diligently provided me with information on power swing phenomenon and trained me continuously for a period of time to improve my understanding on the phenomenon.

I would also like to extend my appreciation to my parents, Mr. Gunasegaran and Mrs. Kalwant Kaur, my fiancé Dr. Vignesvari and other family members for their constant love, personal support, and encouragement throughout my research which has imbued everything in my life with value. On the other hand, I also would like to express gratitude to the Ministry of Higher Education Malaysia for sponsoring my studies through the MyBrain15 program.

My gratitude also goes out to all my supportive friends and UMPEDAC members who have helped me directly and indirectly for the completion of my research. Most importantly, I am humbled and pleased with the privileges and opportunities given to me as a student of University of Malaya. May all the beings of all the worlds, be happy.

TABLE OF CONTENTS

ORIGINAL LITERARY WORK DECLARATION	ii
ABSTRACT	iii
<i>ABSTRAK</i>	iv
ACKNOWLEDGEMENTS	v
TABLE OF CONTENTS	vi
LIST OF FIGURES	x
LIST OF TABLES	xii
LIST OF SYMBOLS AND ABBREVIATIONS	xiii
CHAPTER 1: INTRODUCTION	
1.1 Overview	1
1.2 Problem Statement and Motivation	2
1.3 Objectives	3
1.4 Scope and Limitation	3
1.5 Organization of Thesis	5
CHAPTER 2: LITERATURE REVIEW	
2.1 Introduction	6
2.2 Power Swing	6
2.3 Types of Power Swing	7
2.3.1 Stable Swing	7
2.3.2 Unstable Swing	11
2.4 Causes of Power Swing	13
2.4.1 Change in Load	13

2.4.2	Load Shifting	14
2.5	Impacts of Power Swing	16
2.5.1	Impacts of Power Swing to Utility	16
2.5.1.1	Pole Slip Condition	17
2.5.1.2	Effects of Power Swing to Distance Relay	18
2.5.2	Impacts of Power Swing to Customer	24
2.6	Mitigation of Distance Relay Mal-operation	25
2.6.1	Conventional Methods	25
2.6.1.1	Concentric Characteristics	25
2.6.1.2	Blinder Scheme	27
2.6.1.3	Decreased Resistance Method	29
2.6.1.4	Swing Centre Voltage ($V \cos \phi$)	30
2.6.1.5	Superimposed Current Method	31
2.6.1.6	Three phase power variation	32
2.6.2	Signal Analysis Techniques	33
2.6.2.1	Fast Fourier Transform (FFT) Analysis	33
2.6.2.2	Wavelet Transform (WT)	34
2.6.2.3	S-Transform	36
2.6.2.4	Prony Method	38
2.6.3	Intelligence Based Diagnosis	38
2.6.3.1	Adaptive Neuro-Fuzzy Inference System (ANFIS)	39
2.6.3.2	Support Vector Machine	40
2.7	Impact of Renewable Generation on Power Swing Characteristics	43

CHAPTER 3: METHODOLOGY

3.1	Introduction	45
-----	--------------	----

3.2	System Modelling	45
3.2.1	DIgSILENT Power Factory	45
3.2.2	Network Modeling	45
3.2.3	Synchronous Machine – Generator A	48
3.2.4	Solar Photovoltaic (PV) Generator	48
3.3	Case Studies	49
3.3.1	Analysis on Critical Clearing Time of Synchronous Machines	50
3.3.1.1	Sensitivity Studies for CCT	51
3.3.2	Analysis of on Swing Severity	52
3.3.2.1	Active Power Oscillation	52
3.3.2.2	Impedance Trajectory	53
3.3.3	Analysis on the Risk of Distance Relay Mal-operation	54
3.3.3.1	Varying Fault Duration	54
CHAPTER 4: RESULTS AND DISCUSSIONS		
4.1	Introduction	55
4.2	CCT Analysis	55
4.2.1	Varying types of Generators	55
4.2.2	Varying Fault Location	60
4.2.3	Varying Output Power	64
4.3	Swing Severity Analysis	66
4.3.1	Active Power Oscillation	66
4.3.2	Impedance Trajectory	75
4.4	Analysis on the Risk of Distance Relay Mal-operation	77
4.4.1	Fault Duration Variation	77
4.4.2	Suitable PV Capacity to Prevent Distance Relay Mal-operation	79

CHAPTER 5: CONCLUSIONS AND RECOMMENDATIONS

5.1	Summary of research work	82
5.2	Contribution of Research	84
5.3	Recommendations for Future Works	85
	REFERENCES	86
	LIST OF PUBLICATIONS AND PAPERS PRESENTED	95

University of Malaya

LIST OF FIGURES

Figure 2.1	Power Angle Curve Showing Operating Conditions and Maximum Power Transfer Capabilities	8
Figure 2.2	Transiently Stable System for Self-Clearing Fault	9
Figure 2.3	Transiently Stable System for Permanent Fault	10
Figure 2.4	Transiently Unstable System for Self-Clearing Fault	12
Figure 2.5	Transiently Unstable System for Permanent Fault	12
Figure 2.6	Line Switching	14
Figure 2.7	Unintentional Islanding	15
Figure 2.8	Parallel Generator Outage	15
Figure 2.9	Balance Beam Relay Concept	18
Figure 2.10	Balance Beam Switches Position When Current Force Increases	19
Figure 2.11	Distance Relay Connection to Transmission Line	20
Figure 2.12	Impedance Diagram	21
Figure 2.13	Operating Region for Balance Beam Relay	22
Figure 2.14	An Example of Three Zone Protection	23
Figure 2.15	Z_{total}	23
Figure 2.16	Concentric Impedance Characteristics	26
Figure 2.17	Blinder Scheme Characteristics	28
Figure 2.18	Superimposed Current Detection Technique	32
Figure 3.1	Model of a Complete Network	47
Figure 3.2	Model of Generator A with an Inertia Constant	48
Figure 3.3	Model of PV System with Zero Inertia	49
Figure 3.4	Flow Chart for CCT Analysis Simulation	50
Figure 4.1	Marginally Stable Rotor Angle of Generator G3 for Case 1	57
Figure 4.2	Marginally Stable Rotor Angle of Generator G3 for Case 1	57

Figure 4.3	Unstable Generator G3 for Case 1	58
Figure 4.4	Unstable Generator G4 for Case 1	58
Figure 4.5	Marginally Stable Generator G3 for Case 2	58
Figure 4.6	Marginally Stable Generator G4 for Case 2	59
Figure 4.7	Unstable Generator G3 for Case 2	59
Figure 4.8	Unstable Generator G4 for Case 2	59
Figure 4.9	Active Power Oscillation of Generator G1 for Case 1	68
Figure 4.10	Active Power Oscillation of Generator G1 for Case 2	69
Figure 4.11	Active Power Oscillation of Generator G2 for Case 1	69
Figure 4.12	Active Power Oscillation of Generator G2 for Case 2	70
Figure 4.13	Active Power Oscillation of Generator G3 for Case 1	70
Figure 4.14	Active Power Oscillation of Generator G3 for Case 2	71
Figure 4.15	Active Power Oscillation of Generator G4 for Case 1	71
Figure 4.16	Active Power Oscillation of Generator G4 for Case 2	72
Figure 4.17	Generator A Active Power Oscillation	74
Figure 4.18	Active Power Oscillation of Static Generator (PV)	74
Figure 4.19	Impedance Trajectory seen by Relay R1 for Case 1	76
Figure 4.20	Impedance Trajectory seen by relay R1 for Case 2	76
Figure 4.21	Impedance Swing seen by Relay R1 in the presence of Gen A	78
Figure 4.22	Mal-Operation of Relay R1 in the presence of PV	78
Figure 4.23	Mal-operation of Relay R1 for 80 MW Solar PV Generator	81
Figure 4.24	Impedance Trajectory of Relay R1 for 90 MW solar PV Generator	81

LIST OF TABLES

Table 1.1	Records of Blackouts due to Zone 3 Distance Relay Nuisance Tripping	2
Table 2.1	Condition and Impacts due to Power Swing Occurrence	24
Table 4.1	CCT results for Type of Generators: Case 1	56
Table 4.2	CCT results for Type of Generators: Case 2	57
Table 4.3	CCT result for Fault Location: Case 1	62
Table 4.4	CCT results for Fault Location: Case 2	63
Table 4.5	CCT result for Variable Output Power Case 1	65
Table 4.6	CCT results for Variable Output Power: Case 2	66
Table 4.7	Active Power Oscillation in the Presence for Case 1	73
Table 4.8	Active Power Oscillation in the Presence for Case 2	73
Table 4.9	Suitable PV for Fault duration of 7 Cycles	80

LIST OF SYMBOLS AND ABBREVIATIONS

NERC	North American Electric Reliability Corporation
PV	Photovoltaic
CCT	Critical Clearing Time
E_g	Internal voltage and is proportional to the excitation current
E_l	Load Voltage
X	Reactance between the generator and the load
δ	Angle that the internal voltage leads the load voltage
P_m	Mechanical Turbine Power of the generating unit
P_g	Electromagnetic Power output of the generating unit
P_a	Accelerating Power
E_k	Kinetic Energy
H_i	Inertia
f_n	Nominal Frequency
Pm_i	Instantaneous Mechanical Power
Pe_i	Instantaneous Electrical Power
ΔP_i	Instantaneous Change in Power
V	Voltage
I	Current
$Z_{measured}$	Measured Impedance
Z_{load}	Load Impedance
R	Resistance
X_c	Capacitance
X_L	Inductance
Z_{line}	Line Impedance

Ω	Ohm
SVM	Support Vector Machine
SLT	Statistical Learning Theory
ANN	Artificial Neural Network
SCV	Swing Centre Voltage
kV	Kilovolt
s	Second

University of Malaya

CHAPTER 1: INTRODUCTION

1.1 Overview

Power system stability plays a vital role in ensuring the systems reliability. In steady state, a balance power flow is maintained between the generation and load. However, unpredicted events or large disturbances such as fault, line switching, generator disconnection, and the loss or application of large blocks of loads may interrupt this balance and cause oscillation of power known as power swing in the system (Bakar, Yatim, Yusof, & Othman, 2009; Thakallapelli, Mehra, & Mangalvedekar, 2013). In severe circumstances, the power swing may lead to loss of synchronism between the generator and load, resulting in generator tripping and subsequently risking cascaded power outages and major power blackouts. However, not all power swings are unstable for some of the power swings are stable swing, where the generators can recover from the temporary transient instability. During these stable swing events, the distance relays are very likely to detect a temporary decrement in impedance, which can be wrongly interpreted as a fault by the relay. As oppose to a fault, it is undesirable to trip the line under these stable swing conditions given that the network has the ability to return to stability. Consequently, the undesirable operation of distance relay under a stable swing scenario is termed as mal-operation of distance relay or nuisance tripping.

The North American Electric Reliability Corporation (NERC) reported an alarming statistics where 75% of the major disturbances leading to cascaded outages and major blackouts involved the mal-operation of distance relays (Chen-Ching & Juan, 2008). Table 1.1 lists the countries that experienced major blackout due to nuisance tripping of distance relay.

Table 1.1: Record of Blackouts due to Zone 3 Distance Relay Nuisance Tripping

(Bakar et al., 2009; Chunyan, Yuanzhang, & Xiangyi; Conti, 2010; Corsi & Sabelli, 2004; Pentayya, Gartia, Saha, Anumasula, & Kumar, 2013)

Year	Affected Countries
September 2003	Malaysia - Blackout for five (5) hours including capital Kuala Lumpur
September 2003	Italy major power failure
January 2005	Malaysia – Major blackout in northern region of the country
November 2009	Blackout in eight states of Brazil
July 2012	India – Blackout in the western grid.

1.2 Problem Statement and Motivation

The increasing demand for energy and the pressure on environmental issues over the years gave rise to the penetration of renewable energy into the power system. However, the impact of large penetration of inverter interfaced renewable energy generation has yet to be clearly established. Besides benefiting the environment and generating renewable energies, there are looming concerns that the renewable generations may also significantly impact the power swing characteristics and affect the distance relay operation.

Nowadays, numerous studies are being focused on the solar photovoltaic (PV) research particularly on the development of its technologies and the integration of the system to the grid, as PV serves a great demand in the future. The effect of PV on power swing characteristics have been presented by author in (Yusoff & Abidin, 2013). Tan and Kirschen (Yun Tiam & Kirschen, 2007) had also studied the dynamic stability response during high PV penetration on the IEEE39 bus test system and observed that for a system with higher PV penetration, it takes longer time for the power swing oscillations to settle down. Phuttapatimok et al., had investigated the fault current

contribution from the PV grid connected systems and concluded that higher penetration of the PV into the grid results in higher fault current compared with the case where no PV is present (Phuttapatimok, Sangswang, Seapan, Chenvidhya, & Kirtikara, 2008). S. Eftekharnjad et. al studied the impact of high PV penetration effect on the voltage profile and concluded that high PV penetration levels achieve greater voltage dips (Eftekharnjad, Vittal, Heydt, Keel, & Loehr, 2013).

Up to date, the severity of power swing and its impact on the distance relay operation in a large solar PV integrated network has yet to be established. In addition, the impact of the inertia-less inverter driven machine to the critical clearing time (CCT) of the generator is unknown. Therefore, this research will investigate the impact on CCT of other synchronous generators, the swing severity, and the risk of distance relay mal-operation in a transmission system integrated with large scale solar PV generator.

1.3 Objectives

The main objectives of this project are:

- To investigate the impact of inverter driven solar PV generator to the CCT of other synchronous generator in the transmission system;
- To investigate the severity of power swing in the presence of large solar PV generator;
- To analyze the risk of distance relay mal-operation in the presence of large scale solar PV generator.

1.4 Scope and Limitations

This section will present the scope and limitations of the research. All simulations in this research are conducted using DIgSILENT Power Factory. A two-area four-

machine transmission system proposed by Prabha Kundur as shown in Figure 3.1 is adopted in all the case studies in this research (Kundur, 1994).

The research will first investigate the impact of inverter driven generation to the CCT of the other synchronous generators in the transmission system. Various sensitivity studies are conducted to account for the system variations in a dynamic power system. The sensitivity studies include the types of generator, variation in the generator output power, and fault location variation.

Next, the severity of the power swing in the presence of large solar PV generator will be investigated. In this section, a comparison in the power swing will be made between a network consisting entirely of synchronous machine and another network comprising of certain amount of solar PV generator.

Finally, the research will also analyze the risk of distance relay mal-operation due to the integration of solar PV generator. Here, the distance relay will need to be coordinated first. Then, the impedance trajectory in the resistance-reactance (R-X) plane is investigated. The investigation will be conducted for 2 different cases. The first case study considers the impact of extended fault clearing time and the other case study will consider the impact of increased solar PV generators capacity.

However, the power swing blocking (PSB) schemes are intentionally not considered in this thesis as the swing severity will be limited by the PSB scheme. On the other hand, the intermittency of solar PV generator is also not considered and the output power is set to be constant.

It is also important to note that, the case studies in this research are confined only to the double circuit section of the adopted network (Bus 7, 8 and 9 of Figure 3.1). This is because the permanent fault will cause the faulted line to be isolated. Therefore, the load will be transferred to the parallel healthy line and the network would still be

stable. However, if the single lines are isolated then the respective generators will be disconnected from the network. This will lead to unbalance load dispatch causing the other generators to experience out-of-step condition as they could not supply sufficient power to the loads.

1.5 Organization of Thesis

This thesis comprises of five main divisions:

Chapter One starts with the background of the research. The chapter introduces power swing phenomenon and also states the objectives of the research. Besides that, the scope and limitations of the research are also specified in this chapter.

Chapter Two gives an overview of the power swing phenomenon and its impact to the utility and customer. In addition, the latest updates on the power swing blocking schemes are also presented in this chapter. Besides that, this chapter also describes the impact of renewable energy to the power swing characteristics.

Chapter Three introduces the development of simulation model by using DIGSILENT Power Factory simulation software. Moreover, this chapter presents the methodology of conducting the experiments in order to achieve the objectives of this research.

Chapter Four presents the simulation results from the case studies conducted in this research where the parameters such as power (W), rotor angle (δ), and the impedance locus ($R-X$) are plotted in graphical form. Subsequently, this chapter also discusses and interprets the obtained simulation results.

Chapter Five summarizes the research in this project. In addition, this chapter also presents the possible extension and suggestions to enhance this research project in future.

CHAPTER 2: LITERATURE REVIEW

2.1 Introduction

In earlier chapter, the synopsis of power swing was presented. A detailed explanation about power swing and how it may impact the distance relay operation will be discussed in this chapter. Both types of stable and unstable power swing will be described in this chapter. In addition, the impact of power swing to utility, customer and distance relay will be explained in detail. This section will also explain the power swing blocking schemes used to prevent the mal-operation of distance relay.

2.2 Power swing

The basic principle of electric generation begins by converting mechanical energy to electrical energy. The mechanical power is supplied by a turbine driven by a prime mover through, steam, wind and coal. The turbine is connected to the generator by using a direct shaft and therefore the kinetic energy of the turbine is transferred to the generator. From the electromagnetic induction between the copper winding and magnetic stator, electricity is generated within the generator and this is supplied to the grid after being stepped up to the grid voltage level accordingly.

Nevertheless, the mechanical power supplied to the generator is assumed to remain the same for it is manually set to be constant. The power generated by the generator can be derived as given in equation (2.1) and (2.2).

$$P_g = \frac{E_g E_1}{X} \sin \delta \quad (2.1)$$

Where:

E_g = Internal voltage and is proportional to the excitation current

E_l = Load Voltage

X = Reactance between the generator and the load

δ = Angle that the internal voltage leads the load voltage

$$P_a = P_m - P_g \quad (2.2)$$

P_m = Mechanical Turbine Power of the generating unit

P_g = Electromagnetic Power output of the generating unit

P_a = Accelerating Power

During the steady state condition, the internal voltage E_g is slightly higher than load voltage, E_l . This is to ensure that the power flow condition satisfies the power flow principle from generator to the load. When fault occurs, the changes in both reactance (X) and load voltage (E_l) causes fluctuations in the electrical power and will consequently change the E_g . These fluctuations will cause oscillations in power and change the speed of the generator. Since the speed of the generator is directly proportional to the rotor angle, it will cause the rotor angle to oscillate. This results in power swing phenomenon.

2.3 Types of Power Swing

2.3.1 Stable Swing

The basic concept of stability is derived upon the equal area criterion, which represents the function between the power delivered and the rotor angle of a generator as shown in Figure 2.1 and Figure 2.2 (Hashemi, Hagh, & Seyedi, 2013).

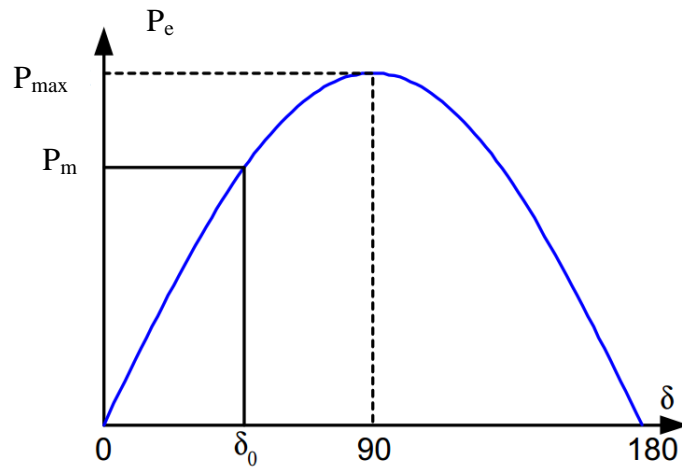


Figure 2.1: Power Angle Curve Showing Operating Conditions and Maximum Power Transfer Capabilities

As shown in Figure 2.1, P_m is the constant mechanical power for the rotor angle at δ_0 , and the maximum power P_{max} is achievable by the mechanical power driving the rotor angle to 90° . Faults that occur may be self-clearing or it may be permanent depending on the nature of the fault. A detailed explanation for both scenarios by using the equal area criterion will be explained below.

Analyzing the transiently stable system for a self-clearing fault as in Figure 2.2, the generator initially operates at point a on the 'pre & post fault' curve during steady state. At the inception of fault, a new rotor angle curve known as fault curve is formed. Hence, the power drops to point b . Here, the rotor angle (δ_0) is the same at the inception of fault but the electrical power during fault is lower than the initial mechanical power, P_m .

It is important to note that, kinetic energy is developed from rate of change of input to output power. Since the mechanical power input, P_m is higher than the electrical power at point b , accelerating power is positive and the rotor angle δ advances towards point

c. The acceleration of rotor stores excess kinetic energy which is represented by Area 1 in Figure 2.2.

At δ_1 , the fault self-clears and the rotor angle returns to the ‘pre & post fault’ curve. The rotor angle now shifts from point c to point d . At this point on the ‘pre & post fault’ curve, electrical power (P_e) is higher than P_m . This causes the rotor to decelerate according to Eq (2). However, the rotor angle will continue its travel until point e where equal amount of kinetic energy to be given up by the rotating masses (Area 2) is reached.

From here on, the rotor will decelerate and oscillate before settling down at steady state operation at the intersection of P_m and δ_0 , which is at point a . Here, the rotor angle experiences damped oscillation according to the machines natural frequency before settling at point a (Mooney & Fischer, 2006).

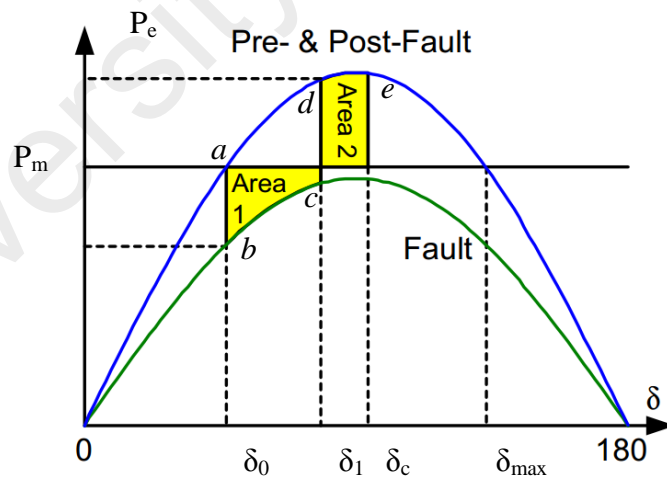


Figure 2.2: Transiently Stable System for Self-Clearing Fault (Gunasegaran, ChiaKwang, & Bakar, 2014)

Faults that occur may be self-clearing or it may be permanent depending on the nature of the fault. If the fault is permanent, the line will be isolated after 3 trials of

reconnections by auto-reclosure (Chothani, Bhalja, & Parikh, 2014). The isolation of a line will cause major changes in the reactance and therefore result in different equal area criterion curve as shown in Figure 2.3.

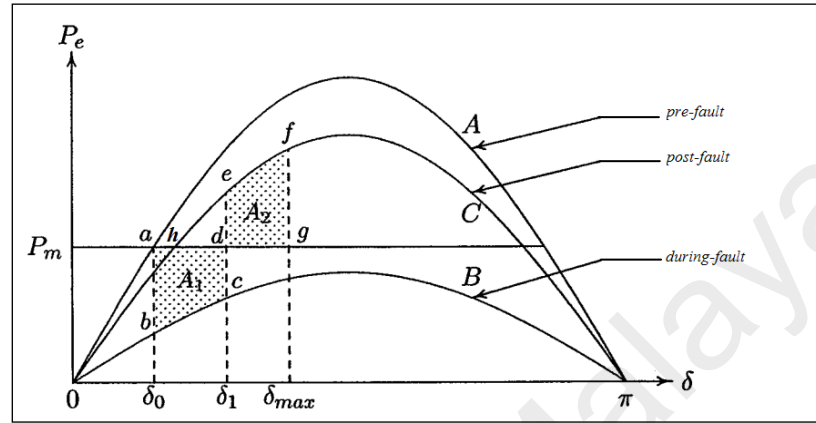


Figure 2.3: Transiently Stable System for Permanent Fault (Gunasegaran et al., 2014)

Analyzing Figure 2.3, the generator initially operates at point a on the pre-fault curve during steady state. At the inception of fault a new rotor angle curve, B , is formed, and the power drops to point b . Here, the rotor angle (δ_0) is the same at the inception of fault but P_e is lower than P_m .

As mentioned before, the kinetic energy is developed from the rate of change of input to output power. Since P_m is higher than electrical power at point b , accelerating power is positive and rotor angle δ advances towards point c . Hence, the acceleration of rotor stores excess kinetic energy which is represented by area A_1 .

Since it is a permanent fault, the circuit breaker opens at δ_1 and this isolates the faulted line, which will change the entire system reactance. As a result, a post-fault rotor angle curve (curve C) will be formed and the rotor angle now shifts from point c to point e . At this point on curve C , P_e is higher than P_m causing deceleration according to Eq (2). However, the rotor angle will continue its travel until point f (δ_{max}) where the equal amount of kinetic energy to be given up by the rotating masses (area A_2) is reached.

From here on, the rotor will decelerate and oscillate before settling down at a new steady state operation at the intersection of P_m and curve C. Here, the rotor angle experiences damped oscillation according to the machine natural frequency before settling at point h .

The oscillation of rotor angle and the changes in power during disturbances is known as power swing. The scenarios that were pictured above are for stable power swings where the generator will be able to recover from the fault and return to a normal operating condition. However, there are cases where the generator could not recover from the disturbances and experiences out-of-step condition which also causes damage to the machine. The next section will present detailed explanation for a transiently unstable system which could occur in the cases of self-clearing and permanent fault.

2.3.2 Unstable Swing

Figure 2.4 shows the equal area criterion for a transiently unstable system. For an unstable swing, Area 1 will be larger than Area 2 as in Figure 2.4. This scenario occurs when the fault clearing time is longer, where the fault happens to be cleared after δ_c , which is the critical rotor angle. It has to be noted that the kinetic energy gained at Area 1 is larger than Area 2. Due to this, the rotor angle will continue to accelerate beyond δ_{max} (the maximum rotor angle) to dissipate the energy gained during fault in Area 1. After the fault is self-cleared, the inertia of the system will cause the rotor angle to surpass point e (δ_c) on the 'pre & post fault' curve in Figure 2.4. Once the rotor angle has traveled beyond point e , the P_m is seen to be larger than the P_e resulting in acceleration of the machine which leads to the increment in δ . Therefore, the machine will not be able to recover as it experiences out-of-step condition.

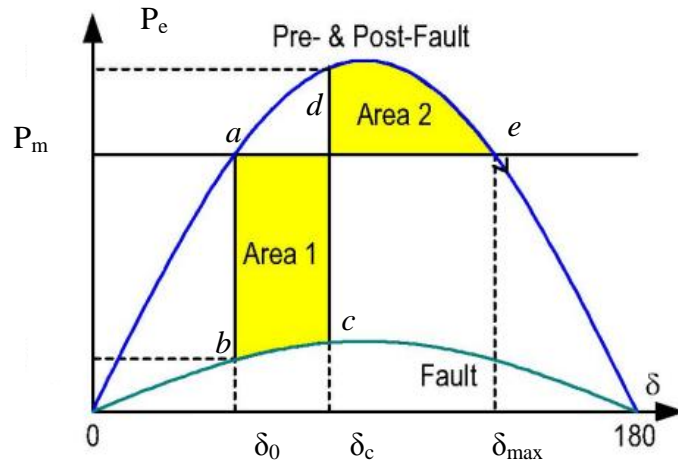


Figure 2.4: Transiently Unstable System for Self-Clearing Fault (Gunasegaran et al., 2014)

The same theoretical analysis can be used to explain a permanent fault. Here, the only difference is that the circuit breaker operates and isolates the faulted line at a time after δ_c . The isolation of the faulted line will cause major changes in the system reactance. Hence, forming a new post fault curve C as shown in Figure 2.5. Since the kinetic energy at Area 1 is larger than Area 2, the speed increases accordingly. As the generator surpasses point f on the curve C , the generator would not be able to recover as the P_m is seen to be larger than the P_e resulting in acceleration of the machine which leads to the increment in rotor angle causing the generator to pole slip.

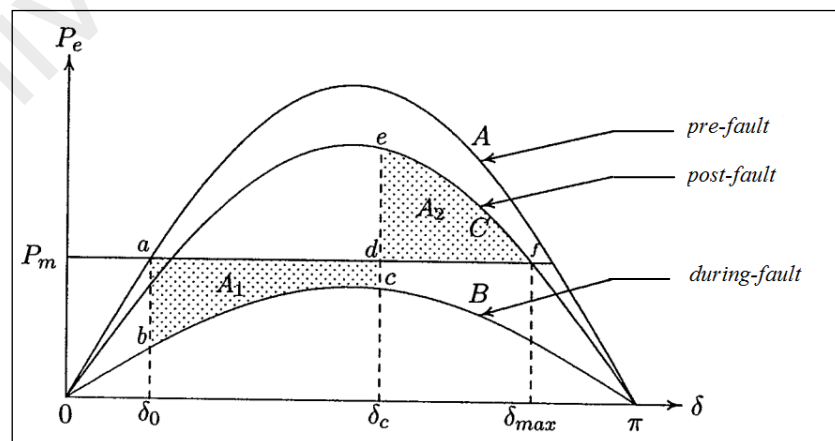


Figure 2.5: Transiently Unstable System for Permanent Fault (Gunasegaran et al., 2014)

When the fault clearing angle (FCA) is equal to critical clearing angle (δ_c) as in Figure 2.5, the machine is said to be critically stable ($A1 = A2$) for it stands a risk of becoming unstable. When FCA is more than δ_c , $A1$ becomes bigger than $A2$. As the rotor angle increases to equalize the kinetic energy ($A1 = A2$), the advancement of rotor angle will surpass δ_{max} in Figure 2.5. Once this happens, P_m will be higher than P_e , causing positive acceleration which will prevent the machine from recovery.

On the other hand, the operation of generator beyond its stable limits will also cause electrical and mechanical stress to the machine as the control system will react accordingly to establish the magnetic contact. In order to save the generator from being damaged, the protection system will operate and trip the breaker leading to a blackout (Fu, He, & Bo, 2008a). The scenarios above are pictured for unstable power swings, where the generator is unable to recover from the disturbances and experiences out-of-step condition. Hence, it is important that the circuit breaker must operate at any point before δ_c is reached.

2.4 Causes of Power Swing

Besides the commonly known faults causing power swing, a change in load and load shifting can also cause power swing. These factors will be described briefly in the next section.

2.4.1 Change in Load

Change in load simply means the variation of load from time to time. Here, it can be divided into two categories which are connection and disconnection of load. In both cases the generator will react accordingly to accommodate to the new condition after the event. Hence, the generator goes through a swing phase until it reaches equilibrium. Eventually, this leads to power swing as stated in Section 2.3 (Abbasi,

Seyedi, & Strunz, 2009). Figure 2.6 illustrates a simple transmission circuit connected to breaker in between which shows line switching.

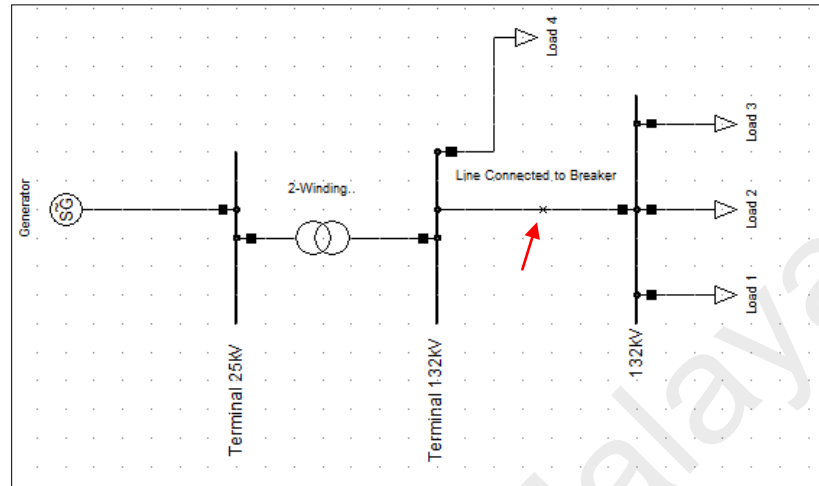


Figure 2.6: Line Switching

2.4.2 Load Shifting

Load shifting simply means a transfer of burden from one machine to another. This occurs in many scenarios (e.g. islanding) where researchers are keen to see the response of a particular machine when load is shifted. In Figure 2.7, the generator and the infinite grid share a common load. In the case of a disturbance on the grid side, the protection device (where the red arrow points) trips the circuit breaker. Now the load remains the same but it is shifted completely to the synchronous generator, where the generator has to undertake and adjust accordingly to the load. In real system, this is called an unintentional islanding where it causes power swing (Brahma, 2007).

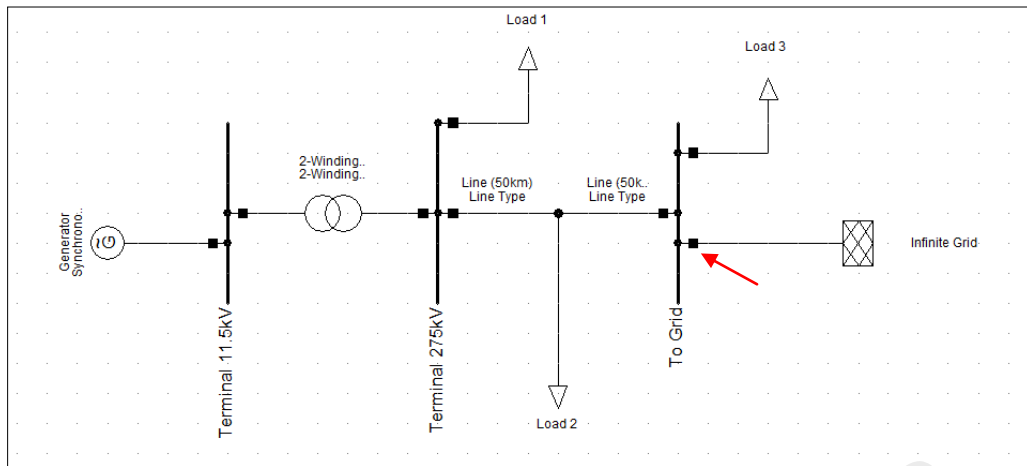


Figure 2.7: Unintentional Islanding

Another scenario that can lead to load shifting characteristic is the sudden outage of parallel generator. Figure 2.8 shows a simple network where the load remains the same and generator 2 is disconnected for maintenance shut down or tripping of circuit breaker. Therefore generator 1 bears the load of the line which results to power swing. From generator view it sees as a sudden increase in load and it has to adjust its dispatch power accordingly to the load change.

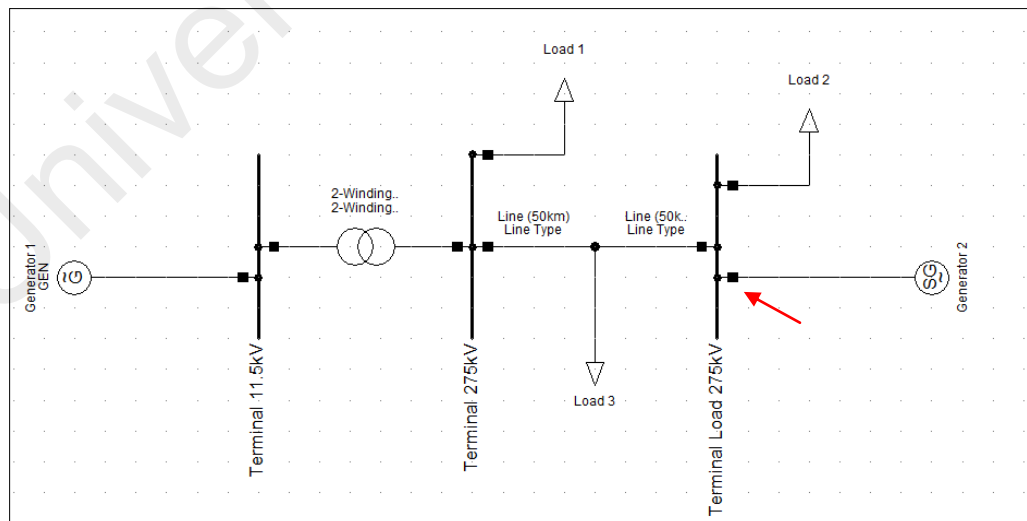


Figure 2.8: Parallel Generator Outage

2.5 Impacts of Power Swing

The occurrence of power swing mainly impact on two important bodies, the utility and its customer. The following sections will describe the impacts in detail.

2.5.1 Impacts of Power Swing to Utility

Severe damages occur to the utility systems especially to the generators when power swing takes place. The main impact that an operator observes is the change in speed of rotor. As known by many, the frequency of a generating system is proportional to the speed of the machine. Therefore, the change in load or generation will cause imbalance in real power and will result to change in system frequency. This happens because the rotating mass tries to adapt to the new condition or disturbances that happen within the overall system. Hence, the kinetic energy (E_k) is used to accommodate any imbalance in the system. If load decreases, the E_k will be stored in the masses causing the rotor to accelerate and at the same time it increases the frequency. If load increases, the required amount of power will be drawn from the masses causing the rotor to decelerate leading to frequency decreament. The responsible property for this operation is the inertia constant (H) which is defined as, time taken for generator to replace its stored E_k when operating at rated speed and apparent power output.

Through the swing equation as in equation (2.3), the inertia constant (H) links to the rate of change of frequency $\left(\frac{df}{dt}\right)$ immediately after the disturbances (Ponal Kundur, 1994; Wall, Gonza, x, lez-Longatt, & Terzija, 2010).

$$\frac{2H_i}{f_n} \frac{df_i}{dt} = Pm_i - Pe_i = \Delta P_i \quad (2.3)$$

Where:

H_i = Inertia

f_n = Nominal Frequency

Pm_i = Instantaneous Mechanical Power

Pe_i = Instantaneous Electrical Power

ΔP_i = Instantaneous Change in Power

As explained in Section 2.3.2, the generator experiences out-of-step condition which results in electrical and mechanical stress due to the effort of its control system to re-establish the magnetic lock. This can cause severe damage to the generator and utility has to bear the cost of replacing or repairing the machine.

2.5.1.1 Pole Slip Condition

Pole slip is also known as out of-step. A stable swing is a swing where the generators (when connected in parallel) do not slip poles (terminal voltage angles exceed 180° with respect to others) and the system reaches a new state of equilibrium after a transient event (Wall et al., 2010). When loss of load takes place, the mechanical power (P_m) will be higher than electrical power (P_e), resulting in high level of transient torque. As mentioned earlier, the system will reach equilibrium after a period of time. As for a small machine such as biomass generator, during the swing and depending on the nature of the fault, it is possible for the power angle (angle between the forces within generator) of the generator to exceed 90° (Berdy et al., 1977).

In synchronous generator, the under-excited or overexcited modes of operation are determined by the excitation control. Commonly, the generator must be overexcited for delivering power. However, the occurrence of pole slip and the angle swings causes

insufficient electromagnetic torque to hold the rotor in synchronism with the stator magnetic flux due to the fact that, P_m is very large which causes large transient torque. This leads the generator to an under-excited mode which draws reactive power to the machine (Mozina, 2012).

In addition to pole slip condition, large currents will flow from the external system into the machine in an attempt to re-establish the magnetic lock. This can cause electrical stress to the system and damage the pole (coil). Therefore, protection devices are installed in the system to avoid the occurrence of such a condition. Hence, the tripping of the protection relay during the condition as mentioned above results in possible blackout (Ambekar & Dambhare, 2012b).

2.5.1.2 Effects of Power Swing to Distance Relay

In high voltage transmission lines, the commonly preferred relays are distance relay due to its speedy reaction. Distance relay measures the impedance of the line by comparing the voltage and current of the bus and line respectively (Ziegler, July 1999). The earliest type of distance relay worked as the balance beam relay and certainly this will be the easiest way to explain the concept of relay.

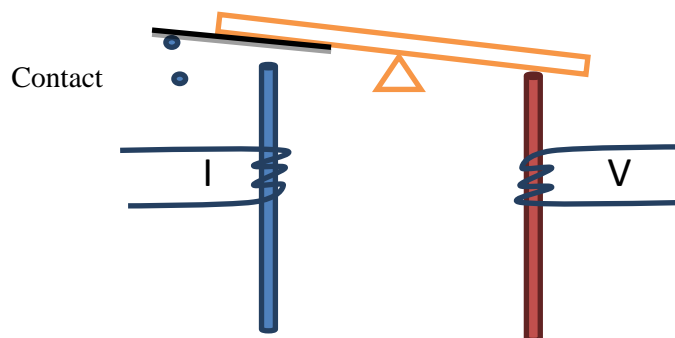


Figure 2.9: Balance Beam Relay Concept

Figure 2.9 shows the balance beam relay concept where the beam is pivoted like a seesaw with the voltage and current coils at its posing ends. The voltage coil is fed from the voltage transformer (VT) on the bus feeding the line, while the current coil is fed from current transformer (CT) on the protected line. Under normal operating condition, the voltage coil attractive force is much stronger than the current coil which makes the beam to remain as in Figure 2.9. When fault occurs, the current increases and therefore increases the attractive force of the current coil, making it greater than the voltage coil. This makes the beam to changes its position as in Figure 2.10.

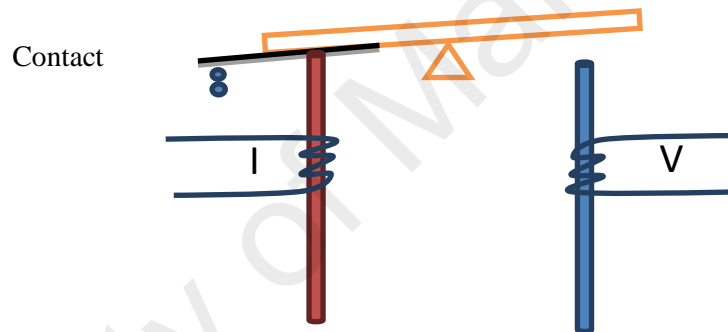


Figure 2.10: Balance Beam Switches Position When Current Force Increases

The pivoted beam seesaws in the opposite direction and closes the contact tripping the circuit breaker of the line. The actual point of tripping can be adjusted by moving the pivot position or by changing the number of turns on the coils.

Either way in real scenario, the point of tripping depends upon the comparison of voltage against current which is the measured impedance as shown in equation 2.4 (Ziegler, July 1999).

$$\frac{V}{I} = Z_{measured} \quad (2.4)$$

Where:

V = Voltage

I = Current

$Z_{measured}$ = Measured Impedance

The relay measures the impedance ($Z_{measured}$) that is being protected and compares with the load impedance (Z_{load}). When a scenario such as a phase to phase fault occurs, the impedance reduces thus increasing the currents magnitude. Therefore the relay is set to operate when it falls below a specific value. In practice, relays do have an error margin of 10%. Hence, to make sure it does not overreach, the limit is set to 90% of the line load. The relay continuously measures the voltage and current and when the measured impedance ($Z_{measured}$) falls below this set point, the relay makes contact to trigger the circuit breaker.

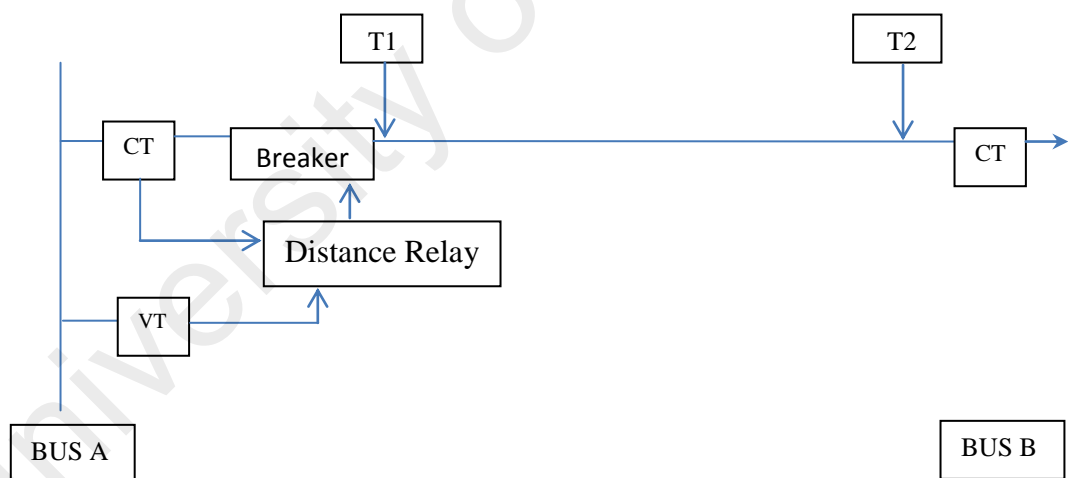


Figure 2.11: Distance Relay Connection to Transmission Line

Figure 2.11 shows an example of transmission system with the protection device connected near to bus A. The line distance in between T1 to T2 in Figure 2.11 is 100km. Since the length of cable is proportional to its impedance, that makes the Z_{line} to be 100Ω with a phase angle of 60 degrees (assuming $1 \Omega/\text{km}$ and phase angle 60 degrees). When relay is set at 90%, it takes up to 90Ω as shown in the impedance diagram in Figure 2.12. When fault occurs and the impedance falls below this region, it will lead to the tripping of the relay resulting in switching of the circuit breaker (Ziegler, July 1999).

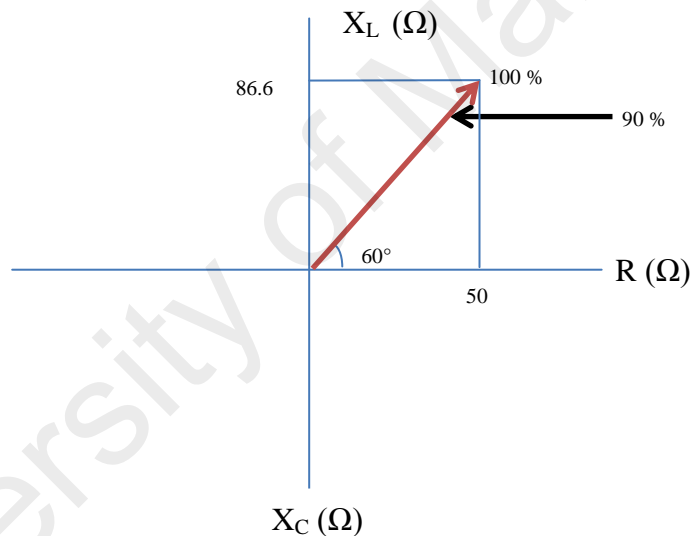


Figure 2.12: Impedance Diagram

Figure 2.12 shows an impedance graph where inductive element is represented in positive vertical axis and resistive element is represented in horizontal axis. The resistive and reactance value is converted from the polar form of $100\Omega \angle 60^\circ$ to rectangular form, which gives $50+j86.6 \Omega$. The capacitive element is represented in the negative region of the vertical axis. Since the relay is set to operate at 90%, it will then form an arc which will cause it to operate when the impedance falls within this region

as shown in Figure 2.13. This means that even though there is a fault at the upstream, the relay will still trip the breaker if the impedance falls within its arc.

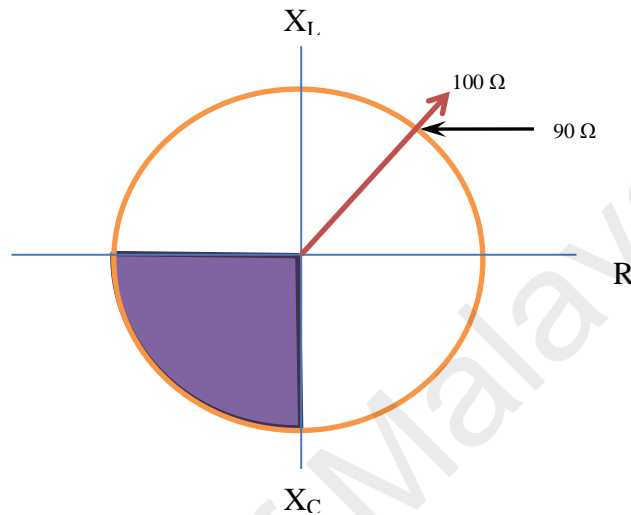


Figure 2.13: Operating Region for Balance Beam Relay

The upstream fault will be at the third quadrant (shaded in color) on the circled diagram as shown in Figure 2.13. Therefore to make sure the relay operates only for the downstream fault, a directional relay is usually attached together with distance relay. When the directional relay is attached together with distance relay, the negative quadrant is eliminated. In this way, distance relay are also known to be directional.

Usually, a second element is installed to protect the remainder of the line and reach out into the second zone. A third element may be added to reach even further and to provide backup protection in case the first and second element fails to operate in time. In the second and third zone, a timer is set. This will result in delay in the relay operation in order to allow the primary protection to operate in its zone. Figure 2.14 shows an example of three zone protection (Prabha Kundur, 1994 ; Ziegler, July 1999).

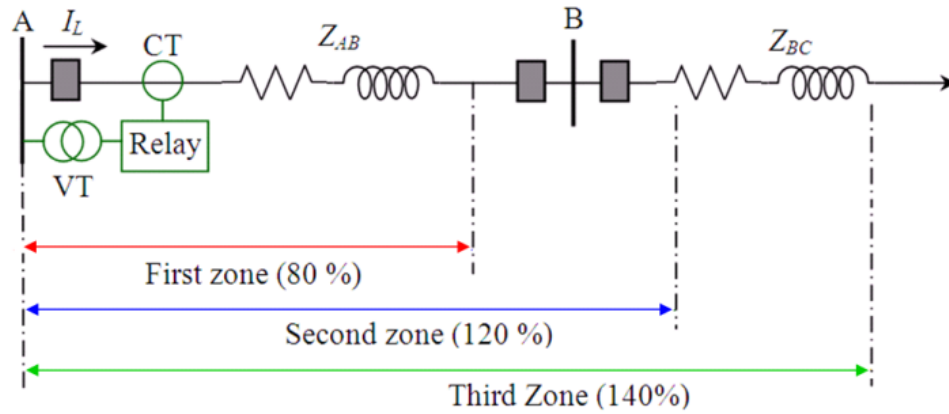


Figure 2.14: An Example of Three Zone Protection

However, not only the load impedance is not taken into consideration when looking into the regions of the relay. The total impedance is defined as the summation of the line impedance (Z_{line}) and the load impedance (Z_{load}) as represented in equation 2.5 (Prabha Kundur, 1994). Figure 2.15 shows the addition of load impedance by vector from all three zones.

$$Z_{total} = Z_{line} + Z_{load} \quad (2.5)$$

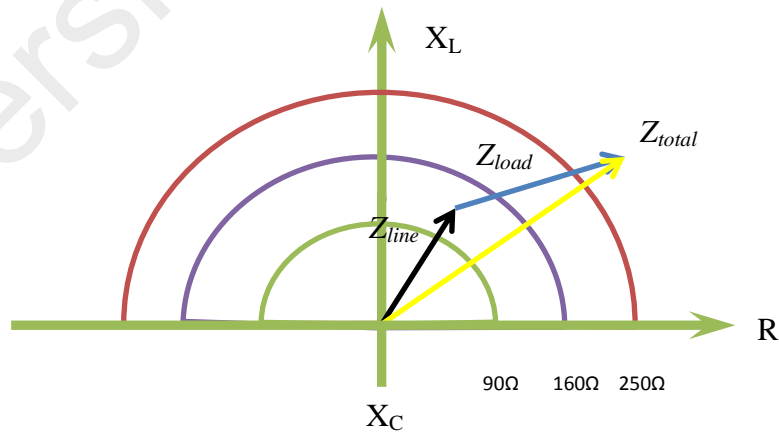


Figure 2.15: Z_{total}

Figure 2.15 shows the impedance diagram for three zone protection where the bold black arrow is the line impedance Z_{line} and the bold blue line is the Z_{load} . Therefore, the relay calculates the total impedance as Z_{total} (yellow line) as shown in equation 2.5.

When power swing occurs in large transmission system, the impedance Z_{total} swings according to the disturbances on the system. When this stable oscillation of impedance enters into the zone of distance relay as shown in Figure 2.15, it will result in relay operation causing the circuit breaker to trip.

2.5.2 Impacts of Power Swing to Customer

When power swing phenomenon causes mal-operation of distance relay and trips the circuit breaker, this causes blackout to the customer. Due to this, giant industries suffer from financial losses for their production is halted for some time. These industries are linked to economy of a country where trading takes places and feeds the country with sufficient economic sustainability. On the other hand, low voltage customers (residential) also suffer from this blackout due to their location in the downstream.

Table 2.1: Condition and Impacts due to Power Swing Occurrence (Yusoff & Abidin, 2013)

Condition	Impact
Loss of Load	Loss of synchronism between voltages
Generator Disconnection	Loss of synchronism between phase angles
Addition of Load	Loss of synchronism between phase sequence
Line Switching	Loss of synchronism between frequencies

Table 2.1 summarizes the impact of power swing phenomenon due to the different types of disturbances (Yusoff & Abidin, 2013).

2.6 Mitigation of Distance Relay Mal-operation

The operating principle of a relay is that it should trip only when fault or unstable swing occurs. As explained from the previous sections, the power swing phenomenon may cause mal-operation of distance relay. Unintended tripping occurs when the impedance trajectory enters the impedance locus of the distance relay (usually zone 3). The subsequent operation of distance protection in response to the power swing will lead to unnecessary outages to consumers. In order to mitigate this problem, researchers have developed power swing blocking (PSB) schemes in distance relays to prevent unwanted tripping during stable swing. The PSB schemes can be generally categorized into conventional methods, signal analysis techniques and intelligence based diagnosis. This section compiles the findings of all the developed power swing blocking schemes up to date.

2.6.1 Conventional Methods

This section will discuss the types of conventional methods used to block the distance relay from tripping during power swing. In addition, their advantages and disadvantages are also presented.

2.6.1.1 Concentric Characteristics

The concentric characteristic is developed such that the inner zone and outer zone for power swing detection in Mho relay is shown in Figure 2.16 (A. Apostolov & Vandiver, 2011; Khoradshadi-Zadeh, 2005; Martuscello, Krizauskas, Holbach, & Yuchen, 2009; Xiangning, Zhengtian, Shuohao, & Yan, 2010).

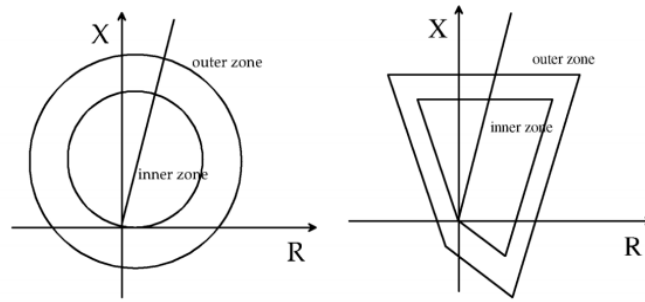


Figure 2.16: Concentric Impedance Characteristics

During fault, the rate of change of impedance is seen larger than the rate of change of impedance during power swing. Therefore, the working principle of concentric impedance is based on observing the difference in the rate of change of impedance (ΔZ) to differentiate between power swing and fault.

Two concentric impedances are set together with threshold (K) timer that record the duration of impedance travel between the outer and inner concentric circles. If the travel of impedance crosses the outer and inner concentric circles before the set time (K), the scheme sees it as a fault. If the impedance crosses the concentric circles for period longer than set time (K), then the scheme sees it as power swing and the relay will be blocked from tripping (Khoradshadi-Zadeh, 2005; P. K. Nayak, J. G. Rao, P. Kundur, A. K. Pradhan, & P. Bajpai, 2010; Xiangning et al., 2010).

During slow swing ($<1\text{Hz}$), the travel of impedance is very slow and it spends longer or sufficient amount of time in each zone (Corsi & Sabelli, 2004). Therefore the scheme can detect the swing and will block the relay from tripping. Zadeh in (Khoradshadi-Zadeh, 2005) reported that this scheme can also detect high resistance ground faults.

However, it was found that this scheme is unable to detect fast swing ($>5\text{Hz}$) due to the fact that the impedance travels very fast across the different zones (Abidin, 2010; Khoradshadi-Zadeh, 2005; Mahamedi, 2010; Martuscello et al., 2009; P. K. Nayak et

al., 2010; Xiangning et al., 2010). Zadeh (Khoradshadi-Zadeh, 2005) simulated a power swing event and proved that this scheme is unable to detect fast swing. From the experiment, Nayak *et.al* in (P. K. Nayak et al., 2010), concluded that the scheme was also unable to detect fast swing during single line to ground fault (P. K. Nayak et al., 2010; Xiangning et al., 2010).

Several authors have also considered a more complicated scenario where a fault occurs during power swing. Zadeh in (Khoradshadi-Zadeh, 2005) simulated a power swing event and intentionally initiated a fault during the power swing. Ideally, the fault has to be isolated by operating the distance relay. However, it was found that, the scheme does not trip the fault during power swing. In this scenario, the relay is unable to reset and subsequently continue to block the relay from tripping. Adding on to its disadvantage, Zadeh [30] stated that this scheme may mal-operate for high impedance fault during a power swing event by blocking the relay from tripping.

2.6.1.2 Blinder Scheme

The blinder scheme or commonly known as double blinder was developed to meet the disadvantages of the concentric characteristic (H. K. Zadeh & Z. Li, 2008). The blinders are usually positioned in parallel to the line impedance as shown in Figure 2.17. Reason being, when out of step condition occurs during power swing, the impedance vectors will enter the protection zones approximately perpendicular to the line impedance. This was discovered to be the most effective way for measuring ΔZ to detect the out of step impedance trajectories (Ambekar & Dambhare, 2012a; Fischer et al., 2012; Holbach, 2006; Martuscello et al., 2009; Tziouvaras & Daqing, 2004; H. K. Zadeh & Z. Li, 2008). Figure 2 shows the blinder scheme elements.

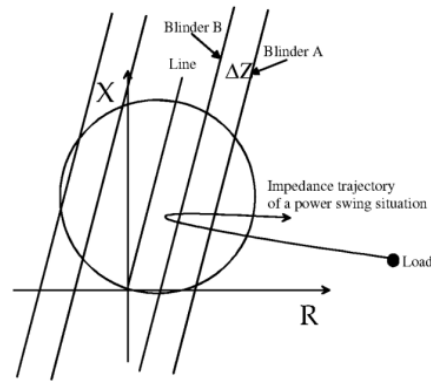


Figure 2.17: Blinder Scheme Characteristics

The working principle for blinder is the same as concentric characteristics. A timer starts when impedance vector crosses blinder A (outer element) and stops when blinder B (inner element) is crossed. If the measured time is more than the threshold (K), power swing is detected. Vice versa, a fault is detected when the measured time is less than the threshold (K).

The advantages of blinder scheme are that it can be applied independently in each zone, load impedance can lie inside the blinder impedances, and slow swing will not cross blinder A. Therefore the relay will not trip unnecessarily (Ambekar & Dambhare, 2012a; Fischer et al., 2012; Holbach, 2006).

Solving the disadvantages of concentric scheme, the blinder scheme comes with its own disadvantages. In order to implement the blinder scheme, sophisticated grid analysis is required to identify the partition between the inner and outer elements. In addition, the relay may mal-operate for stable swing unless very precise threshold estimation is made to differentiate between a fault and a power swing event as experimented by Ambekar and Dambhare in (Ambekar & Dambhare, 2012a).

2.6.1.3 Decreased Resistance Method

Since the blinder scheme needs thorough grid studies and may mal-operate for stable swing, the decreased resistance method was introduced as an alternative solution. Through experiment, it was found that the resistance element of measured impedance seems to show continuous changes during power swing (Khoradshadi-Zadeh, 2005; P. K. Nayak et al., 2010). As for fault, the resistance element changes drastically only during the inception of fault and remains the same during the fault period. These characteristics were used to differentiate between a power swing and fault for distance relay blocking.

It must be noted that this blocking scheme can detect fault during power swing as experimented by Zadeh (Khoradshadi-Zadeh, 2005). When a fault occurs during power swing, the scheme will reset and allows the relay to trip. Zadeh (Khoradshadi-Zadeh, 2005), experimented different scenarios and proved that this method works for all the simulated situation. In addition, this detection method does not require as thorough understanding of the system as in the blinder scheme (Kang, Subramanian, Hassan, & Yao, 2010).

However, this detection scheme comes with its unique disadvantages. It must be noted that when fault occurs, the resistance drops significantly. Nayak et.al in (P. K. Nayak et al., 2010) reported that during swing with low slip frequency at the power angle of 180° , the change in resistance over time (ΔR) drops significantly. Therefore, a swing with low slip frequency will be treated as a fault by this detection scheme. The change in resistance during different slip frequencies was also presented in (Khoradshadi-Zadeh, 2005). Additionally, when a three phase fault occurs during slow swing, it will also be difficult for this scheme to distinguish between power swing and fault resulting to mal-operation of relay. On the other hand, when a three phase fault occurs at power angle close to 180° , the value of resistance element is already low. Hence, it is difficult

to recognize fault during slow and fast swing at power angle close to 180° . Moreover, a time delay is needed for the detection scheme even when the unblocking condition is satisfied due to the initial transient of fault (P. K. Nayak et al., 2010).

2.6.1.4 Swing Center Voltage ($V\cos\phi$)

All the above mentioned schemes are dependent on the line and bus impedance unlike, the Swing Center Voltage (SCV). SCV is best represented by using $V\cos\phi$, where V is the magnitude of locally measured voltage and ϕ is the angle between locally measured voltage (V) and current (I) (Fischer et al., 2012).

During power swing SCV changes continuously, but when fault occurs SCV remains constant. This criterion is used to distinguish between a power swing and a fault. Relay can be controlled by setting a threshold (k) using the criteria of $dV\cos\phi/dt$. When $dV\cos\phi/dt > k$, stable swing is identified and if $dV\cos\phi/dt$ less than k , then it is an unstable swing or fault (P. K. Nayak et al., 2010).

The advantage of SCV is that it is independent of source impedances and line impedances. Therefore sophisticated grid analysis is not required. Besides that, the previously mentioned schemes require the user to have some understanding on the overall grid and distance relay configurations. In contrast, SCV is bounded with a lower limit of zero and an upper limit of one per unit. This allows the user to successfully apply power swing detection with limited knowledge on the dynamic response of the power system.

However, several literatures presented the disadvantages of this scheme. Nayak *et.al* in (P. K. Nayak et al., 2010) carried out an experiment and found that when a three phase fault is initiated, there is some delay in the detection due to the inception of fault. Similar findings were reported by Ambekar and Dambhare in (Ambekar & Dambhare, 2012a). On the other hand, when power swing occurs at power angle close to 180° , the

threshold (k) must be at a very low value to detect the power swing (Ambekar & Dambhare, 2012a). Furthermore, when single line to ground fault with high ground resistance was simulated, Nayak *et.al* found that the SCV did not remain constant (P. K. Nayak et al., 2010). Consequently, the relay will not trip as the SCV characteristic is similar to that of a power swing. In addition, Zadeh simulated a three phase fault during a slow swing at a maximum angle of 180° and found that the scheme continues to block the relay from tripping even after the fault had occurred (Khoradshadi-Zadeh, 2005).

2.6.1.5 Superimposed Current Method

The occurrence of power swing produces continuous superimposed current when the present value of currents is compared with a buffer that is taken two cycles earlier. Figure 2.18 shows the working principle of superimposed current detection technique (Verzosa, 2013).

A change in the rate of current (ΔI) is detected if the difference in current is greater than 5% of the nominal current. Continuous ΔI measurement for three cycles indicates a power swing condition and the relay will be blocked from tripping. The advantages of this method are that, it will detect fast and slow swing and ensure the correct blocking of zones. Besides that, this method is also reported to work efficiently for faults occurring during a power swing (A. Apostolov & Vandiver, 2011; A. P. Apostolov, Tholomier, & Richards, 2004).

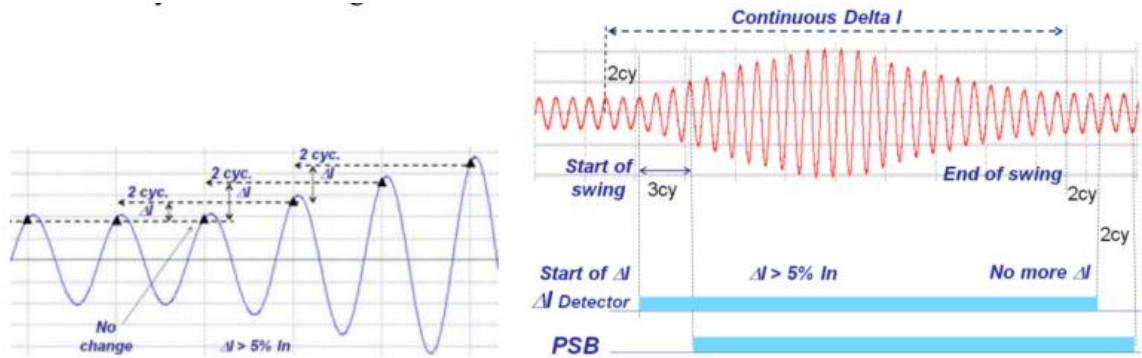


Figure 2.18: Superimposed Current Detection Technique

However, Nayak *et.al* (P. K. Nayak et al., 2010) reported that the scheme prevents the relay from tripping when three phase fault occurs at power angle close to 180° and single phase high resistance ground fault occurs during the power swing. Reason being, the small ΔI as in both scenarios. Similar findings were reported by Zadeh in (Khoradshadi-Zadeh, 2005).

2.6.1.6 Three phase power variation

This scheme, also known as power derivation method is proposed by Xiangning *et.al* in (Xiangning, Yan, & Pei, 2008). During power swing, it is found that the three-phase active and reactive power changes. Both the rate of change of active power (dP/dt) and reactive power (dQ/dt) are proportional to the angular speed ($\omega = d\delta/dt$) (Esmaeilian, Ghaderi, Tasdighi, & Rouhani, 2011). During power swing the normalized value of $|dP/dt|$ and $|dQ/dt|$ is greater than 0.7, while during fault both values drop and stays close to zero. The normalized value of $|dP/dt|$ and $|dQ/dt|$ are used for the swing detection.

It is reported that this method has improved sensitivity in detecting power swing. According to Xiangning *et.al* (Xiangning et al., 2008), the scheme is not affected by factors like fault inception time and system parameters.

However, several studies presented few limitations in this scheme. First, it might operate incorrectly during a stable power swing, because the speed might reach zero when the power angle nears its maximum limit. Besides that, it only works for symmetrical faults. In addition, the latest discovery by Esmailian *et.al* in (Esmailian et al., 2011) found that, it has a longer delay in detection as compared to SCV due to the transient from the inception of fault. To improve the disadvantages of this scheme, Mahamedi in (Mahamedi, 2010) proposed an enhanced scheme based on this method to detect power swing phenomenon. Esmailian *et.al* in (Esmailian et al., 2011) did the latest comparison between SCV and this three phase power method but the comparison did not include the scheme proposed by Mahamedi in (Mahamedi, 2010).

2.6.2 Signal Analysis Techniques

The parameters that vary during power swing can also be observed through waveforms. When digital signal processing (DSP) field expands, numerous researchers have proposed various methods using DSP to detect power swing. This section will compile the methods developed for detecting power swing using DSP.

2.6.2.1 Fast Fourier Transform (FFT) Analysis

Various FFT techniques have been proposed by different authors over the years for power swing detection. Each of the proposed technique carries its own strengths and weaknesses.

Karegar and Mohamedi in (Karegar & Mohamedi, 2009) used FFT approach based on DC component of the current to detect fault during power swing occurrence for both symmetrical and asymmetrical fault. In this method, each phase current is measured and scrutinized by using FFT analysis. The DC component obtained from the FFT

analysis will be compared to settable threshold (K). If the threshold is higher than K , then fault is detected.

Another approach based on FFT analysis is presented in (Mahamedi, 2010), where only symmetrical faults were discussed. The method proposed by the authors in (Mahamedi, 2010) is done by detecting the frequency component of three phase active power using FFT analysis with fundamental of 50Hz. The author also demonstrated that during power swing, the three phase real power frequency is equivalent to its slip frequency (f_{slip}). In contrast, when fault occurs, the three phase real power's frequency will be equivalent to the nominal frequency.

However, the above literatures did not offer any insights for a value of threshold (K) to be selected. As such, a novel approach to determine the threshold (K) was presented by Mahamedi and Jian Gao in (Mahamedi & Jian Guo, 2012). All of these techniques require a proper selection of the threshold value for the fault to be detected (D'Apuzzo & D'Arco, 2008; Karegar & Mohamedi, 2009; Mahamedi, 2010; Mahamedi & Jian Guo, 2012).

2.6.2.2 Wavelet Transform (WT)

Wavelet transform has been used in many power system applications (Chengzong & Kezunovic, 2010; Fu, He, & Bo, 2008b; Parameswariah & Cox, 2002). The WT was introduced to overcome the disadvantage of FFT where the WT is able to retain the time information (Brahma, 2006). However despite this advantage, WT fails in frequency location. Most of the recent research using WT are concentrated in addressing this disadvantage.

The authors in (Brahma, 2006; Chengzong & Kezunovic, 2010; Dubey & Samantaray, 2013; Dubey, Samantaray, Tripathy, Babu, & Ehtesham, 2012a; Fu et al., 2008b; Mahamedi, 2011) stated that during power swing, the frequency of a system varies

over a range around the nominal frequency. Due to the fact that fault causes transient, WT is efficient for power system transient analysis and feature extraction. Bramha in (Bramha, 2006) studied the different sampling frequency (f_s) used for the WT to detect power swing and symmetrical fault during power swing. Bramha claimed that the sampling frequency of 40.96kHz, is ideal for detecting power swing and symmetrical fault at any location to capture the rise and fall of the frequency variation. Even though it is better to use higher f_s , but most numerical relays cannot accommodate high sampling rate. Thus, Bramha developed a relay logic as in (Bramha, 2007) to utilize the information captured for numerical relay using $f_s = 40.96\text{kHz}$.

On the other hand, Chengzong and Kezunovic in (Chengzong & Kezunovic, 2010) developed a high speed WT algorithm to detect symmetrical fault during power swing with $f_s = 10\text{kHz}$. This sampling frequency will fit most of the presently available numerical relays without the need of further modifications.

In (Mahamedi, 2011), Mahamedi *et.al* performed WT on the impedance variation to detect power swing and faults. The authors presented that a maximum delay of 30 ms was observed for fault detection using this method. Using f_s as low as 1 kHz, this method is claimed to be suitable for high voltage (HV) and extra high voltage (EHV) transmission system (Mahamedi, 2011).

In contrast, Dubey *et.al* (Dubey, Samantaray, Tripathy, Babu, & Ehtesham, 2012b) used WT to analyze the current variation for detecting faults of various resistances during power swing. Here, the authors selected $f_s = 20\text{ kHz}$ for the WT. The output of the WT is then reduced to 10 kHz before being fed into the numerical relay. Correspondingly, Dubey *et.al* proposed an algorithm to detect fault in the presence of power swing. The latest studies using WT was presented by the authors in (Dubey et al., 2012b) through the introduction of entropy as in (Dubey & Samantaray, 2013). It

was found that this method detects both stable and unstable swing and offers reliable decision to the relay besides its capability to detect fault during power swing.

2.6.2.3 S-Transform

S-transform can be derived from two methods which are Gaussian function on short time Fourier transform (STFT) and phase correction on WT (N. Z. Mohamad & A. F. Abidin, 2012). However, most research has only derived it using Gaussian function, where the derivation is as stated in (A. F. Abidin, A. Mohamed, & H. Shareef, 2011; Nor Zulaily Mohamad & Ahmad Farid Abidin, 2012; N. Z. Mohamad & A. F. Abidin, 2012; Mohamad, Abidin, & Munim, 2012; Mohamad, Abidin, Munim, & Yahya, 2012; Mohamad, Abidin, & Musirin, 2013; Samantaray, Dubey, Tripathy, & Babu, 2011). Most importantly, it has shown to have absolute referenced phase information and frequency invariant amplitude response. Another key feature is its accurate time-frequency (amplitude-phase) information (Ahmad Farid Abidin, Azah Mohamed, & Hussain Shareef, 2011; A. F. Abidin et al., 2011; Mohamad et al., 2013).

Abidin *et.al* in (Ahmad Farid Abidin et al., 2011) introduced an analysis by using S-Transform to extract information and characterize fault, stable swing, and unstable swing. This information is used as input signals to the probabilistic neural network (PNN) based arrangement scheme as presented in (Ahmad Farid Abidin et al., 2011) to differentiate between stable and unstable power swing conditions and to detect fault during power swing. The authors also compared the performance of multi-layer perceptron neural network (MLPNN) with PNN and reported that PNN performs better than MLPNN in detecting and classifying stable swing and unstable swing, fault, and fault during power swing.

Mohamad *et.al* in (Mohamad, Abidin, & Munim, 2012) introduced the use of S-transform in detecting fault during power swing. This was done using IEEE 9 bus

system. This scheme analyses the input signals to distance relay including the voltage, current, three phase active and reactive power. It was demonstrated that when fault occurs, S-transform of the active and reactive power will deliver value larger than 0, and during power swing the value equals to 0.

Mohamad *et.al* also presented another method to detect symmetrical fault during power swing in (Mohamad, Abidin, Munim, et al., 2012). Here the input signals (voltage and current) to distance relay are calculated and processed using S-Transform tools to generate the S-matrix. The magnitude of S-matrix are as presented by the authors in (Mohamad, Abidin, Munim, et al., 2012). From the S-matrix, the minimum value of voltage and current magnitude are plotted. It was reported that during power swing, less samples was observed and when fault occurs during power swing more samples was observed. However, the schemes in (Mohamad, Abidin, & Munim, 2012; Mohamad, Abidin, Munim, et al., 2012) may face detection problem for high resistance fault. To resolve this disadvantage, the authors proposed a new scheme as in (N. Z. Mohamad & A. F. Abidin, 2012) using IEEE 14 bus system as the test case. A three phase fault with up to 200 Ω resistances were simulated. The advantage of this developed scheme is that, fault during power swing can be detected at any inception time.

The latest findings in this particular area was presented by Mohamad *et.al* in (Mohamad et al., 2013), which applies S-transform analysis on active power at the distance relay. The authors calculated the magnitude of S-matrix using equation as stated in (Mohamad et al., 2013), a standard deviation σ , is evaluated. The detection criterion is defined as such that, if $\sigma > 1$ the power swing is of unstable type, whereas if $\sigma \leq 1$ the power swing is of stable type (Mohamad et al., 2013). The authors simulated the scenario using IEEE 39 bus system.

2.6.2.4 Prony Method

Very recently prony method has been introduced in power system protection field (Lotfifard, Faiz, & Kezunovic, 2010; Thakallapelli, Mehra, & Mangalvedekar, 2013) and it was reported to have better result than FFT (Trujillo G, Conde E, & Leonowicz, 2013). In order to estimate the analyzed signal parameters, Prony converts the complex damped sinusoidal signal into samples in time. This is done as per the mathematical equations as presented by Lobos *et.al* in (Lobos, Rezmer, & Koglin, 2001).

Lotfifard *et.al* in (Lotfifard et al., 2010) had proposed an algorithm by using the current waveform to detect a three phase fault during power swing. The method is based on the exponential drop in the DC current which signifies fault. The authors simulated a three phase fault during power swing and reported that this algorithm can unblock the relay if fault occurs during swing (Lotfifard et al., 2010), thus allowing the relay to trip and isolate the fault.

However, it was found that the algorithm does not unblock the relay for other types of fault. To overcome this disadvantage, Thakallapeli *et.al* in (Thakallapelli et al., 2013) proposed an algorithm based on DC component of current waveform. Unlike (Lotfifard et al., 2010) where low impedance faults were discussed, high impedance faults were simulated in this paper and Prony method was used to differentiate between power swing and high impedance faults.

2.6.3 Intelligence Based Diagnosis

Artificial intelligence (AI) is widely used for pattern recognition and classification which is essential for developing protection techniques. Several AI based methods have been implemented in the blocking scheme of protection system and have been proven to not be affected by parameters variation in the system (Cho et al., 1999; Feilat & Al-Tallaq, 2004; Vaidya & Venikar, 2012).

2.6.3.1 Adaptive Neuro-Fuzzy Inference System (ANFIS)

A fuzzy logic system (FLS) is an intelligent system developed to generate its own decision making. It is pre-trained and registered to ensure the correct output. The advantage of FLS is that it can have many inputs. Very commonly, the FLS composed of five layers which are, input, fuzzifiers, rules, inference, and de-fuzzifiers.

One of the methods to develop a fuzzy network is Adaptive neuro-fuzzy inference network (ANFIS). ANFIS is an enhanced version of FLS with extraordinary features such as, generalization capability, noise immunity, robustness, and fault tolerance (Esmailian & Astinfeshan, 2011; Sanaye-Pasand & Jafarian, 2011; Hassan Khorashadi Zadeh & Zuyi Li, 2008).

Zadeh and Li in (Hassan Khorashadi Zadeh & Zuyi Li, 2008) used the rates of positive sequence impedance, positive and negative sequence current, and the SCV as input signals to ANFIS. In the output layer, the ANFIS has only one node, which can have value from 0 to 1. For blocking scheme classification purposes, the authors pre-specified a threshold (k) of 0.5 where in case of power swing, the output will be more than or equal to 0.5 and the blocking scheme will be activated. When the output is less than 0.5, it will be identified as fault and the relay will be unblocked to allow it to trip. The ANFIS approach uses Gaussian membership function for fuzzy sets, linear function for rule outputs and Sugeno's inference mechanism (Hassan Khorashadi Zadeh & Zuyi Li, 2008). The authors presented test results at various fault location, fault inception time, various load, single pole open condition, different slip frequencies and the test results are available in (Hassan Khorashadi Zadeh & Zuyi Li, 2008). They concluded that the scheme was able to operate for high resistance fault, clear the blocking if fault occur during swing, detect slow and fast swing, detect fault during power swing even for fault that occurs at power swing centre at 180° , operates during single pole open condition, and reset the relay in case of fault during power swing.

On the other hand, Esmailian *et.al* in (Esmailian & Astinfeshan, 2011) presented another algorithm using ANFIS. Here, the authors used three inputs which are the rate of change of currents (positive and negative sequence), normalized active power, and normalized reactive power. The first order Sugeno's fuzzy model were implemented in ANFIS, linear functions for the rules output and bell functions for membership functions. The authors concluded that the method was able to detect the feature as in (Hassan Khorashadi Zadeh & Zuyi Li, 2008). In addition, this method (Esmailian & Astinfeshan, 2011) is not be affected by factors such as system parameters, fault inception time, fault position, and pre fault load flow condition.

2.6.3.2 Support Vector Machine

Support vector machine (SVM) is a new solution for separating functions in classification tasks such as pattern recognition (Seethalekshmi, Singh, & Srivastava, 2010). As mentioned in (Kampeerawat, Buangam, & Chusanapiputt, 2010; Seethalekshmi et al., 2010; Vapnik, 1995), SVM has been known as a very potential tool in solving the classification problems. Being introduced by Vapnik (Vapnik, 1995) from the Statistical Learning Theory (SLT), it is found that SVM performs better than Artificial Neural Networks (ANN) because, SVM's essence follows on Structural Risk Minimization (SRM) while ANN is based on the Empirical Risk Minimization (ERM) (Chothani et al., 2014; Kampeerawat et al., 2010; Kampeerawat, Buangam, & Chusanapiputt, 2012; Seethalekshmi et al., 2010; Seethalekshmi, Singh, & Srivastava, 2012). The typical steps for SVM comprised of extracting the input features, and training the SVM classifier. The SVM classifier can be categorized into few sections depending on the necessity. For power swing detection, most researchers divide it into power swing classifier, fault classifier and ground fault classifier for discriminating purposes.

Kampeerawat *et.al* (Kampeerawat et al., 2010) proposed a new power swing blocking method using a least square support vector machine (LS-SVM) approach. This approach is claimed to be another signal processing method to be used with numerical distance relay. The authors used the current and voltage signal at the relaying point as an input for LS-SVM. In the paper, the event classifications are based on the rate of change of different measured quantities such as rate of change in positive sequence impedance (ΔZ_p), rate of change in positive current (ΔI_p), rate of change in negative sequence current (ΔI_n) and rate of change in power swing center voltage (ΔV_{scv}). Three (3) LS-SVM classification such as LS-SVM1, LS-SVM2, and LS-SVM3 were developed to identify fault, power swing and ground fault detection respectively. During fault, the schemes uses fault current signal as input for fault detection. When power swing occurs, the scheme uses ΔZ_p and ΔV_{scv} as input for detection. For ground fault, the scheme uses zero sequence component of fault current signal to detect ground faults. Therefore, the method uses three-layer LS-SVM classifier to distinguish power swing and fault in order to ensure the correct relay operation. The authors have simulated all types of fault, and concluded that this scheme is able to differentiate between fault, power swing, and fault during power swing.

Kampeerawat *et.al* proposed another approach in (Kampeerawat et al., 2012), where Wavelet Packet Transform (WPT) and LS-SVM were used. The authors generated a double circuit transmission line model and simulated a power swing by inducing a three-phase fault. Here, the extracted features were decomposed from the current and voltage signal at relaying point by using WPT Daubechies based on multi-resolution analysis. The authors selected $fs = 10\text{kHz}$. The training of LS-SVM results were obtained using wavelet entropy (WPE_n) and the rate of change of wavelet packet total energy (ΔWPE_{tot}). The authors concluded that the proposed method is able to distinguish between power swing, fault and fault during power swing.

Seethalekshmi *et.al* (Seethalekshmi et al., 2010) proposed another scheme using two separate logic blocks for the summation of AND gate in relay in order to distinguish between power swing and fault using SVM based classifier. The input features are positive sequence magnitude and angle of voltage, positive sequence magnitude of the current, real power, and reactive power. These parameters are selected based on the Principal Component Analysis (PCA) by utilizing the voltage and current signal at the relaying point. The authors also compared the performance of SVM scheme with ANFIS scheme and concluded that the SVM performs better than ANFIS due to the selection of the input features using PCA and a better generalization capability of SVM.

On the other hand, Chotani *et.al* (Chothani et al., 2014) has proposed another power swing and fault discrimination using SVM based technique. The proposed algorithm uses $f_s = 1$ kHz at 50 Hz nominal frequency and the inputs are the half cycle samples of three phase current signals at the relaying point. A half cycle waveform is used to distinguish a fault and a power swing (Chothani et al., 2014). Subsequently, the necessary steps are taken to block or unblock the distance relay from tripping. The accuracy of the algorithm is reported to be 98.71% for a half cycle waveform and 98.93% for a full cycle waveform. However, the authors used a half cycle waveform to reduce the computing burden and decision making time. Simulations were carried out for all types of fault at different distances on the line and fault during power swing. The authors also used a maximum of 50 Ω for ground fault at different lines considering various factors such as variation in mechanical torque, line isolation and line switching. It was reported that the algorithm delivered promising results under these varied scenarios.

2.7 Impact of Renewable Generation on Power Swing Characteristics

The escalating fuel price has promoted the interest in large scale renewable energy generations. However, the penetration of these renewable generations into the grid might significantly impact the power swing characteristics. As such, few literatures have conducted studies in this area. Yusoff *et.al* initiated power swing by simulating a three phase bolted fault using IEEE 9-bus system with and without Photovoltaic (PV) generators. The authors found that the integration of solar PV generator will lead to decrease in active power after installing the PV generators (Yusoff & Abidin, 2013).

Besides that, the application of large scale power converters produces interharmonic and subharmonic frequencies component which can contaminate the input voltage and current signal to the distance relay. The current filters (Cosine and Fourier digital filters) which are used in distance relay are unable to reject the interharmonics and subharmonics frequency components. As a consequence, an error estimation of impedance will cause the distance relay to underreach and overreach. Consequently, Trujillo and Leonowicz designed a Butterworth analog filter using the Prony method to mitigate the problem (Trujillo G et al., 2013). The authors reported that the proposed method when compared to cosine filter managed to reduce the reach error from 210% to 75%, and the operation time of the relay was also reduced from 15.05% to 0.86%. This finding has opened up new possibilities in designing new families of digital filters for power system protection. Authors in (Ding et al., 2016) has mentioned that being a static generator, PV will not contribute in power angle oscillation which could have detrimental and beneficial effect on rotor angle stability. Especially when there is centralized large scale PV system integration in to the grid, the impact on system stability will be more intense. Authors in (Li & Ying-Hao, 2000) have presented a novel approach based on eigenvalue approach and nonlinear model simulation to investigate both transient and steady state performance of a PV array connected to a

large utility grid. This study has opened new opportunity in transient analysis for of inverter integrated generation. The next chapter will present the methodology to achieve the objectives as stated in Chapter 1. In addition, the method used to construct the network model and the components in for the power swing simulation and further analysis will also be presented in Chapter 3.

University of Malaya

- Abbasi, E., Seyedi, H., & Strunz, K. (2009, 26-30 July 2009). *Simulation and analysis of the effect of single-pole auto-reclosing on HV transmission lines switching overvoltages*. Paper presented at the Power & Energy Society General Meeting, 2009. PES '09. IEEE.
- Abidin, A. F., Mohamed, A., & Shareef, H. (2011). Intelligent detection of unstable power swing for correct distance relay operation using S-transform and neural networks. *Expert Systems with Applications*, 38(12), 14969-14975. doi: <http://dx.doi.org/10.1016/j.eswa.2011.05.050>
- Abidin, A. F., Mohamed, A., & Shareef, H. (2011, 6-7 June 2011). *Power swing detection for correct distance relay operation using S-transform and neural networks*. Paper presented at the 2011 5th International Power Engineering and Optimization Conference (PEOCO), .
- Abidin, F. b. (2010). *Adaptive Distance Protection to Prevent False Relay Tripping during Voltage Collapse and Power Swing*. (PhD), Universiti Kebangsaan Malaysia.
- Ambekar, V. A., & Dambhare, S. S. (2012a, 19-22 Dec. 2012). *Comparative evaluation of out of step detection schemes for distance relays*. Paper presented at the 2012 IEEE FifthPower India Conference, .
- Ambekar, V. A., & Dambhare, S. S. (2012b, 19-22 Dec. 2012). *Comparative evaluation of out of step detection schemes for distance relays*. Paper presented at the Power India Conference, 2012 IEEE Fifth.
- Apostolov, A., & Vandiver, B. (2011, 11-14 April 2011). *Requirements for testing of power swing blocking functions in protection IEDs*. Paper presented at the 2011 64th Annual Conference for Protective Relay Engineers,.
- Apostolov, A. P., Tholomier, D., & Richards, S. H. (2004, 10-13 Oct. 2004). *Superimposed components based sub-cycle protection of transmission lines*. Paper presented at the 2004 IEEE Power Systems Conference and Exposition, .
- Berdy, J., Elmore, W. A., -Goff, L. E., New, W. C., Parr, G. C., Summers, A. H., & Wagner, C. L. (1977). Out of step relaying for generators working group report. *IEEE Transactions on Power Apparatus and Systems*, , 96(5), 1556-1564. doi: 10.1109/t-pas.1977.32484
- Brahma, S. M. (2006, 0-0 0). *Use of wavelets for out of step blocking function of distance relays*. Paper presented at the IEEE Power Engineering Society General Meeting.
- Brahma, S. M. (2007). Distance Relay With Out-of-Step Blocking Function Using Wavelet Transform. *IEEE Transactions on Power Delivery*,, 22(3), 1360-1366. doi: 10.1109/tpwrd.2006.886773
- Chengzong, P., & Kezunovic, M. (2010). Fast Distance Relay Scheme for Detecting Symmetrical Fault During Power Swing. *IEEE Transactions on Power Delivery*, 25(4), 2205-2212. doi: 10.1109/tpwrd.2010.2050341
- Cho, K. R., Kang, Y. C., Kim, S. S., Park, J. K., Kang, S. H., & Kim, K. H. (1999). An ANN based approach to improve the speed of a differential equation based distance relaying algorithm. *IEEE Transactions on Power Delivery*, , 14(2), 349-357. doi: 10.1109/61.754073
- Chothani, N. G., Bhalja, B. R., & Parikh, U. B. (2014). New support vector machine-based digital relaying scheme for discrimination between power swing and fault. *IET Generation, Transmission & Distribution*,, 8(1), 17-25. doi: 10.1049/iet-gtd.2013.0020
- Corsi, S., & Sabelli, C. (2004, 6-10 June 2004). *General blackout in Italy Sunday September 28, 2003, h. 03:28:00*. Paper presented at the IEEE Power Engineering Society General Meeting, .
- D'Apuzzo, M., & D'Arco, M. (2008). A Time-Domain Approach for the Analysis of Nonstationary Signals in Power Systems. *IEEE Transactions on Instrumentation and Measurement*, , 57(9), 1969-1977. doi: 10.1109/tim.2008.919903

- Ding, M., Xu, Z., Wang, W., Wang, X., Song, Y., & Chen, D. (2016). A review on China's large-scale PV integration: Progress, challenges and recommendations. *Renewable and Sustainable Energy Reviews*, 53, 639-652. doi: <http://dx.doi.org/10.1016/j.rser.2015.09.009>
- Dubey, R., & Samantaray, S. R. (2013). Wavelet singular entropy-based symmetrical fault-detection and out-of-step protection during power swing. *IET Generation, Transmission & Distribution*, 7(10), 1123-1134. doi: 10.1049/iet-gtd.2012.0528
- Dubey, R., Samantaray, S. R., Tripathy, A., Babu, B. C., & Ehtesham, M. (2012a, 16-18 March 2012). *Wavelet based energy function for symmetrical fault detection during power swing*. Paper presented at the Students Conference on Engineering and Systems (SCES).
- Dubey, R., Samantaray, S. R., Tripathy, A., Babu, B. C., & Ehtesham, M. (2012b, 16-18 March 2012). *Wavelet based energy function for symmetrical fault detection during power swing*. Paper presented at the Students Conference on Engineering and Systems (SCES).
- Esmailian, A., & Astinfeshan, S. (2011, 17-19 July 2011). *A novel power swing detection algorithm using adaptive neuro fuzzy technique*. Paper presented at the International Conference on Electrical Engineering and Informatics (ICEEI), .
- Esmailian, A., Ghaderi, A., Tasdighi, M., & Rouhani, A. (2011, 8-11 May 2011). *Evaluation and performance comparison of power swing detection algorithms in presence of series compensation on transmission lines*. Paper presented at the 10th International Conference on Environment and Electrical Engineering (EEEIC), .
- Feilat, E. A., & Al-Tallaq, K. (2004, 8-8 Sept. 2004). *A new approach for distance protection using artificial neural network*. Paper presented at the UPEC 2004. 39th International Universities Power Engineering Conference, 2004. .
- Fischer, N., Benmouyal, G., Daqing, H., Tziouvaras, D., Byrne-Finley, J., & Smyth, B. (2012, 2-5 April 2012). *Do system impedances really affect power swings; Applying power swing protection elements without complex system studies*. Paper presented at the 65th Annual Conference for Protective Relay Engineers, .
- Fu, L., He, Z. Y., & Bo, Z. Q. (2008a, 17-20 March 2008). *Wavelet Transform and Approximate Entropy Based Identification of Faults in Power Swings*. Paper presented at the Developments in Power System Protection, 2008. DPSP 2008. IET 9th International Conference on.
- Fu, L., He, Z. Y., & Bo, Z. Q. (2008b, 17-20 March 2008). *Wavelet Transform and Approximate Entropy Based Identification of Faults in Power Swings*. Paper presented at the IET 9th International Conference on Developments in Power System Protection (DPSP), .
- Gunasegaran, M. K., ChiaKwang, T., & Bakar, A. H. A. (2014, 24-26 Nov. 2014). *Investigation of power swing phenomenon and verification of critical clearing time through theoretical calculations and simulated studies*. Paper presented at the Clean Energy and Technology (CEAT) 2014, 3rd IET International Conference on.
- Hashemi, S. M., Hagh, M. T., & Seyed, H. (2013). Transmission-Line Protection: A Directional Comparison Scheme Using the Average of Superimposed Components. *IEEE Transactions on Power Delivery*, 28(2), 955-964. doi: 10.1109/tpwrd.2012.2226609
- Holbach, J. (2006, 14-17 March 2006). *New Out of Step Blocking Algorithm for Detecting Fast Power Swing Frequencies*. Paper presented at the Power Systems Conference: Advanced Metering, Protection, Control, Communication, and Distributed Resources, 2006. PS '06.
- Kampeerawat, W., Buangam, W., & Chusanapiputt, S. (2010, 24-28 Oct. 2010). *New swing-blocking methods for digital distance protection using Support Vector Machine*. Paper presented at the International Conference on Power System Technology (POWERCON), .
- Kampeerawat, W., Buangam, W., & Chusanapiputt, S. (2012, 27-29 March 2012). *The Swing-Blocking Methods for Digital Distance Protection Based on Wavelet Packet Transform*

- and Support Vector Machine. Paper presented at the Asia-Pacific Power and Energy Engineering Conference (APPEEC),.
- Kang, H., Subramanian, S., Hassan, F., & Yao, L. (2010, March 29 2010-April 1 2010). *Distance protection under extreme conditions*. Paper presented at the 10th IET International Conference on Managing the Change, Developments in Power System Protection (DPSP),.
- Karegar, H. K., & Mohamedi, B. (2009, 6-9 May 2009). *A new method for fault detection during power swing in distance protection*. Paper presented at the 6th International Conference on Electrical Engineering/Electronics, Computer, Telecommunications and Information Technology (ECTI-CON), .
- Khoradshadi-Zadeh, H. (2005, 12-16 June 2005). *Evaluation and performance comparison of power swing detection algorithms*. Paper presented at the IEEE Power Engineering Society General Meeting,.
- Kundur, P. (1994). *Power System Stability Control*. New York: McGraw-Hill.
- Kundur, P. (1994). *Power System Stability and Control: Introduction to the Power System Stability Problem*. New York: Electric Power Research Institute.
- Li, W., & Ying-Hao, L. (2000, 2000). *Dynamic stability analyses of a photovoltaic array connected to a large utility grid*. Paper presented at the Power Engineering Society Winter Meeting, 2000. IEEE.
- Lobos, T., Rezmer, J., & Koglin, H. J. (2001, 2001). *Analysis of power system transients using wavelets and Prony method*. Paper presented at the IEEE Porto Power Tech Proceedings, .
- Lotfifard, S., Faiz, J., & Kezunovic, M. (2010). Detection of Symmetrical Faults by Distance Relays During Power Swings. *IEEE Transactions on Power Delivery*, 25(1), 81-87. doi: 10.1109/tpwrd.2009.2035224
- Mahamed, B. (2010, 27-29 Oct. 2010). *A very fast unblocking scheme for distance protection to detect symmetrical faults during power swings*. Paper presented at the International Power Electronics Conference Proceedings (IPEC),.
- Mahamed, B. (2011, 15-17 Nov. 2011). *A new power swing blocking function based on wavelet transform*. Paper presented at the 2nd International Conference on Electric Power and Energy Conversion Systems (EPECS), .
- Mahamed, B., & Jian Guo, Z. (2012). A Novel Approach to Detect Symmetrical Faults Occurring During Power Swings by Using Frequency Components of Instantaneous Three-Phase Active Power. *IEEE Transactions on Power Delivery*, 27(3), 1368-1376. doi: 10.1109/tpwrd.2012.2200265
- Martuscello, L., Krizauskas, E., Holbach, J., & Yuchen, L. (2009, March 30 2009-April 2 2009). *Tests of distance relay performance on stable and unstable power swings reported using simulated data of the August 14 2003 system disturbance*. Paper presented at the 62nd Annual Conference for Protective Relay Engineers,.
- Mohamad, N. Z., & Abidin, A. F. (2012). A New Technique for High Resistance Fault Detection during Power Swing for Distance Relay. *AASRI Procedia*, 2(0), 50-55. doi: <http://dx.doi.org/10.1016/j.aasri.2012.09.013>
- Mohamad, N. Z., & Abidin, A. F. (2012, 23-25 March 2012). *S-Transform based technique to detect high resistance symmetrical fault during power swing*. Paper presented at the IEEE 8th International Colloquium on Signal Processing and its Applications (CSPA), .
- Mohamad, N. Z., Abidin, A. F., & Munim, W. N. W. A. (2012, 6-7 June 2012). *A new tracking method of symmetrical fault during Power Swing Based on S-Transform*. Paper presented at the IEEE International Power Engineering and Optimization Conference (PEDCO) Melaka, Malaysia,.
- Mohamad, N. Z., Abidin, A. F., Munim, W. N. W. A., & Yahya, M. (2012, 5-6 Dec. 2012). *Symmetrical fault detection technique during power swing based on S-Transform*. Paper presented at the IEEE Student Conference on Research and Development (SCORED),.

- Mohamad, N. Z., Abidin, A. F., & Musirin, I. (2013, 3-5 Dec. 2013). *The use of S-Transform for distance relay's power swing detection*. Paper presented at the IEEE Jordan Conference on Applied Electrical Engineering and Computing Technologies (AEECT),.
- Mooney, J., & Fischer, N. (2006, 0-0 0). *Application guidelines for power swing detection on transmission systems*. Paper presented at the 59th Annual Conference for Protective Relay Engineers, 2006. .
- Mozina, C. J. (2012, 7-10 May 2012). *Impact of power system instability on generator protection*. Paper presented at the Transmission and Distribution Conference and Exposition (T&D), 2012 IEEE PES.
- P. K. Nayak, J. G. Rao, P. Kundur, A. K. Pradhan, & P. Bajpai. (2010, 20-23 Dec. 2010). *A comparative assessment of power swing detection techniques*. Paper presented at the Power India Joint International Conference on Power Electronics, Drives and Energy Systems (PEDES).
- Parameswariah, C., & Cox, M. (2002). Frequency characteristics of wavelets. *IEEE Transactions on Power Delivery*, , 17(3), 800-804. doi: 10.1109/tpwrd.2002.1022806
- Samantaray, S. R., Dubey, R. K., Tripathy, L. N., & Babu, B. C. (2011, 28-30 Dec. 2011). *Spectral energy function for fault detection during power swing*. Paper presented at the International Conference on Energy, Automation, and Signal (ICEAS),.
- Sanaye-Pasand, M., & Jafarian, P. (2011). An Adaptive Decision Logic to Enhance Distance Protection of Transmission Lines. *IEEE Transactions on Power Delivery*, , 26(4), 2134-2144. doi: 10.1109/tpwrd.2011.2159404
- Seethalekshmi, K., Singh, S. N., & Srivastava, S. C. (2010, 25-29 July 2010). *SVM based power swing identification scheme for distance relays*. Paper presented at the IEEE Power and Energy Society General Meeting,.
- Seethalekshmi, K., Singh, S. N., & Srivastava, S. C. (2012). A Classification Approach Using Support Vector Machines to Prevent Distance Relay Maloperation Under Power Swing and Voltage Instability. *IEEE Transactions on Power Delivery*,, 27(3), 1124-1133. doi: 10.1109/tpwrd.2011.2174808
- Thakallapelli, A., Mehra, R., & Mangalvedekar, H. A. (2013, 6-8 Dec. 2013). *Differentiation of faults from power swings and detection of high impedance faults by distance relays*. Paper presented at the IEEE 1st International Conference on Condition Assessment Techniques in Electrical Systems (CATCON),.
- Trujillo G, L. A., Conde E, A., & Leonowicz, Z. (2013, 5-8 May 2013). *Application of the Prony method for compensation of errors in distance relays*. Paper presented at the 12th International Conference on Environment and Electrical Engineering (EEEIC),.
- Tziouvaras, D. A., & Daqing, H. (2004, 30 Mar-1 Apr 2004). *Out-of-step protection fundamentals and advancements*. Paper presented at the 57th Annual Conference for Protective Relay Engineers,.
- Vaidya, A. P., & Venikar, P. A. (2012, 30-31 March 2012). *ANN based distance protection of long transmission lines by considering the effect of fault resistance*. Paper presented at the Advances in Engineering, Science and Management (ICAESM), 2012 International Conference on.
- Vapnik, V. (1995). The nature of statistical learning theory
- Verzosa, Q. (2013, 8-11 April 2013). *Realistic testing of power swing blocking and out-of-step tripping functions*. Paper presented at the 2013 66th Annual Conference for Protective Relay Engineers, .
- Wall, P., Gonza, x, lez-Longatt, F., & Terzija, V. (2010, Aug. 31 2010-Sept. 3 2010). *Demonstration of an inertia constant estimation method through simulation*. Paper presented at the 45th International Universities Power Engineering Conference (UPEC), .
- Xiangning, L., Yan, G., & Pei, L. (2008). A Novel Scheme to Identify Symmetrical Faults Occurring During Power Swings. *IEEE Transactions on Power Delivery*, , 23(1), 73-78. doi: 10.1109/tpwrd.2007.911154

- Xiangning, L., Zhengtian, L., Shuohao, K., & Yan, G. (2010). Theoretical Fundamentals and Implementation of Novel Self-Adaptive Distance Protection Resistant to Power Swings. *IEEE Transactions on Power Delivery*, , 25(3), 1372-1383. doi: 10.1109/tpwrd.2010.2043450
- Yusoff, N., & Abidin, A. F. (2013, 19-20 Aug. 2013). *The effect of solar Photovoltaic (PV) system to the characteristic of power swing*. Paper presented at the IEEE 3rd International Conference on System Engineering and Technology (ICSET),.
- Zadeh, H. K., & Li, Z. (2008, 20-24 July 2008). *Artificial neural network based load blinder for distance protection*. Paper presented at the IEEE Power and Energy Society General Meeting - Conversion and Delivery of Electrical Energy in the 21st Century,.
- Zadeh, H. K., & Li, Z. (2008). A novel power swing blocking scheme using adaptive neuro-fuzzy inference system. *Electric Power Systems Research*, 78(7), 1138-1146. doi: <http://dx.doi.org/10.1016/j.epsr.2007.09.007>
- Ziegler, G. (July 1999). *Numerical Distance Protection: Principle and Application* (Vol. 1). Germany: Publicis MCD.

University of Malaysia

CHAPTER 3: METHODOLOGY

3.1 Introduction

In the earlier chapter, a literature review on the power swing, its impact, and the PSB schemes were presented. This chapter will present the methodology to achieve the objectives of this research. In the first part, the simulation software used in this research is described briefly. This is followed by network modeling which will be used in this research for simulation and analysis purposes. The modelling of an additional synchronous machine and a solar PV generator will also be presented. It is important to note that, these additional generators will be used for comparison studies which comprise of critical clearing time analysis, swing severity analysis and the risk in distance relay mal-operation. The methodology on achieving the above mentioned analyses will be presented in this chapter.

3.2 System Modelling

3.2.1 DIgSILENT Power Factory

DIgSILENT Power Factory is a program commonly used to simulate complex power and control systems. The experiments in this research are completely done using the DIgSILENT Power Factory simulation software.

3.2.2 Network Modelling

The double circuit transmission line configuration is commonly found in a transmission system for increased reliability. The analysis in this research is conducted using the 230kV, 60Hz, two-area and four-machine system shown in Figure 3.1, adopted from (Dubey & Samantaray, 2013). Generator G1, connected to Bus 1 is rated at 20kV and 900MVA. It is the reference machine, operating at a power angle of

20.2 degree and delivering 700 MW and 185 Mvar of power, amounting to 81.1% of its capacity. The initial value of generator 2, 3 and 4 (G2, G3 and G4 respectively) are set to deliver 700MW+235MVAR, 719MW+176MVAR and 700MW+202MVAR respectively. All of the transformers are rated at 900 MVA and they are connected in between the generators busbar and high voltage busbar to step up the voltage from 20 kV to 230 kV. All the overhead transmission lines are rated at 230 kV. The network also consists of 2 sections of double circuit transmission lines, between Bus 7 and Bus 8, and between Bus 8 and Bus 9. There are two loads at Bus 7 and Bus 9 and they are consuming 967 MW, 100 Mvar and 1767 MW, 100 Mvar respectively. Two shunt capacitances are also connected to Bus 7 and Bus 9 which are rated at 200 Mvar and 350 Mvar to provide compensation during low power factor (Hashemi, Hagh, & Seyedi, 2014). A Mho type distance relay (R1) is placed at the end of Line-1 and the relay is set with its zone 1, zone 2 and zone 3 to cover for 80%, 120%, and 150% of the length of Line-1 respectively. In addition, zone 1 is set to trip instantaneously while a delay of 300 ms and 3 s is set for zone 2 and zone 3 respectively.

In addition to the 4 machines in the network in Figure 3.1, an additional of two other generators are also connected to Bus 2 for the comparative analysis. The two generators are synchronous Generator A and solar PV generator of equal capacity which will be explained in subsequent section. The simulation and analysis in this thesis will be conducted considering the 2 cases below:

Case 1: The connection of synchronous Generator A and the disconnection of solar PV generator in the network in Figure 3.1.

Case 2: The connection of solar PV generator and the disconnection of synchronous Generator A in the network in Figure 3.1.

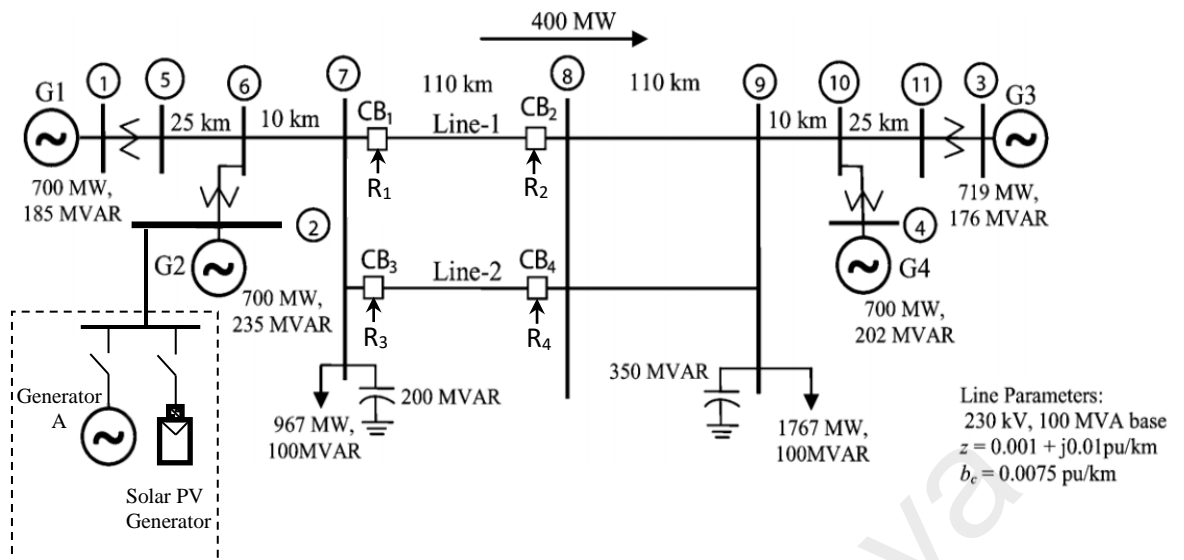


Figure 3.1: Model of a Complete Network (Rao & Pradhan, 2015)

Legend

Synchronous Machine		Switch	
Solar Photovoltaic Generator		Load	
20/230 kV Transformer		Capacitor	
Circuit Breaker		Earth	
<u>Busbar</u>			

3.2.3 Synchronous Machine – Generator A

Besides the four existing synchronous generators, another 50 MVA Generator A is connected to Bus 2, operating in parallel to generator G2. This Generator A is intended to be exchanged with a solar PV generator of similar capacity for comparison purposes during the analysis. Therefore bus 6 will act as the point-of-common coupling (PCC). In the simulation, Generator A will be operated at its maximum capacity, generating 50 MVA at unity power factor. The parallel connection of Generator A to generator G2 will result in the loading of transformer in between Bus 2 and Bus 6 to be 87.4% of its capacity as shown in Figure 3.2. As a result to the increment of the transformers loading, G2 is seen to deliver an addition of 28.3MVAR to cater the loading. As a rotating machine and under the influence of mechanical power, it is important to note that Generator A has an inertia constant of 4.351858 s.

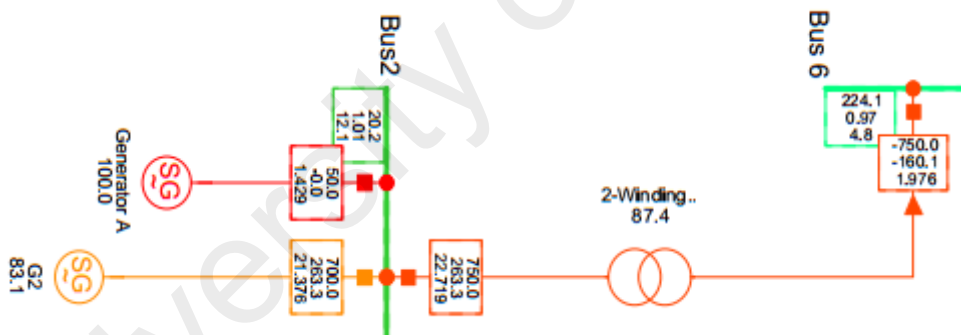


Figure 3.2: Model of Generator A with an Inertia Constant

3.2.4 Solar Photovoltaic (PV) Generator

A Solar PV farm of similar capacity to the Generator A will be modelled in DIgSILENT Power Factory for comparison purposes in the analysis. The 50MW solar PV system used in this study is also connected to Bus 2 at a nominal voltage of 20kV. The combination of solar PV generator and generator G2 will also load the transformer to

87.4%. As shown in Figure 3.3, the PV system that is used in this simulation is developed by DIgSILENT Power Factory and it comes with a built in ideal inverter. However, there is no maximum power point tracking (MPPT) module included in this solar PV system and instead, the total dispatched power can be manually decided by the user. In this study, the solar PV generator is set to deliver a constant power at 100% of its rated capacity. The parallel connection of solar PV generator to generator G2 will result in the loading of transformer in between Bus 2 and Bus 6 to be 87.4% of its capacity as shown in Figure 3.3. As a result to the increment of the transformers loading, G2 is seen to deliver an addition of 28.3MVAR to cater the loading. It is also important to note that the PV system is an inertia-less machine (Wandhare & Agarwal, 2014).

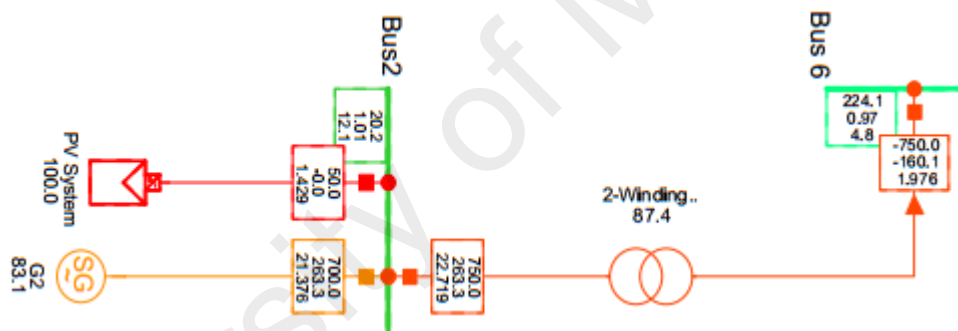


Figure 3.3: Model of PV System with Zero Inertia

3.3 Case studies

The simulation is conducted for three (3) different parts where:

1. The CCT of the synchronous machines will be analyzed in the first part.
2. The second part will investigate the severity of the swing by observing the active power oscillations of other generators. In addition, the impedance trajectory at the distance relay R1 of the Line-1 in Figure 3.1 will also be evaluated.
3. The third part will investigate the risk of distance relay mal-operation by increasing the fault clearing time and observing relay R1's impedance trajectory.

All the three parts of the experiment will be conducted for both Case 1 and Case 2.

3.3.1 Analysis on Critical Clearing Time of Synchronous Machines

Figure 3.4 shows the flowchart for the CCT analysis methodology.

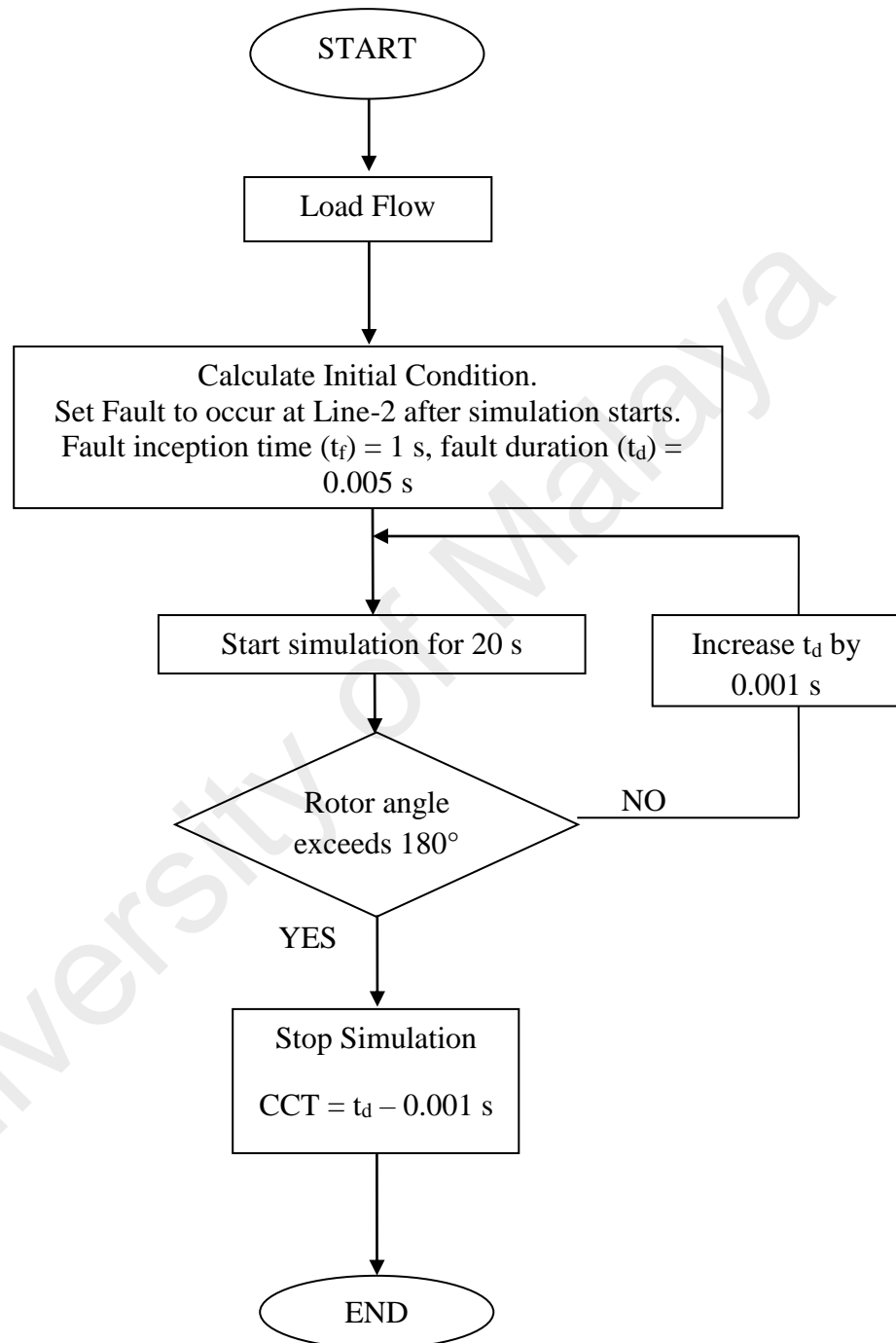


Figure 3.4: Flow Chart for CCT Analysis Simulation

The simulation will begin with Case 1 where the synchronous Generator A is connected to Bus 2 while the solar PV generator is disconnected. A permanent 3-phase bolted fault

is then initiated at 1 s after the simulation is started. The fault is set to occur at 100% length of Line-2 and the fault clearing time for R3 and R4 (t_d) are set at 0.005 s. The rotor angles of generator G3 and G4 are then checked to see if it has exceeded 180 degree (out-of-step condition). If the generators rotor angle did not experience out-of-step condition, the simulation is repeated by increasing the fault duration (t_d) by 0.001 s. The simulation will be repeated until out-of-step condition is met. Once the rotor angles of the generators have exceeded 180 degree, the simulation is stopped and the CCT of the generators are calculated by deducting 0.001 s from the last set t_d .

After that, the above steps are repeated for Case 2 where the solar PV generator is connected and Generator A is disconnected.

3.3.1.1 Sensitivity Studies for CCT

The CCT of a machine will allow the generator to withstand fault for a maximum period of time. However, the CCT of the machine may vary according to few factors which are varying types of generators, faults at different locations, and varying output power of generator. Since the consequences of the mentioned factors to the CCT of the generators are unknown, the sensitivity studies simulation which comprise of types of generators, varying fault location and varying output power will be conducted. Section 3.3.1 presents the methodology for the first part of the sensitivity studies which is the varying types of generators. For the second part, the fault location is varied and the same methodology is repeated. The fault is simulated only at the double circuit section of the 230 kV transmission line. This includes busbar 7, 8, and 9 which comprise of Line-1 and Line-2 as in Figure 3.1. The fault location is varied from 0% to 200% in between bus 7 and 9 in steps of 20%. Therefore, it has to be noted that the fault location at 0%, 100% and 200% represents bus 7, 8 and 9 respectively and the other fault locations represent the line in between the two busses. For the final part, the output power of the

synchronous machine and solar PV generator is varied in the range from 20% to 100% in a step of 20%. The differences in CCT for all these simulated factors will be analyzed and discussed.

3.3.2 Analysis on Swing Severity

The analysis on swing severity will consist of 2 parts:

- a) Active power oscillation
- b) Impedance trajectory

3.3.2.1 Active Power Oscillation

To analyze the severity of the swing, the active power of the other generators (G1 to G4) will be plotted and analyzed. The simulation will start with Case 1 where the synchronous Generator A is connected to Bus 2 while the solar PV generator is disconnected. A 3-phase bolted fault is then initiated at 0.5 s after the simulation is started. The fault location is set to be at Line-2 close to bus 7. The circuit breaker on the faulted line (CB3 and CB4) will then isolate Line-2 at 0.1 s after the fault is initiated due to the instantaneous tripping. The relay R3 and R4 fault clearing duration of 0.1 s, equivalent to 6 cycles is considered in this simulation taking into account the relay operating time, the signal travelling time, circuit breaker operating time, and arc extinction time. Subsequently, the entire load from Line-2 is transferred onto the other healthy line (Line-1). After this simulation, the active power oscillation at all the terminals of the generators (G1 to G4) throughout the simulation duration is observed. The above steps are then repeated for Case 2 where the solar PV generator is connected and the synchronous Generator A is disconnected. To achieve a fair comparison, the generating capacities for both the Generator A and solar PV generator are set to 100%. It is important to note that the Power Swing Blocking scheme (PSB scheme) is not

considered as this will limit the evaluation of swing severity. The differences in active power oscillation for all these simulated factors will be analyzed and discussed.

3.3.2.2 Impedance Trajectory

Ideally, for faults that occurred in one circuit of a double circuit transmission line, only the faulted line should be isolated while the other healthy line remains connected. In the case of power swing, the impedance trajectory may fall into the healthy line relay zones. If the duration of the impedance trajectory exceeds the delay time of the healthy line distance relay zones (Zone 2 and Zone 3), it will lead to the nuisance tripping of the relay leading to the opening of the circuit breaker to isolate the healthy line. This will result in major blackout as the entire double circuit transmission lines will be disconnected. Therefore this section will analyze the impedance trajectory seen by distance relay R1 on the healthy line (Line-1) for Case 1 and Case 2.

In this experiment, the simulation will begin with Case 1 where the synchronous Generator A is connected to Bus 2 while the solar PV generator is disconnected. A permanent 3-phase bolted fault is then initiated at 0.5 s after the simulation is started. The fault location is set to be at Line-2 close to bus 7. The circuit breaker on the faulted line (CB3 and CB4) will then isolate Line-2 after 6-cycles which is, 0.1 s after the fault is initiated due to the instantaneous tripping. Subsequently, the entire load from Line-2 is transferred onto the other healthy line (Line-1). The impedance trajectory seen by the distance relay R1 will be analyzed. The above steps are then repeated for Case 2. The impedance trajectory results will then be used to analyze the risk of distance relay mal-operation in the next section.

3.3.3 Analysis on the Risk of Distance Relay Mal-operation

3.3.3.1 Varying Fault Duration

When fault occurs, the distance relay detects the impedance in its zones and send a tripping signal to the circuit breaker. However, it is common to have sluggishness in the circuit breakers operation due to mechanical failures (Canay, 2001; Das, 2008). This sluggishness will cause longer fault sustenance on the faulted line. Therefore, this section of the experiment will analyze the impact on impedance trajectory seen by distance relay R1 of the healthy line for varying fault duration.

In this experiment, the simulation will begin with Case 1 where the synchronous Generator A is connected to Bus 2 while the solar PV generator is disconnected. A permanent 3-phase bolted fault is then initiated at 0.5 s after the simulation is started. The fault location is set to be at Line-2 close to bus 7. The circuit breaker on the faulted line (CB3 and CB4) will then isolate Line-2 after 7-cycles which is, 0.1167 s after the fault is initiated due to the sluggishness of the circuit breaker. Subsequently, the entire load from Line-2 is transferred onto the other healthy line (Line-1). The impedance trajectory seen by the distance relay R1 will be analyzed to evaluate the risk of distance relay mal-operation. The above steps are then repeated for Case 2.

CHAPTER 4: RESULTS AND DISCUSSION

4.1 Introduction

This chapter will present the simulated results from the developed power system model in Chapter Three. Before running the simulation, the load flow analysis is performed to ensure that the system is operating in a stable condition. Next, the simulation is executed for a duration of 10 s. The simulation duration is sufficient to be set at 10 s for the reason that any protection device would operate faster than this period of time. The results and discussions that will be presented in this chapter comprise of the sensitivity studies for critical clearing time (CCT) analysis, severity of the swing and analysis on the risk of distance relay mal-operation.

4.2 CCT Analysis

4.2.1 Varying types of Generators

Table 4.1 and 4.2 show the result of critical clearing time (CCT) for Case 1 and Case 2 respectively. It has to be noted that the CCT of generator G1 could not be observed due to its nature of being the reference machine in the network as in Figure 3.1. On the other hand, the CCT for generator G2 could not be identified because generator G1 and G2 are located in the same area. Hence, the power flow from the reference machine (generator G1) will not allow generator G2 to pole slip or to become unstable.

However, for the purpose of comparison between Case 1 and Case 2, the CCT of generator G3 and G4 will be observed and analyzed. By repetitive trial and error in setting the fault clearing time (FCT), the CCTs for generator G3 and G4 for Case 1 are identified to be 1.6706 s and 1.6705 s respectively. When the same simulation is conducted for Case 2, the CCTs of generator G3 and G4 are seen to reduce to 1.5274 s and 1.5273 s. It can be clearly seen that the CCT for generator G3 and G4 is longer in

Case 1 when compared to Case 2. A difference of 0.1432 s exists in the CCT for both generators G3 and G4 when the synchronous generator is interchanged with a solar PV generator of equal capacity.

The rotor angle graph for both marginally stable and unstable scenarios which are simulated for Case 1 and Case 2 is as shown from Figure 4.1 to Figure 4.8. Figure 4.1 and Figure 4.2 shows the marginally stable condition of generator G3 and G4 for Case 1. It can be clearly observed that the maximum rotor angle is -141.015° and -149.091° for generator G3 and G4 respectively. It is important to note from here that, generator G4 will pole slip faster compared to generator G3 due to a larger rotor angle in generator G4 than the rotor angle of generator G3. In addition, Figure 3.1 shows that the location of generator G4 is nearer to fault location when compared to generator G4. The distance of the generator to the fault location will result in lower fault impedance value seen by generator G4 in comparison to generator G3. Hence, these are the reasons for the small differences in their CCT values.

Increasing the FCT value by 0.0001 s to 1.6707 s and 1.6706 s leads both the generators G3 and G4 to out-of-step condition as shown in Figure 4.3 and Figure 4.4. As mentioned earlier, generator G4 experiences out-of-step condition earlier (4.082 s) than generator G3 (4.142 s).

Table 4.1: CCT results for Type of Generators: Case 1

Generators	CCT
G1	ref machine
G2	no pole slip for 10 s
G3	1.6706 s
G4	1.6705 s

Table 4.2: CCT results for Case 2 for Type of Generators: Case 2

Generators	CCT
G1	ref machine
G2	no pole slip for 10 s
G3	1.5274 s
G4	1.5273 s

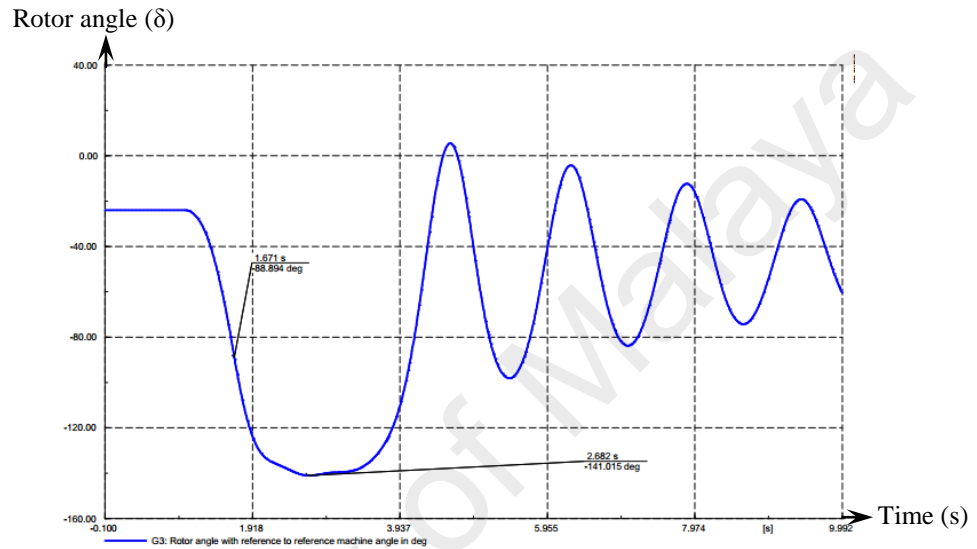


Figure 4.1: Marginally Stable Rotor Angle of Generator G3 for Case 1

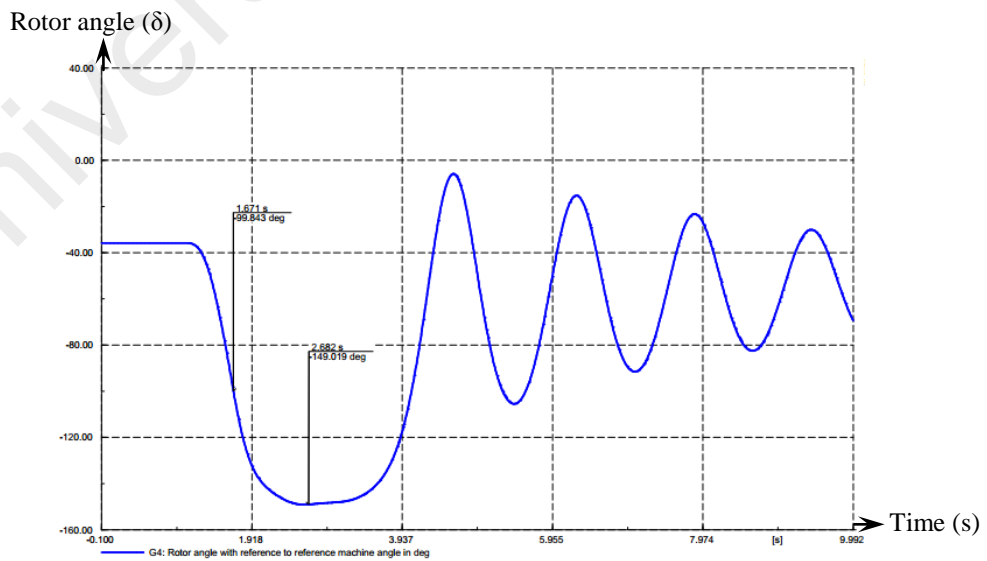


Figure 4.2: Marginally Stable Rotor Angle of Generator G4 for Case 1

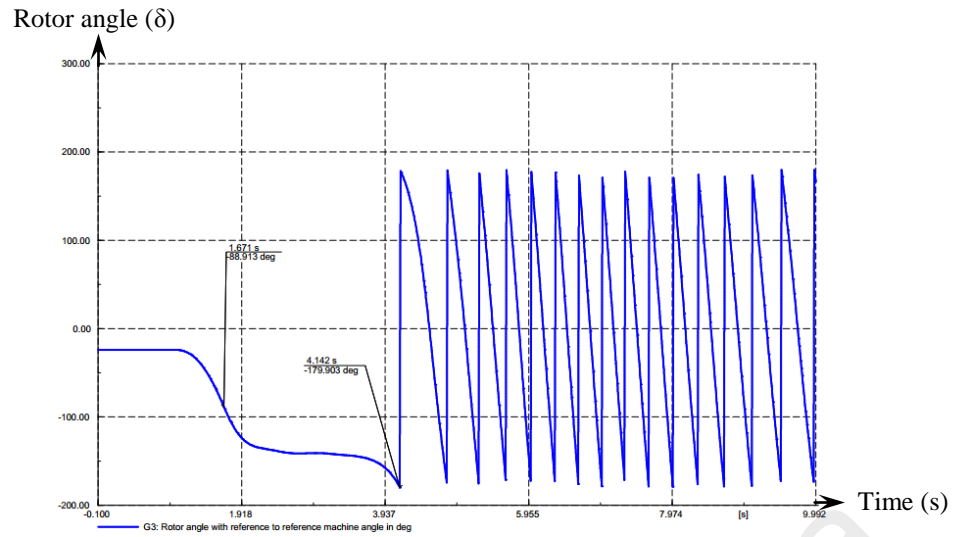


Figure 4.3: Unstable Generator G3 for Case 1

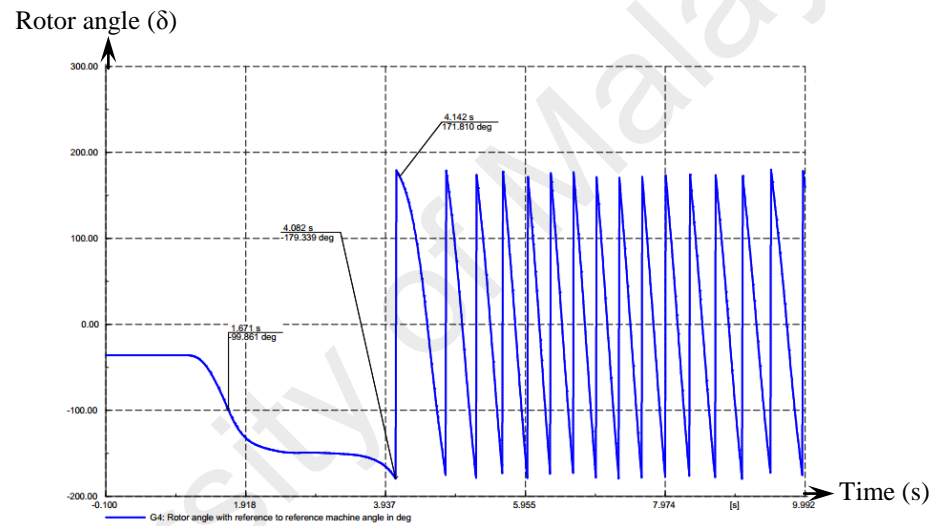


Figure 4.4: Unstable Generator G4 for Case 1

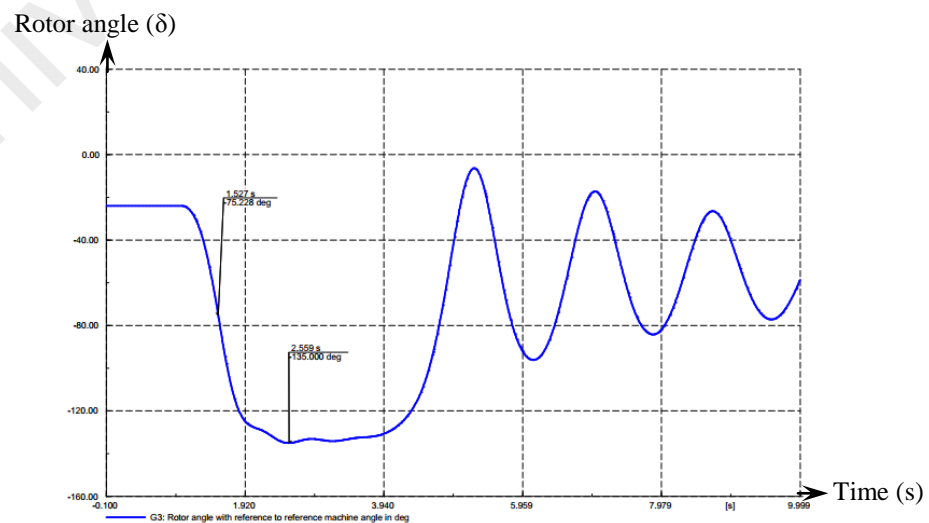


Figure 4.5: Marginally Stable Generator G3 for Case 2

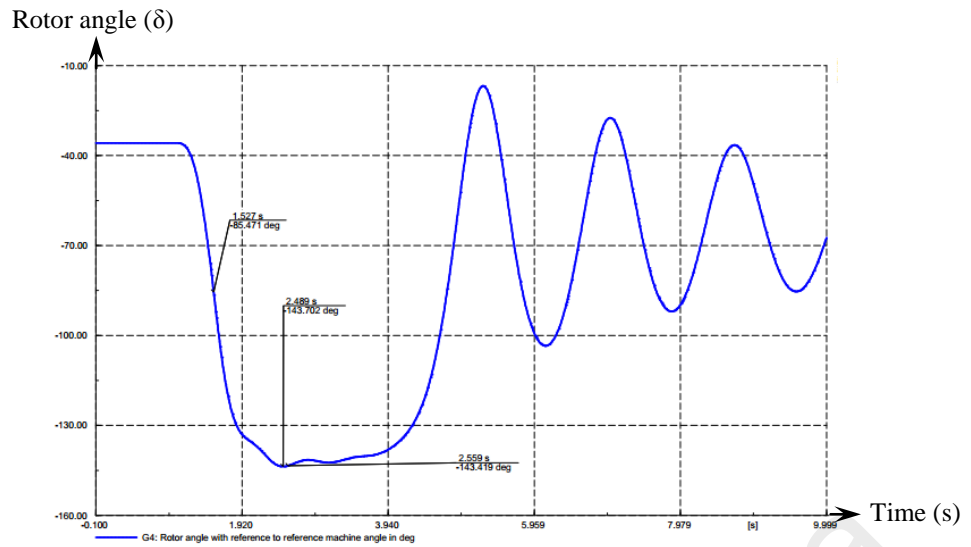


Figure 4.6: Marginally Stable Generator G4 for Case 2

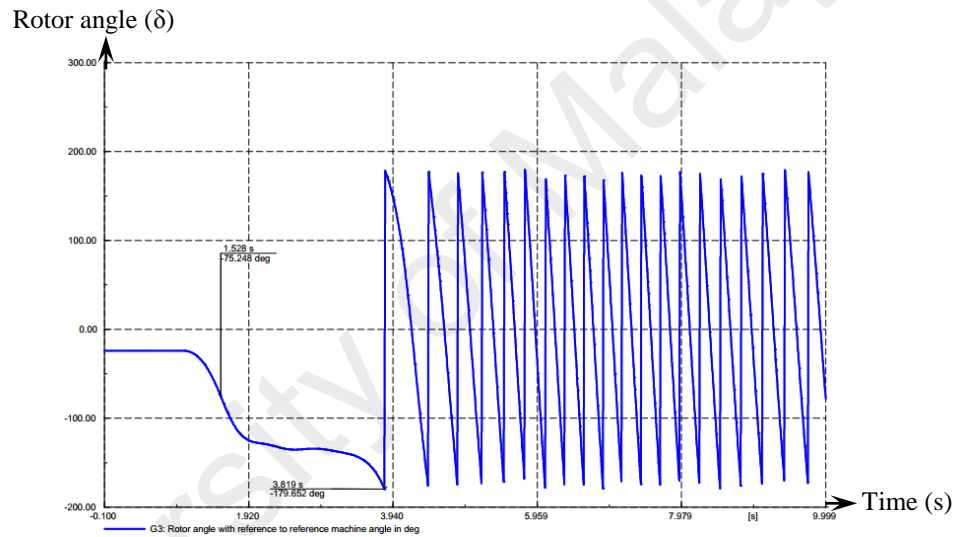


Figure 4.7: Unstable Generator G3 for Case 2

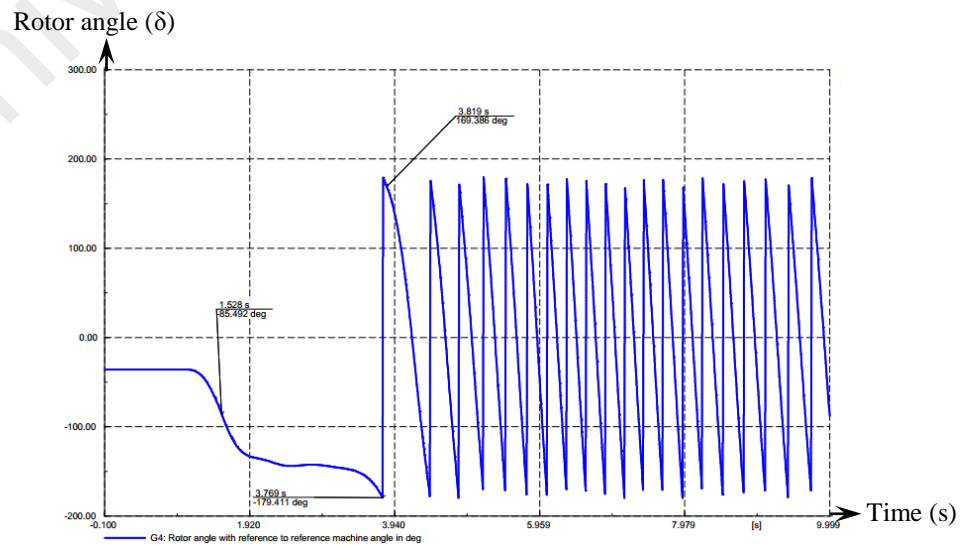


Figure 4.8: Unstable Generator G4 for Case 2

Figure 4.5 and Figure 4.6 shows the marginally stable condition of generator G3 and G4 for Case 2. It can be clearly observed that the maximum rotor angle is -135.000° and -143.419° for generator G3 and G4 respectively. It is important to note from here that, generator G4 will pole slip faster compared to generator G3 due to the larger rotor angle in generator G4 than the rotor angle of generator G3. In addition, Figure 3.1 shows that the location of generator G4 is nearer to fault location when compared to generator G3. Due to shorter distance of the generator G4 to the fault location, a lower fault impedance value is seen by generator G4 in comparison to generator G3. Hence, these are the reasons for the small differences in their CCT values.

Increasing the FCT values by 0.0001 s to 1.5275 s and 1.6274 s leads both the generators G3 and G4 to out-of-step condition as shown in Figure 4.7 and Figure 4.8. As mentioned earlier, generator G4 experiences out-of-step condition earlier (3.769 s) than generator G3 (3.819 s).

In order to understand the reason behind these differences, the analyses are taken to another level by observing the CCT for varying fault location as in the next section.

4.2.2 Varying Fault Location

Table 4.3 and 4.4 shows the result for varying fault locations of Case 1 and Case 2 respectively. The fault location is adjusted at a step size of 20% on Line-2 and the FCT is adjusted at a step size of 0.0001 s. For Case 1, Table 4.3 shows that when the fault location is set to be at 0% of Line-2, the CCT of generator G3 and G4 are 1.0963 s and 1.0962 s respectively. The fault location is changed to 20% of Line-2 length and it results in the increment of CCT for generator G3 and G4 to 1.1484 s and 1.1483 s respectively. Next, the fault location is change to 40% of Line-2 length. The simulation at this location further increases the CCT of generator of G3 and G4 to 1.2160 s and 1.2159 s respectively. Further simulation was done by changing the fault

location to 60% of Line-2 length, and it was found that the CCT of generator G3 and G4 becomes 1.3067 s and 1.3066 s respectively. When fault location is advanced to 80% of the Line-2 length, the simulated result for CCT of generator G3 and G4 escalates to 1.4421 s and 1.4420 s. Next, when the fault location is set to be at 100% of Line-2 length, the result of CCT for generator G3 and G4 becomes 1.6706 s and 1.6705 s respectively. Extension of the fault location to 120% results in a largest value of CCT which is 1.8289 s and 1.8288 s for G3 and G4 respectively. The fault location is then changed to 140% and the CCT is observed to reduce to 1.3729 s and 1.3728 s for G3 and G4 respectively. Extending the fault location to 160% shortens the CCT even further to 1.2251 s and 1.2250 s for G3 and G4 respectively. Next the CCT for G3 and G4 are observed when the fault location is at 180% and the generators experience marginal stability at 1.1385 s and 1.1384 s. Finally, to complete the sensitivity studies at double circuit transmission line, the fault location is set at 200% of Line-2 length which falls at Busbar 9. Here, the CCT values are recorded to be 1.0796 s and 1.0795 s for generator G3 and G4 respectively.

For Case 2, Table 4.4 shows that when the fault location is set to be at 0% of Line-2, the CCT of generator G3 and G4 are 1.0677 s and 1.0676 s respectively. The fault location is changed to 20% of Line-2 length and it results in the increment of CCT for generator G3 and G4 to, 1.1141 s and 1.1140 s respectively. Next, the fault location is changed to 40% of Line-2 length. The simulation at this fault location further increases the CCT of generator of G3 and G4 to 1.1711 s and 1.1710 s respectively. Further simulation was done by changing the fault location to 60% of Line-2 length, and it was found that the CCT of generator G3 and G4 becomes 1.2480 s and 1.2479 s respectively.

Table 4.3: CCT result for Fault Location: Case 1

Fault Location	CCT			
	G1	G2	G3	G4
0%	ref machine	no pole slip	1.0963	1.0962
20%	ref machine	no pole slip	1.1484	1.1483
40%	ref machine	no pole slip	1.2160	1.2159
60%	ref machine	no pole slip	1.3067	1.3066
80%	ref machine	no pole slip	1.4421	1.4420
100%	ref machine	no pole slip	1.6706	1.6705
120%	ref machine	no pole slip	1.8289	1.8288
140%	ref machine	no pole slip	1.3729	1.3728
160%	ref machine	no pole slip	1.2251	1.2250
180%	ref machine	no pole slip	1.1385	1.1384
200%	ref machine	no pole slip	1.0796	1.0795

When fault location is advanced to 80% of the Line-2 length, the simulated result for CCT of generator G3 and G4 escalates to 1.3637 s and 1.3636 s. Next, when the fault location is set to be at 100% of the Line-2 length, the result of CCT for generator G3 and G4 becomes 1.5274 s and 1.5273 s respectively. Extension of the fault location to 120% results in a largest value of CCT which is 1.7578 s and 1.7577 s for G3 and G4 respectively. The fault location is then changed to 140% and the CCT is observed to reduce to 1.2392 s and 1.2391 s for G3 and G4 respectively. Extending the fault location to 160% shortens the CCT even further to 1.1568 s and 1.1567 s for G3 and G4 respectively. Next the CCT for G3 and G4 are observed by setting the fault location to 180% and the generators experience marginal stability at 1.1006 s and 1.1005 s. Finally, to complete the sensitivity studies at double circuit transmission line, the fault location is set at 200% of Line-2 length which falls at busbar 9. Here, the CCT values are recorded to be 1.0451 s and 1.0450 s for generator G3 and G4 respectively.

Table 4.4: CCT results for Fault Location: Case 2

Fault Location	CCT			
	G1	G2	G3	G4
0%	ref machine	no pole slip	1.0677	1.0667
20%	ref machine	no pole slip	1.1141	1.1140
40%	ref machine	no pole slip	1.1711	1.1710
60%	ref machine	no pole slip	1.2480	1.2479
80%	ref machine	no pole slip	1.3637	1.3636
100%	ref machine	no pole slip	1.5274	1.5273
120%	ref machine	no pole slip	1.7578	1.7577
140%	ref machine	no pole slip	1.2392	1.2391
160%	ref machine	no pole slip	1.1568	1.1567
180%	ref machine	no pole slip	1.1006	1.1005
200%	ref machine	no pole slip	1.0451	1.0452

By analyzing the result from Table 4.3 and 4.4, it is observed that as the fault location increases further from the reference machine, the CCT of the generator G3 and G4 increases for Case 1 and Case 2. The maximum value of CCT for both Case 1 and Case 2 is observed when the fault location is set to be at 120% of Line-2 length. This shows that the generators would be able to sustain fault for its maximum time if fault occurs at this particular location. This is because the fault impedance is the largest at the fault location of 120% when compared to other places. Therefore from Eq. 2.1, the CCT sustenance is longer as the fault impedance assists in lengthening the CCT value for both cases. However, the important point here is to compare Case 1 and Case 2 which consists of the presence of synchronous machine and the presence of solar PV generator respectively. By comparing both Case 1 and Case 2, it is found that the CCT for generator G3 and G4 is longer for Case 1 compared to Case 2.

As explained earlier, one of the factors that affect the CCT for synchronous machine is the impedances between the fault and the machine. The presence of these sub-transient and transient reactances in synchronous machine contributes to the longer fault

sustenance of the generator G3 and G4 in Case 1. In contrast, the absence or negligible level sub-transient and transient reactances in the solar PV generator does not contribute to the longer fault sustenance for generator G3 and G4 as in Case 2. Hence, this causes the differences between Case 1 and Case 2. In a monopolized synchronous machine environment, the installation of a static generator will result in shorter CCT. If preventive measure such as re-analysis of the protection system is not taken, the other synchronous machines might risk out-of step condition. Therefore, it is important for a utility team to study the entire system in such a case for future network expansion.

4.2.3 Varying Output Power

This section presents the simulation results of various output power from the generators (synchronous machine and solar PV generator) as in Case 1 and Case 2 in order to analyze the change in CCT for generator G3 and G4. The output power for both cases are varied from 20%, 40%, 60%, 80% and 100%. From Table 4.5 for Case 1, it is seen that when the synchronous machine is operated at 20% of its maximum power (50 MVA), the CCT of generator G3 and G4 are 1.6592 s and 1.6591 s respectively. Subsequently, when the generator power is increased to 40% of its maximum capacity the CCT value increases to 1.6616 s and 1.6615 s for generator G3 and G4 respectively. At 60% at its maximum generating capacity, generator G3 and G4 is seen to have a CCT value of 1.6634 s and 1.6633 s respectively. Next, the output power is increased to 80% of the synchronous machines maximum power and the same simulation is repeated. The CCT of generator G3 and G4 increase to 1.6676 s and 1.6675 s. Finally, at the maximum power output from the synchronous machine, the CCT of the generator G3 and G4 are 1.6706 s and 1.6705 s respectively.

The simulation is repeated for Case 2 and the results obtained are as presented in Table 4.6.

Table 4.5: CCT result for Variable Output Power: Case 1

Output power	CCT			
	G1	G2	G3	G4
20%	ref machine	no pole slip	1.6592	1.6591
40%	ref machine	no pole slip	1.6616	1.6615
60%	ref machine	no pole slip	1.6634	1.6633
80%	ref machine	no pole slip	1.6676	1.6675
100%	ref machine	no pole slip	1.6706	1.6705

From Table 4.6 for Case 2, it is seen that when the solar PV generator is operated at 20% of its maximum power (50 MW), the CCT of generator G3 and G4 are 1.4981 s and 1.4980 s respectively. Subsequently, when the generator power is increased to 40% of its maximum capacity, the CCT value increases to 1.5057 s and 1.5056 s for generator G3 and G4 respectively. At 60% of its maximum generating capacity, generator G3 and G4 are observed to have a CCT value of 1.5178 s and 1.5177 s respectively. Next, the output power is increased to 80% of the solar PV generator maximum power and the same simulation is repeated. The CCT of generator G3 and G4 increase to 1.5226 s and 1.5225 s. Finally, at the maximum power output from the solar PV generator, the CCT of the generator G3 and G4 are 1.5274 s and 1.5273 s respectively.

From the obtained results it can be concluded that, the variation of output power leads to very minimal change in the CCT of the corresponding generators for both Case 1 and Case 2. Therefore the change in output power will have minimal impact to the CCT and setting of generators relay. This is also due to the small ratio of solar PV generator power delivery value compared to other generators. On the other hand, by comparing both the cases the CCT value for Case 2 is seems to be shorter than Case 1.

Table 4.6: CCT results for Variable Output Power: Case 2

Output power	CCT			
	G1	G2	G3	G4
20%	ref machine	no pole slip	1.4981	1.4980
40%	ref machine	no pole slip	1.5057	1.5056
60%	ref machine	no pole slip	1.5178	1.5177
80%	ref machine	no pole slip	1.5226	1.5225
100%	ref machine	no pole slip	1.5274	1.5273

As explained in Section 4.2.2, this is due to the presence of sub-transient and transient reactances in the synchronous machine. The sub-transient and transient reactances in synchronous machine assisted in increasing the sustenance of generator to the fault. Accordingly, the CCT value also becomes longer in Case 1 compared to Case 2. Therefore, this part of the sensitivity study proves that the presence of solar PV generator in a synchronous machine monopolized environment will shorten the CCT of other generators. It is important to note that the utility team have to consider the recalibration of the relay for the entire system in such a case for future network expansion.

4.3 Swing Severity Analysis

4.3.1 Active Power Oscillation

In this section, the swing severity will be analyzed by observing the active power oscillation of generator G1, G2, G3 and G4. The simulation is conducted for both Case 1 and Case 2.

As the simulation is started, the constant active power recorded in the first 0.5 s is the steady state power throughout the pre-fault duration. At 0.5 s, the fault is initiated at Line-2 close to Bus 7 and the active power falls drastically to a low value. The faulted

line is isolated after 0.1 s, which occurred at 0.6 s in the simulation. Upon isolation, the load is transferred to the healthy line (Line-1) and the power oscillation is initiated in the post-fault period.

Figure 4.9 to Figure 4.16 show the active power oscillation of generator G1, G2, G3 and G4 during fault and the subsequent transfer of load to the healthy Line-1 for both Case 1 and Case 2. The active power output of Generator A and solar PV generator during the simulation are also shown in Figure 4.17 and Figure 4.18 respectively. In addition, the active power output during pre-fault, fault, and post-fault period for all the generators are also measured during the simulation for both Case 1 and Case 2. The results are summarized in Table 4.7 and Table 4.8 respectively. Since all generators in the network have equal capacities, all the generator's pre-fault active power are similar for both Case 1 and Case 2. Because of differences in electrical properties between the synchronous generator and the inertia-less inverter driven generator in solar PV, the during-fault active power for Case 1 and Case 2 are different. Comparing Table 4.7 and Table 4.8, it can be observed that the drop in active power during fault is more severe in Case 2 compared to Case 1. Referring to Figure 4.17 and Figure 4.18, it can be noticed that the active power for Generator A during fault period is -2.393 MW while the static generator (solar PV) recorded an active power of 33.367 MW during fault. The reversed active power flow in the synchronous Generator A during fault will lead it to pole-slip condition which will require the ceasing of its operation as explained in Section 2.3.1. The ceasing of the synchronous Generator A will pose further stability problem to the grid. In contrast, the solar PV generator which maintains a positive active power during fault will remain connected to the grid and is advantageous in this scenario. The solar PV generator is a static generator and does not have the impact of inertia on it. As the intermittent is constant, it still delivers power during fault and the reduction of power during fault is due to the changes that occur in

voltage and current during the fault. It can be observed from Figure 4.17 and 4.18 that the initial response of both the generators from the inception of fault to its clearance is the same. However, due acceleration and increase in rotor angle of the synchronous Generator A leads to faster drop of power compared to solar PV generator. Since solar PV generator is a static machine and is not affected by any means of dynamic, therefore the drop in power during fault is seen to be slower. This results in higher power delivery by the solar PV generator during fault.

It must be noted that the post-fault active power recorded in both Table 4.7 and Table 4.8 correspond to the maximum deviation of active power from its nominal value. This convention is used because the post-fault active power oscillates in both the positive and negative directions. The maximum active power deviation from the simulated result is calculated as per Eq (4.1).

$$\Delta P_{\max} = | P_n - P_{LP/HP} | \quad (4.1)$$

Where:

ΔP_{\max} = Maximum active power deviation

P_n = Nominal power

$P_{LP/HP}$ = Lowest/ Highest peak value after fault

Observing the results obtained from Table 4.7 and Table 4.8, the active power reduction for all the Generator G1, G2, G3 and G4 during fault (at 0.6 s) is more severe in Case 2 compared to Case 1. The differences in active power deviations would have an impact on the impedance trajectory in the distance relay R1. Therefore, the next section will perform a comparative study between the synchronous generator and inverter driven generation for the risk of distance relay mal-operation during power swing phenomenon.

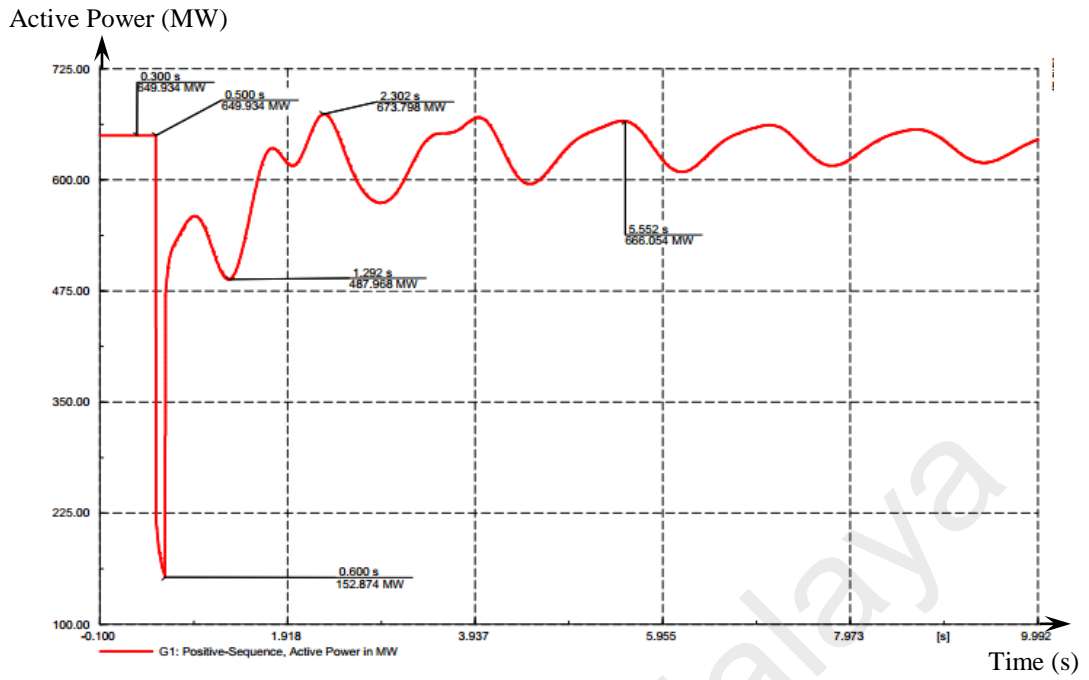


Figure 4.9: Active Power Oscillation of Generator G1 for Case 1

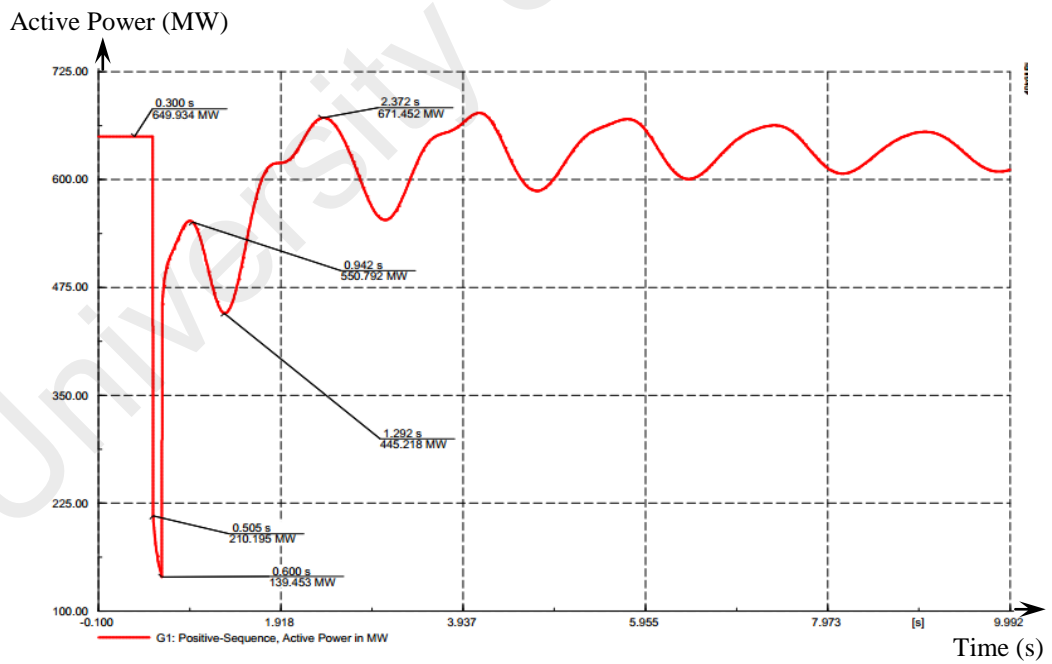


Figure 4.10: Active Power Oscillation of Generator G1 for Case 2

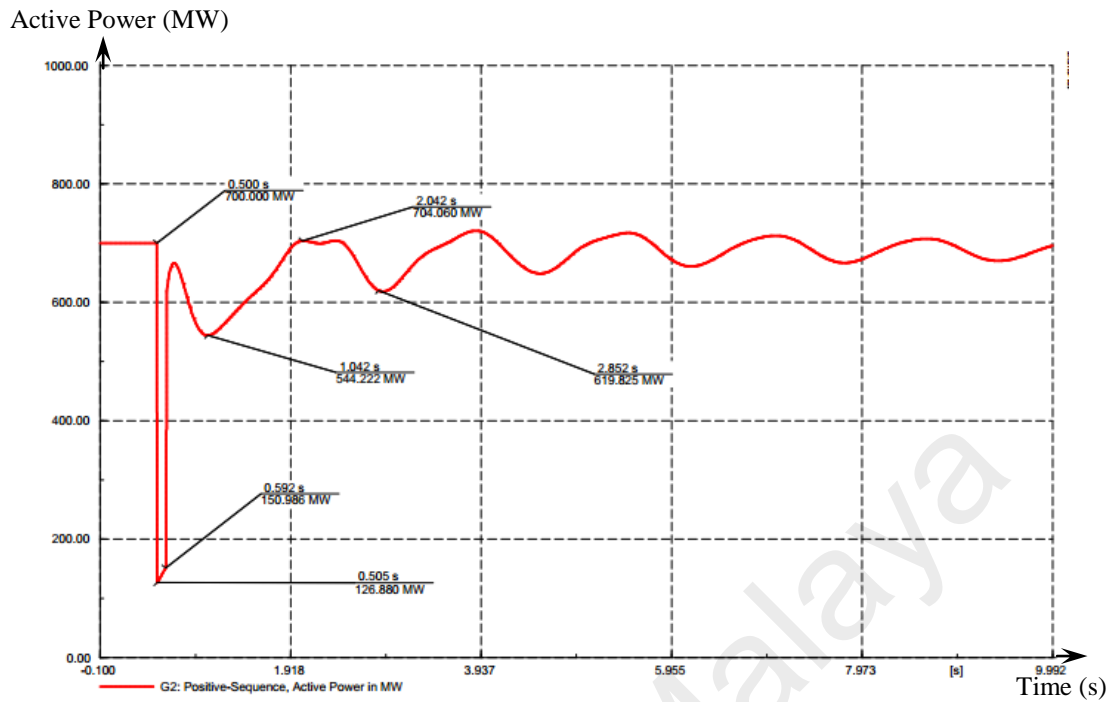


Figure 4.11: Active Power Oscillation of Generator G2 for Case 1

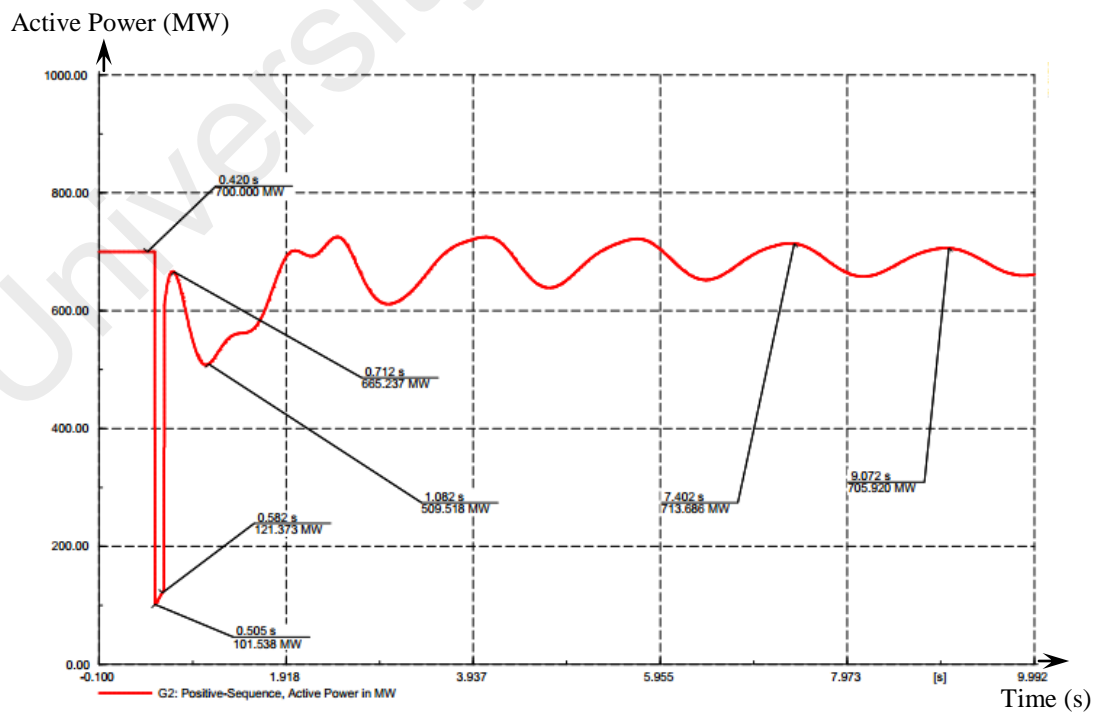


Figure 4.12: Active Power Oscillation of Generator G2 for Case 2

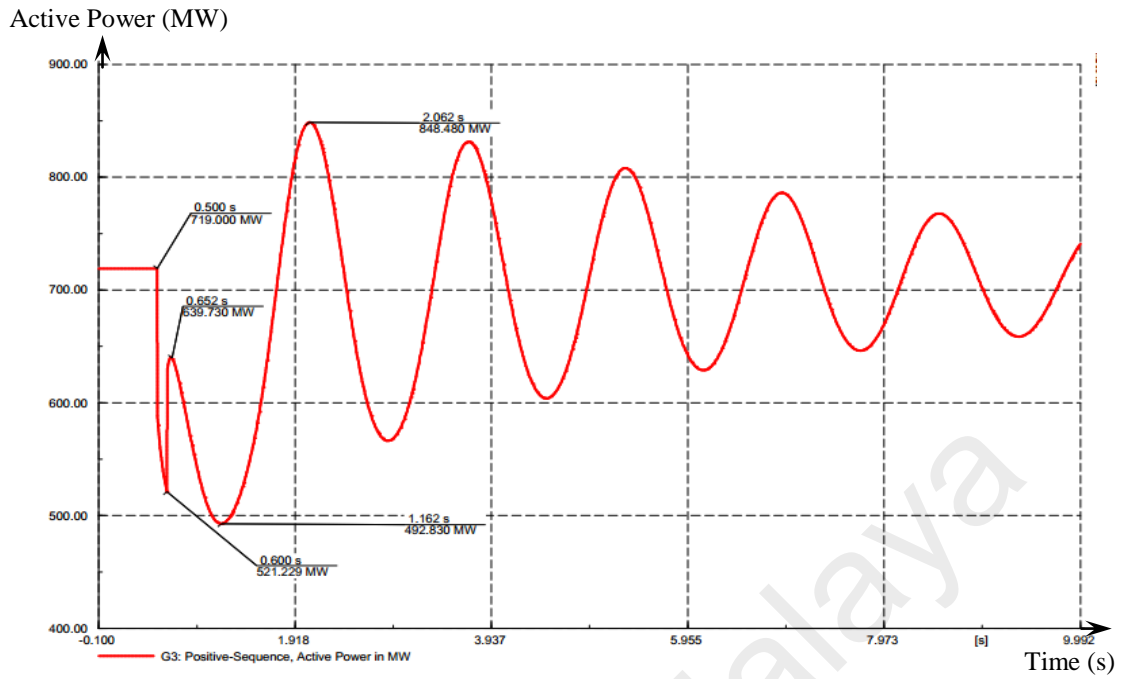


Figure 4.13: Active Power Oscillation of Generator G3 for Case 1

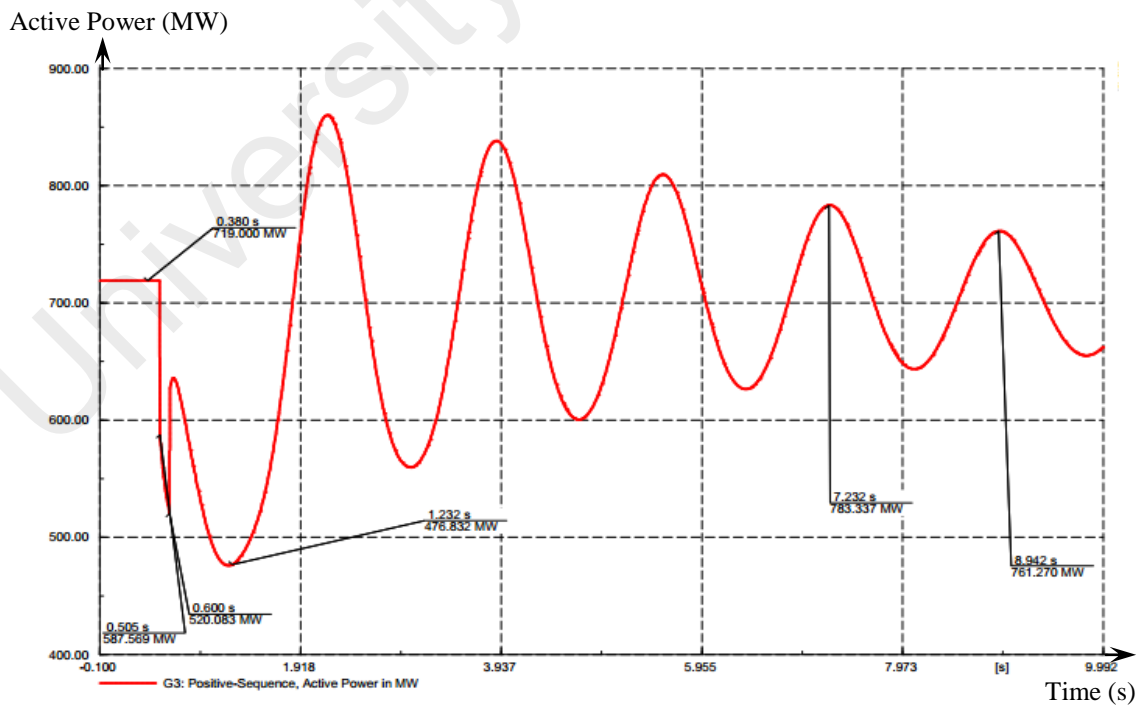


Figure 4.14: Active Power Oscillation of Generator G3 for Case 2

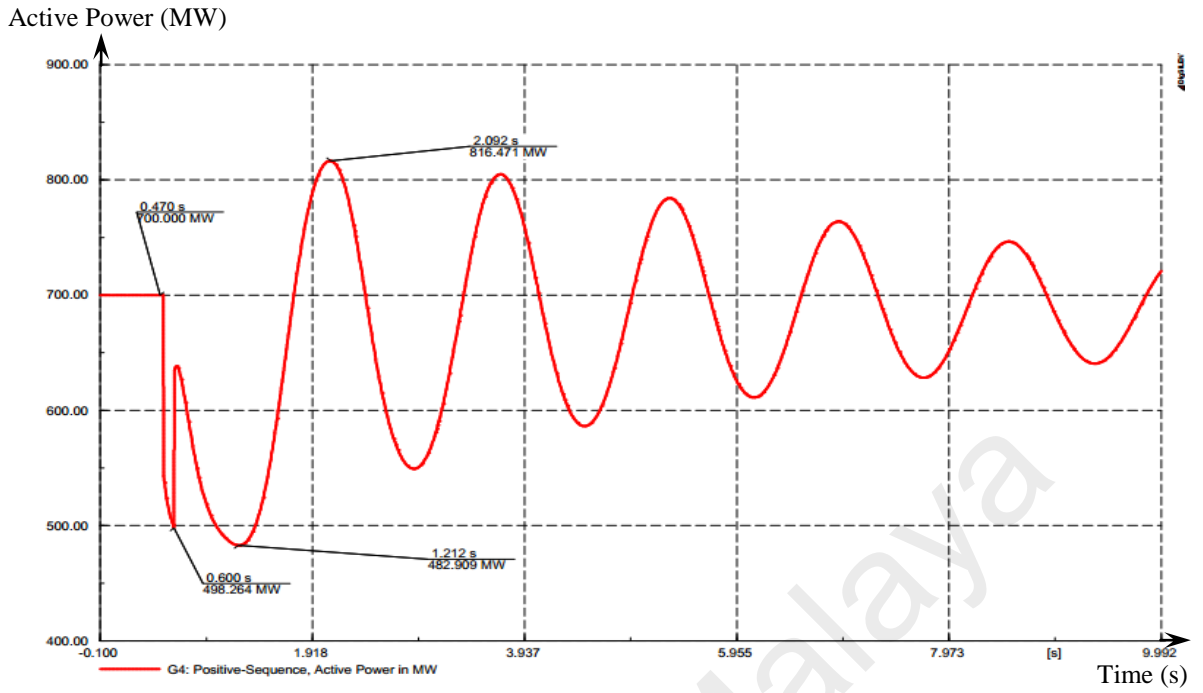


Figure 4.15: Active Power Oscillation of Generator G4 for Case 1

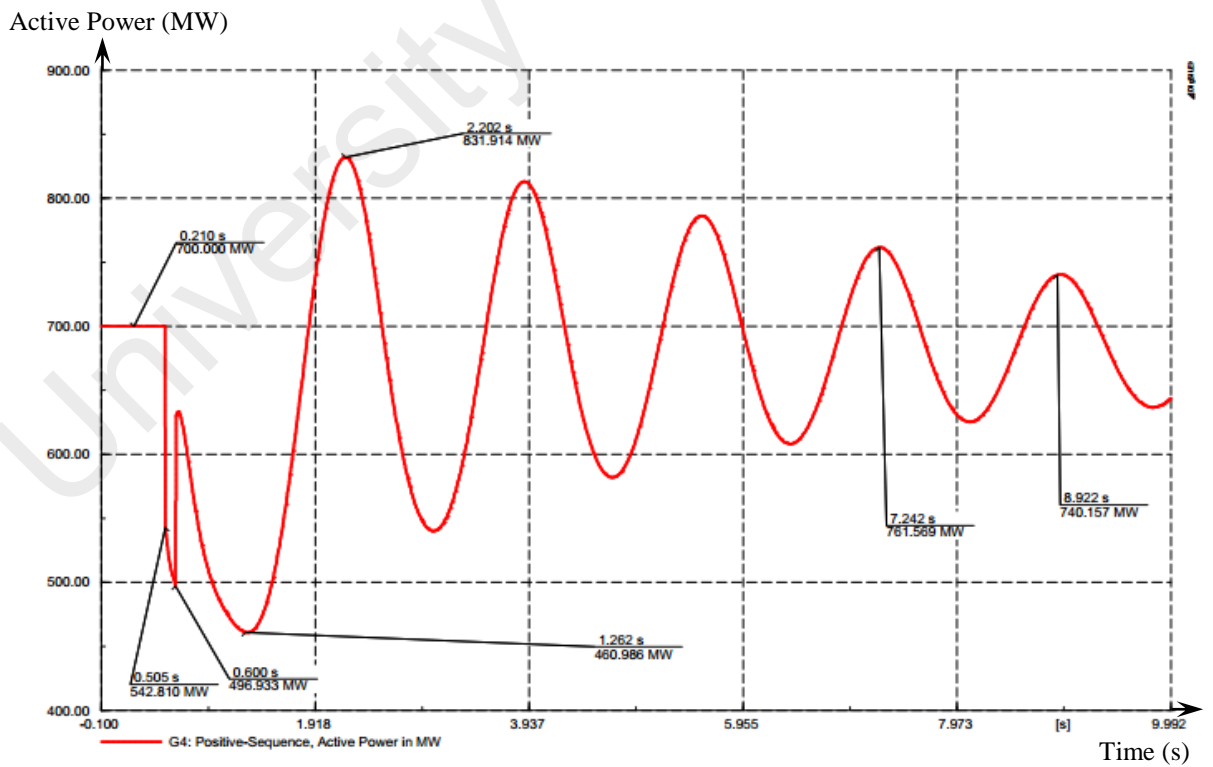


Figure 4.16: Active Power Oscillation of Generator G4 for Case 2

Table 4.7: Active Power Oscillation in the Presence for Case 1

Condition/ Case	Case 1			
	G1	G2	G3	G4
	<i>Active Power (MW)</i>	<i>Active Power (MW)</i>	<i>Active Power (MW)</i>	<i>Active Power (MW)</i>
Pre fault	649.934	700	719	700
During fault 0.6 s	152.874	150.986	521.229	498.26
Post fault -Max deviation	161.966	155.778	226.17	217.09

Table 4.8: Active Power Oscillation in the Presence for Case 2

Condition/ Case	Case 2			
	G1	G2	G3	G4
	<i>Active Power (MW)</i>	<i>Active Power (MW)</i>	<i>Active Power (MW)</i>	<i>Active Power (MW)</i>
Pre fault	649.934	700	719	700
During fault 0.6 s	139.453	121.373	520.083	496.93
Post fault -Max deviation	204.716	190.482	242.168	239.01

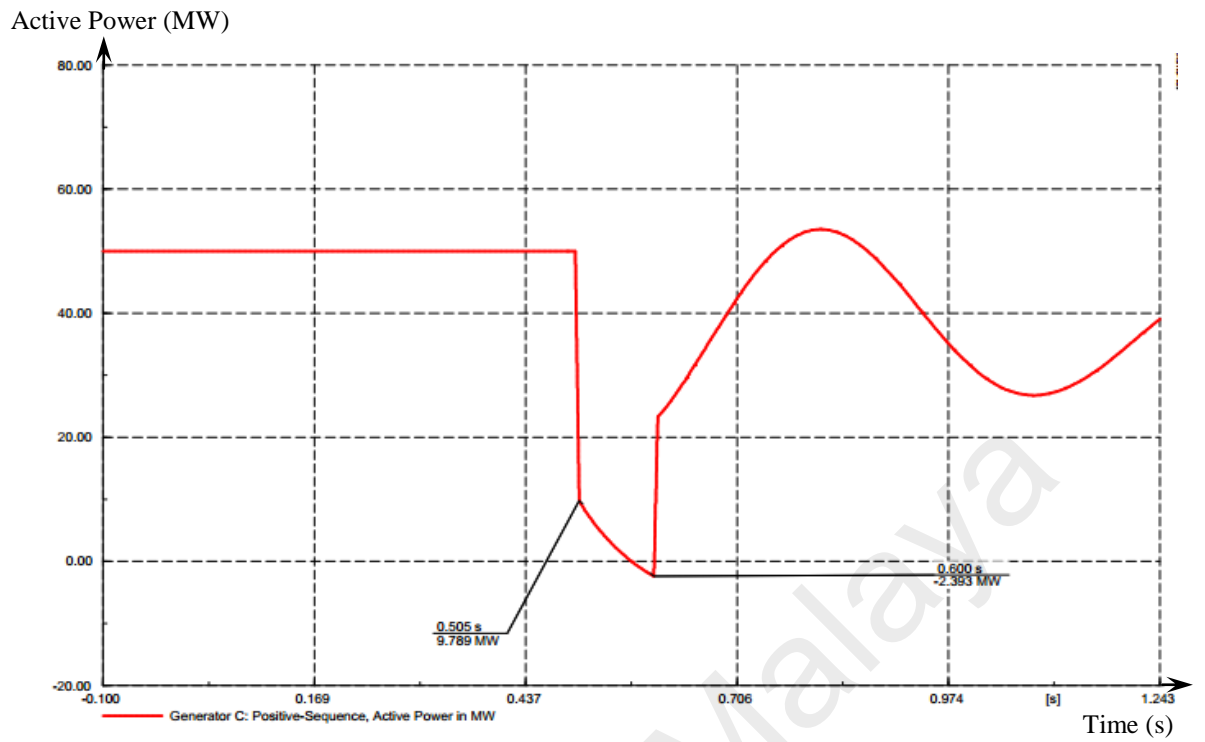


Figure 4.17: Generator A Active Power Oscillation

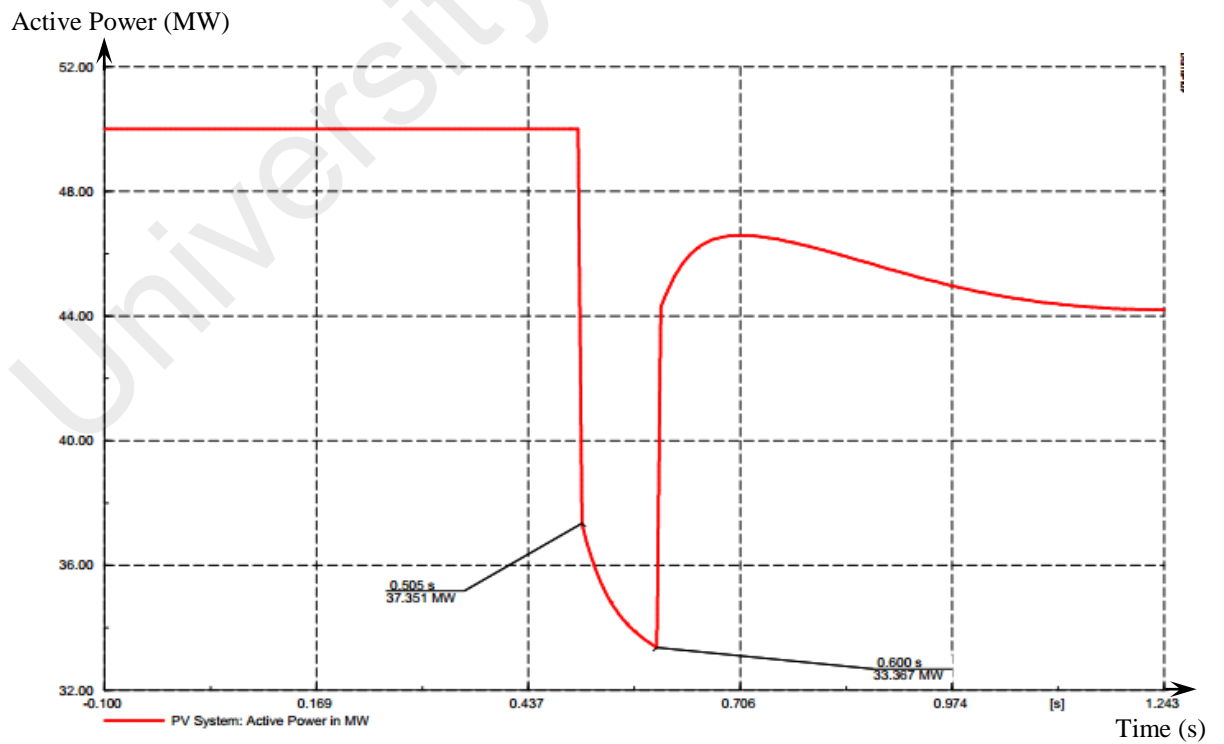


Figure 4.18: Active Power Oscillation of Static Generator (PV)

4.3.2 Impedance Trajectory

In this section, the swing severity will be analyzed by observing the impedance trajectory seen by relay R1. The simulation is conducted for both Case 1 and Case 2. Figure 4.19 shows the relay R1 impedance trajectory for 6-cycle fault clearing time in circuit breaker CB3 and CB4 for Case 1, while that for Case 2 is shown in Figure 4.20. For both Case 1 and Case 2, as the simulation is started in the pre-fault period, the impedance value is high, indicated by A in the R-X plane. When the fault is initiated at 0.5 s, the impedance drops to a small value as shown by B at 0.505 s and C at 0.6 s in the R-X plane. At 0.6 s, the fault is terminated by isolating Line-2 through relay R3 and R4. At this instant, the impedance increases to D. Thereafter, the impedance oscillates between E and F around D.

For the case of integrating a 50MW synchronous Generator A to the grid (Case 1), Figure 4.19 shows that the resistance (R) is 64.903 Ω and reactance (X) is 5.961 Ω at the point of Line-2 isolation at point C. As for the case of integrating a 50MW solar PV generator to the grid (Case 2), Figure 4.20 shows that the resistance is 63.168 Ω and the reactance is 6.423 Ω at point C. By comparing both results, it is seen that Case 2 causes a steeper drop in resistance and increase in reactance value. After clearing the fault at D, power swing takes place due to the dynamic responses amongst the synchronous generators in the system. The power swing will translate to impedance swing between E and F in the R-X plane in relay R1.

For Case 1, E travelled very close to the boundary of zone 3 as shown in Figure 4.11. In this case, there is no risk of distance relay mal-operation. In comparison, point E travelled inside zone 3 of relay R1 for Case 2. Although that seems to pose a problem, however, the 3 s delay in zone 3 operation of distance relay R1 is long. Before the 3 s delay is reached, the impedance trajectory had already left zone 3 and the relay would not have operated.

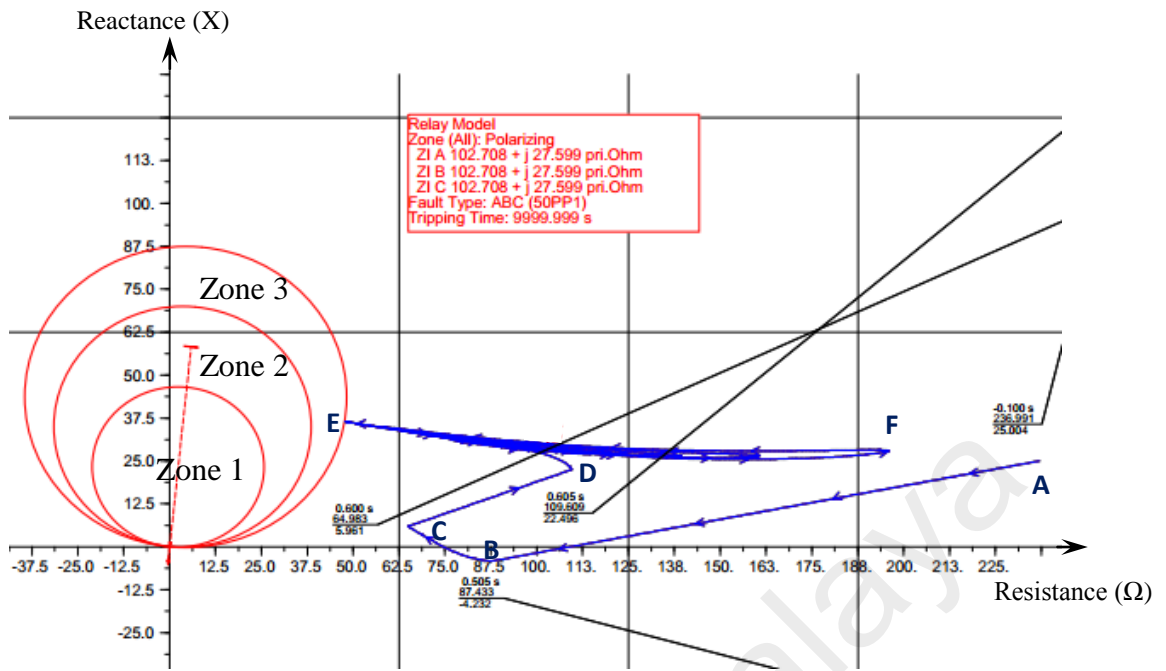


Figure 4.19: Impedance Trajectory seen by Relay R1 for Case 1

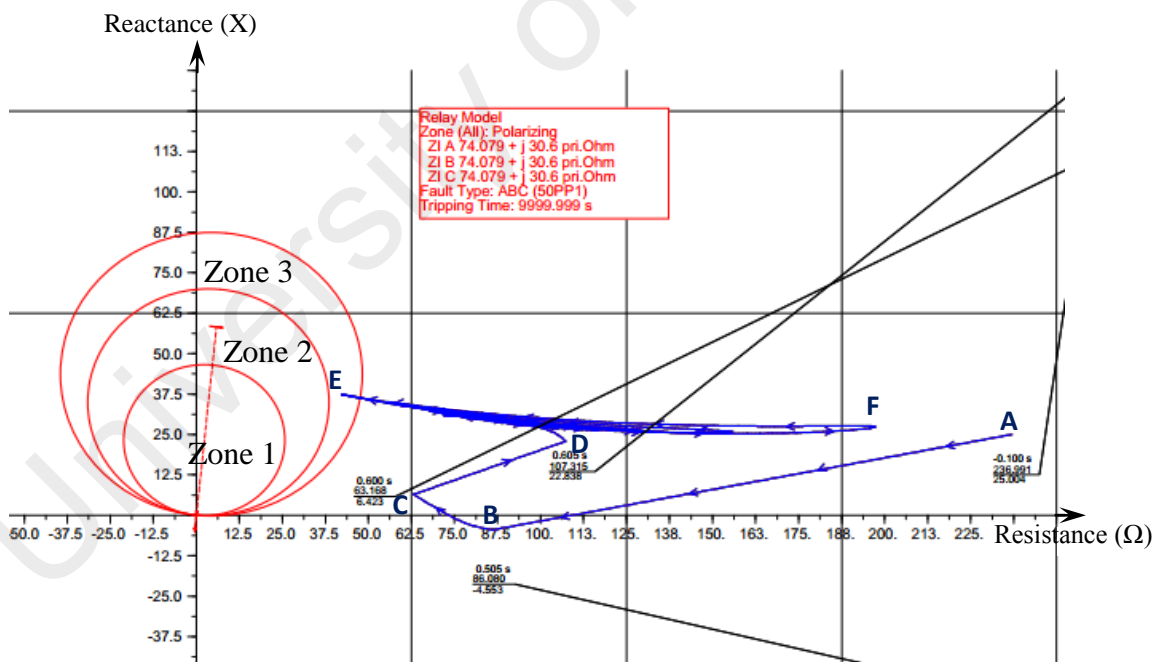


Figure 4.20: Impedance Trajectory seen by relay R1 for Case 2

The above analysis is conducted considering the ideal 6-cycle fault clearing time. However, the impact of delayed fault clearing time to the risk of distance relay mal-

operation is unknown. As such, the next section will analyze the role of fault clearing time in causing distance relay mal-operation.

4.4 Analysis on the Risk of Distance Relay Mal-operation

The impedance trajectory results from the previous section will now be used to analyze the risk of distance relay mal-operation in this section.

4.4.1 Fault Duration Variation

As mentioned in Chapter 3 subsection 3.3.3.1, the fault clearing time is the summation of the circuit breaker operation time and arc extinction time. However, undesirable delays in these times may result in longer fault clearing time (Canay, 2001; Das, 2008). As such, a 7-cycle delayed fault clearing time is considered in this section and the impedance trajectory analysis will be repeated for both Case 1 and Case 2.

Figure 4.21 shows the relay R1 impedance trajectory for 7-cycle fault clearing time in Case 1. As the simulation is started in the pre-fault period, the impedance value is high, indicated by A in the R-X plane. When fault is initiated at 0.5 s, the impedance drops to a small value as shown by B at 0.505 s and C at 0.617 s in the R-X plane. At 0.617 s, the fault is terminated after 7-cycles by isolating Line-2 through relay R3 and R4. At this instant, the impedance increases to D. Thereafter, the impedance oscillates between E and F around D.

In contrast, the impedance trajectory for Case 2 is shown in Figure 4.22. After the fault is cleared at point C, the impedance travel increases to point D and the subsequent power oscillations resulted in the impedance encroachment into the zone 3 and zone 2 of the relay R1. Since the impedance travel is slow, it has exceeded the timer threshold of zone 2 which is 0.3 s from the point of zone 2 entry till point E. Consequently, the relay R1 operated at E as the 0.3 s is also the delay for zone 2 operations in relay R1.

The tripping occurred at 1.409 s in the simulation. Due to the complete disconnection of the double circuit transmission line, the impedance travelled to infinitely large value after point E.

In summary, a delay of 1 cycle from the ideal 6-cycle fault clearing time had resulted in the mal-operation of distance relay R1 in the case of integrating 50MW of solar PV farm. The complete disconnection of the double circuit transmission line would have detrimental effect to initiating a cascaded blackout in the grid.

Given that the integration of solar PV farm increases the risk of distance relay mal-operation as compared to the integration of synchronous generators, the effect of varying solar PV farm capacity to the risk of distance relay mal-operation will be investigated in the next section.

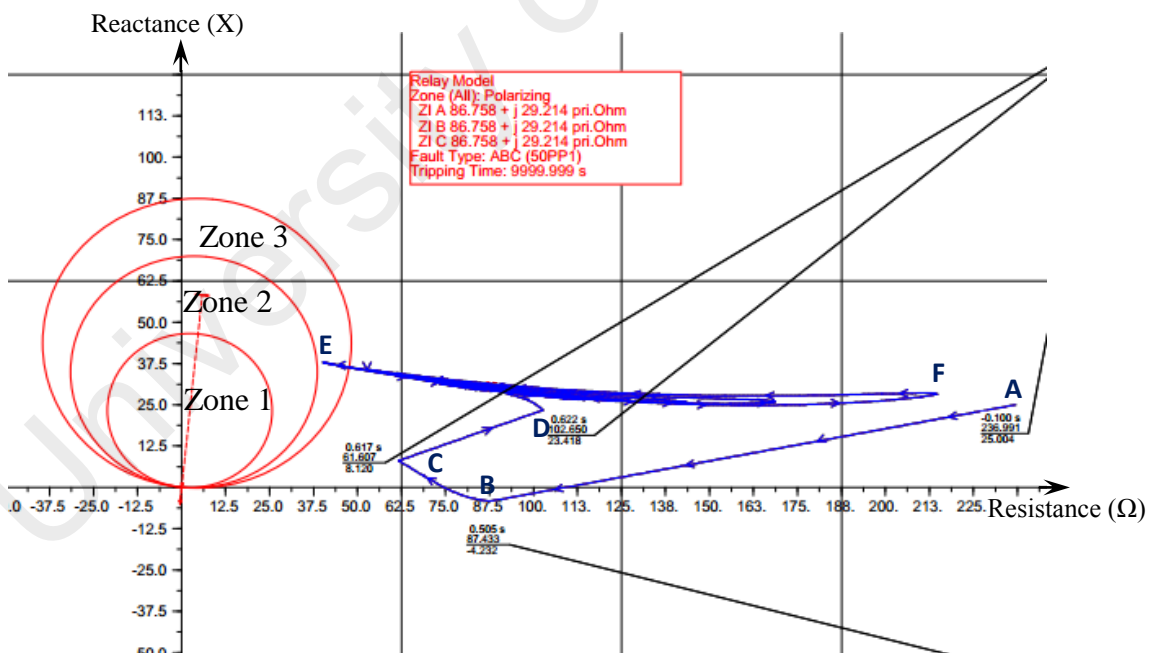


Figure 4.21: Impedance Swing seen by Relay R1 for Case 1

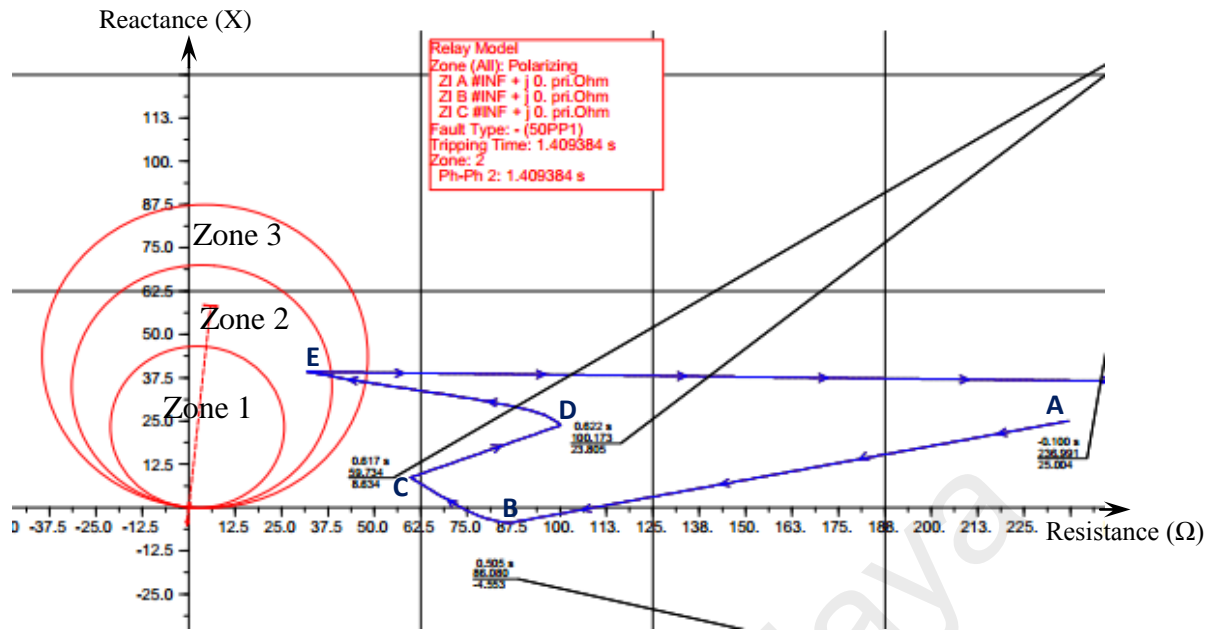


Figure 4.22: Mal-Operation of Relay R1 for Case 2

4.4.2 Suitable PV Capacity to Prevent Distance Relay Mal-Operation

Besides investigating the role of delays in fault clearing time to the increasing risk of distance relay mal-operation, simulations are also conducted to identify the risk of distance relay mal-operation with varying capacity of solar PV farm. In this section, the solar PV capacity is increased from 50MW in steps of 10 MW until 200MW and the impedance trajectory is observed. It is important to note that, the capacity of the transformer which is connected in between Bus 2 and Bus 6 has been maintained at the same loading of 87.4% by increasing its capacity in proportion to the increasing solar PV capacity. This is done in order to ensure that the transformer does not saturate which may lead to other complications. The result for the solar PV capacity increment and its risks to distance relay mal-operation for the 7-cycle fault clearing time are summarized in Table 4.9.

From Table 4.9, it can be observed that the solar PV generator of 90 MW and above do not cause mal-operation of distance relay R1. Figure 4.23 and Figure 4.24 show the impedance trajectory seen by relay R1 from the integration of 80 MW and 90 MW of

solar PV generator respectively. It can be observed that, as the solar PV generator's capacity is increased from 80 MW to 90 MW, the impedance trajectory at point E moves outwards from the distance relay zones. As such, the distance relay R1 did not mal-operate. Besides that, as the solar PV generator's capacity is increased, the tripping time for relay R1 increases gradually as well. Hence, it can be concluded that the higher the capacity of solar PV generator, the lower risk of distance relay mal-operation is observed.

Next, the fault clearing time was extended to 8-cycles. However, it was found that the voltage in per unit at the PCC (Bus 7) drops to 0.84 p.u. Therefore, the simulation was discontinued as this would have triggered the under voltage relay to operate once a voltage drop of 0.9 p.u. is detected.

The next chapter will conclude the findings of this research and match it with the objectives.

Table 4.9: Suitable PV for Fault duration of 7 Cycles

Size of PV (MW)	Distance Relay (R1) Mal-operate	Tripping Time (s)	In Zone
60	Yes	1.422	2
70	Yes	1.433	2
80	Yes	1.458	2
90	No	-	3
100	No	-	3
110	No	-	3
120	No	-	3
130	No	-	3
140	No	-	3
150	No	-	3
160	No	-	3
170	No	-	3
180	No	-	3
190	No	-	Outside
200	No	-	Outside

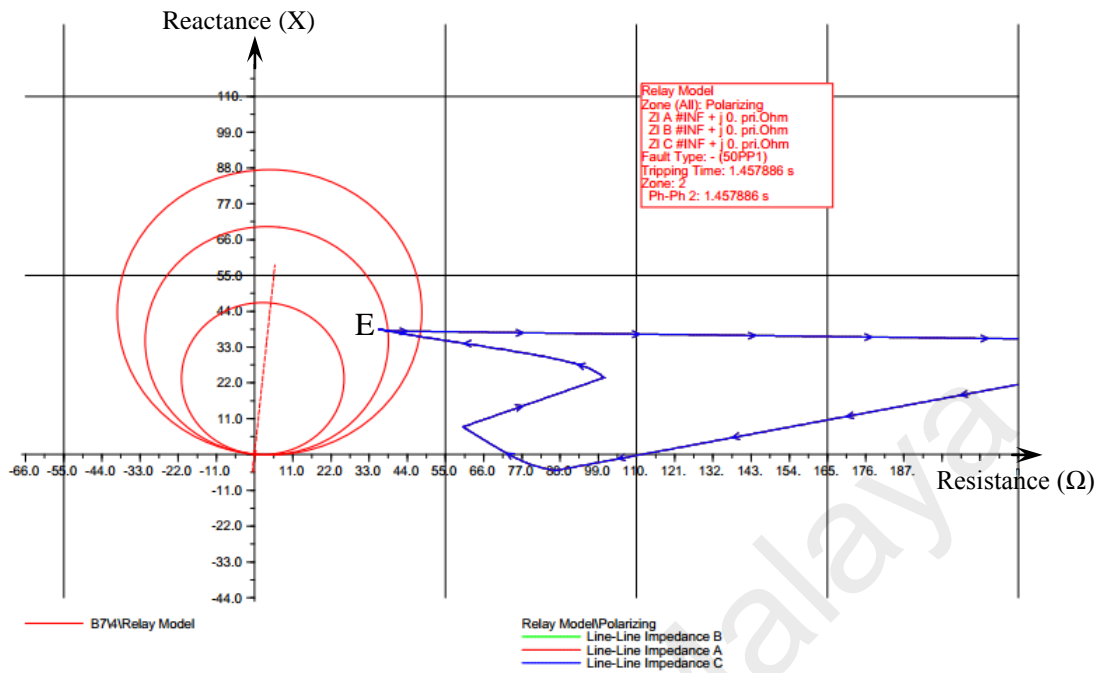


Figure 4.23: Mal-operation of Relay R1 for 80 MW Solar PV Generator

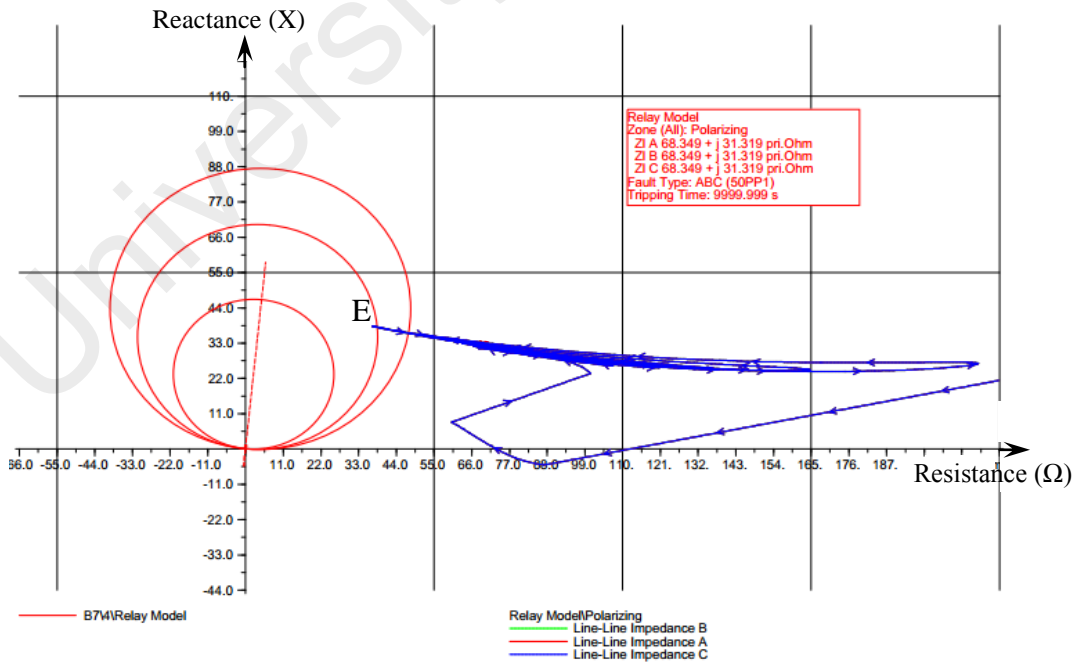


Figure 4.24: Impedance Trajectory of Relay R1 for 90 MW solar PV Generator

- Canay, I. M. (2001). Comparison of generator circuit-breaker stresses in test laboratory and real service condition. *Power Delivery, IEEE Transactions on*, 16(3), 415-421. doi:10.1109/61.924820
- Das, J. C. (2008). Reducing Interrupting Duties of High-Voltage Circuit Breakers by Increasing Contact Parting Time. *Industry Applications, IEEE Transactions on*, 44(4), 1027-1033. doi:10.1109/TIA.2008.926235

CHAPTER 5: CONCLUSION

5.1 Summary of the research work

The investigation of power swing phenomenon in a network integrated with inverter driven generation is inspired from the Malaysia 2003 and 2005 major blackout. The power swing characteristic due to the integration of large scale solar PV generator to the transmission system has yet to be established. Therefore this research aims to analyze the CCT of other generators in the network, swing severity and the risk of distance relay mal-operation in the presence of a synchronous machine compared to an equivalent static generator.

Following the objectives in Chapter 1, the outcomes of this research are as follows:

- 1. To investigate the impact of inverter driven solar PV generator to the CCT of other synchronous generator in the transmission system**

Firstly, the investigation was conducted towards identifying the critical clearing time of other synchronous generators. The simulation was conducted until the other synchronous generators become marginally stable and the simulated CCT is compared. From the investigation, it can be concluded that the presence of sub-transient and transient reactances in the Generator A increases the CCT of other generators. The absence or negligible sub-transient and transient reactances in solar PV generator resulted in smaller value of CCT. As such, the protection engineers have to ensure that the protection relay operating time in the future grid integrated with inverter based generator is less than this shorter CCT.

2. To investigate the severity of power swing in the presence of large solar PV generator

Secondly, this research focused on the severity of swing observed from the distance relay at the transmission level. The simulation was first conducted for the case where synchronous Generator A is present, and next the synchronous Generator A is replaced with a solar PV generator where both their output power are kept constant. By simulating the impedance trajectory, the power swing is observed on the parallel healthy line after the faulted line is isolated. From the obtained results, it can be concluded that the severity of swing increases in the presence of solar PV generator in the network compared to synchronous Generator A.

3. To analyze the risk of distance relay mal-operation in the presence of large scale solar PV generator

Thirdly, this research analyzes the risk of distance relay mal-operation in the presence of solar PV generator compared to synchronous machine. For the case of synchronous Generator A, no mal-operation was observed. However, in the case of solar PV generator, the impedance trajectory enters to the zone 2 of distance relay resulting in the mal-operation of distance relay leading to the isolation of the healthy line.

The impact on distance relay mal-operation with the increased in solar PV capacity was also investigated. From the findings, it is proposed that a larger capacity of PV is to be integrated on the network to prevent the mal-operation of distance relay as the swing resides outside of the distance relay zone.

Hence, all the three objectives has been successfully accomplished and achieved in this research project.

5.2 Contribution of Research

The investigation of power swing phenomenon in a network integrated with inverter driven generation is inspired by the 50 MW solar PV farm which is to be integrated in the northern region of Malaysia. Therefore, the findings of this research will serve as a guide for the integration of renewable energy generators into the future network especially in Malaysia. From this research, the following contributions can be delivered:

- This research had demonstrated that the integration of solar PV generator into the grid reduces the CCT of other generators. As such, it is imperative that the utility engineers reanalyze the resultant CCT in a solar PV integrated grid and ensure that the protection relay operating time does not exceed the new CCT.
- This research had also demonstrated that the risk of distance relay mal-operation is higher for a grid integrated with solar PV generator compared to a grid consisting entirely of synchronous machine. In addition, the risk of distance relay mal-operation reduces with increasing solar PV generator capacity. In order to prevent cascaded blackouts caused by the integration of inverter driven generation, the utility engineers have to consider the suitable capacity of solar PV generator that can be safely integrated into the network.

5.3 Recommendations for Future Works

For future works, the following tasks are recommended to enhance this research project:

- Investigate the effectiveness of power swing blocking schemes in the presence of inverter driven generation.
- Analyze the severity of swing by taking into account the intermittence present in a practical solar PV generator at transmission level.
- Perform hardware in the loop testing using real time digital simulator.

University of Malaya

REFERENCES

- Abbasi, E., et al. (2009, 26-30 July 2009). *Simulation and analysis of the effect of single-pole auto-reclosing on HV transmission lines switching overvoltages*. Paper presented at the 2009 IEEE Power & Energy Society General Meeting, PES '09.
- Abidin, A. F., et al. (2011). Intelligent detection of unstable power swing for correct distance relay operation using S-transform and neural networks. *Expert Systems with Applications*, 38(12), 14969-14975. doi: <http://dx.doi.org/10.1016/j.eswa.2011.05.050>
- Abidin, A. F., et al. (2011, 6-7 June 2011). *Power swing detection for correct distance relay operation using S-transform and neural networks*. Paper presented at the 2011 5th International Power Engineering and Optimization Conference (PEOCO), .
- Abidin, F. b. (2010). *Adaptive Distance Protection to Prevent False Relay Tripping during Voltage Collapse and Power Swing*. PhD, Universiti Kebangsaan Malaysia.
- Ambekar, V. A., & Dambhare, S. S. (2012a, 19-22 Dec. 2012). *Comparative evaluation of out of step detection schemes for distance relays*. Paper presented at the 2012 IEEE Fifth Power India Conference,.
- Ambekar, V. A., & Dambhare, S. S. (2012b, 19-22 Dec. 2012). *Comparative evaluation of out of step detection schemes for distance relays*. Paper presented at the 2012 IEEE Fifth Power India Conference, .
- Apostolov, A., & Vandiver, B. (2011, 11-14 April 2011). *Requirements for testing of power swing blocking functions in protection IEDs*. Paper presented at the 2011 64th Annual Conference for Protective Relay Engineers,.
- Apostolov, A. P., et al. (2004, 10-13 Oct. 2004). *Superimposed components based sub-cycle protection of transmission lines*. Paper presented at the 2004 IEEE Power Systems Conference and Exposition, .
- Bakar, A. H. A., Yatim, F. M., Yusof, S., & Othman, M. R. (2009). Analysis of overload conditions in distance relay under severe system contingencies. *Electrical Power and Energy Systems, Elsevier*, 32(2010), 345-350.

- Berdy, J., et al. (1977). Out of step relaying for generators working group report. *IEEE Transactions on Power Apparatus and Systems*, , 96(5), 1556-1564. doi: 10.1109/t-pas.1977.32484
- Brahma, S. M. (2006, 0-0 0). *Use of wavelets for out of step blocking function of distance relays*. Paper presented at the IEEE Power Engineering Society General Meeting.
- Brahma, S. M. (2007). Distance Relay With Out-of-Step Blocking Function Using Wavelet Transform. *IEEE Transactions on Power Delivery*,, 22(3), 1360-1366. doi: 10.1109/tpwrd.2006.886773
- Canay, I. M. (2001). Comparison of generator circuit-breaker stresses in test laboratory and real service condition. *Power Delivery, IEEE Transactions on*, 16(3), 415-421. doi:10.1109/61.924820
- Chen-Ching, L., & Juan, L. (2008, 20-24 July 2008). *Patterns of cascaded events in blackouts*. Paper presented at the IEEE Power and Energy Society General Meeting - Conversion and Delivery of Electrical Energy in the 21st Century, .
- Chengzong, P., & Kezunovic, M. (2010). Fast Distance Relay Scheme for Detecting Symmetrical Fault During Power Swing. *IEEE Transactions on Power Delivery*, 25(4), 2205-2212. doi: 10.1109/tpwrd.2010.2050341
- Cho, K. R., et al. (1999). An ANN based approach to improve the speed of a differential equation based distance relaying algorithm. *IEEE Transactions on Power Delivery*, , 14(2), 349-357. doi: 10.1109/61.754073
- Chothani, N. G., et al. (2014). New support vector machine-based digital relaying scheme for discrimination between power swing and fault. *IET Generation, Transmission & Distribution*,, 8(1), 17-25. doi: 10.1049/iet-gtd.2013.0020
- Chunyan, L., Yuanzhang, S., & Xiangyi, C. (3-6 Dec. 2007). *Analysis of the blackout in Europe on November 4, 2006*. Paper presented at the International Power Engineering Conference, IPEC 2007.
- Conti, J. P. (2010). The day the samba stopped. *Engineering & Technology*, 5(4), 46-47.

- Corsi, S., & Sabelli, C. (2004, 6-10 June 2004). *General blackout in Italy Sunday September 28, 2003, h. 03:28:00*. Paper presented at the IEEE Power Engineering Society General Meeting,
- Das, J. C. (2008). Reducing Interrupting Duties of High-Voltage Circuit Breakers by Increasing Contact Parting Time. *IEEE Transactions on Industry Applications*, 44(4), 1027-1033. doi:10.1109/TIA.2008.926235
- D'Apuzzo, M., & D'Arco, M. (2008). A Time-Domain Approach for the Analysis of Nonstationary Signals in Power Systems. *IEEE Transactions on Instrumentation and Measurement*, 57(9), 1969-1977. doi: 10.1109/tim.2008.919903
- Ding, M., Xu, Z., Wang, W., Wang, X., Song, Y., & Chen, D. (2016). A review on China's large-scale PV integration: Progress, challenges and recommendations. *Renewable and Sustainable Energy Reviews*, 53, 639-652. doi: <http://dx.doi.org/10.1016/j.rser.2015.09.009>
- Dubey, R., & Samantaray, S. R. (2013). Wavelet singular entropy-based symmetrical fault-detection and out-of-step protection during power swing. *IET Generation, Transmission & Distribution*, 7(10), 1123-1134. doi: 10.1049/iet-gtd.2012.0528
- Dubey, R., et al. (2012a, 16-18 March 2012). *Wavelet based energy function for symmetrical fault detection during power swing*. Paper presented at the Students Conference on Engineering and Systems (SCES).
- Dubey, R., et al. (2012b, 16-18 March 2012). *Wavelet based energy function for symmetrical fault detection during power swing*. Paper presented at the Students Conference on Engineering and Systems (SCES),.
- Eftekharijad, S., Vittal, V., Heydt, G. T., Keel, B., & Loehr, J. (2013). Impact of increased penetration of photovoltaic generation on power systems. *IEEE Transactions on Power Systems*, 28(2), 893-901. doi: 10.1109/TPWRS.2012.2216294
- Esmailian, A., & Astinfeshan, S. (2011, 17-19 July 2011). *A novel power swing detection algorithm using adaptive neuro fuzzy technique*. Paper presented at the International Conference on Electrical Engineering and Informatics (ICEEI), .
- Esmailian, A., et al. (2011, 8-11 May 2011). *Evaluation and performance comparison of power swing detection algorithms in presence of series compensation on*

transmission lines. Paper presented at the 10th International Conference on Environment and Electrical Engineering (EEEIC), .

Feilat, E. A., & Al-Tallaq, K. (2004, 8-8 Sept. 2004). *A new approach for distance protection using artificial neural network*. Paper presented at the 39th International Universities Power Engineering Conference, 2004, UPEC 2004.

Fischer, N., et al. (2012, 2-5 April 2012). *Do system impedances really affect power swings; Applying power swing protection elements without complex system studies*. Paper presented at the 65th Annual Conference for Protective Relay Engineers, .

Fu, L., et al. (2008a, 17-20 March 2008). *Wavelet Transform and Approximate Entropy Based Identification of Faults in Power Swings*. Paper presented at the IET 9th International Conference on Developments in Power System Protection, 2008. DPSP 2008.

Fu, L., et al. (2008b, 17-20 March 2008). *Wavelet Transform and Approximate Entropy Based Identification of Faults in Power Swings*. Paper presented at the IET 9th International Conference on Developments in Power System Protection (DPSP),.

Hashemi, S. M., et al. (2013). *Transmission-Line Protection: A Directional Comparison Scheme Using the Average of Superimposed Components*. *IEEE Transactions on Power Delivery*, 28(2), 955-964. doi: 10.1109/tpwr.2012.2226609

Hashemi, S. M., Hagh, M. T., & Seyedi, H. (2014). *A Novel Backup Distance Protection Scheme for Series-Compensated Transmission Lines*. *IEEE Transactions on Power Delivery*, 29(2), 699-707. doi:10.1109/TPWRD.2013.2272765

Holbach, J. (2006, 14-17 March 2006). *New Out of Step Blocking Algorithm for Detecting Fast Power Swing Frequencies*. Paper presented at the Power Systems Conference: Advanced Metering, Protection, Control, Communication, and Distributed Resources, 2006. PS '06.

Kampeerawat, W., et al. (2010, 24-28 Oct. 2010). *New swing-blocking methods for digital distance protection using Support Vector Machine*. Paper presented at the International Conference on Power System Technology (POWERCON), .

Kampeerawat, W., et al. (2012, 27-29 March 2012). *The Swing-Blocking Methods for Digital Distance Protection Based on Wavelet Packet Transform and Support Vector Machine*. Paper presented at the Asia-Pacific Power and Energy Engineering Conference (APPEEC),.

- Kang, H., et al. (2010, March 29 2010-April 1 2010). *Distance protection under extreme conditions*. Paper presented at the 10th IET International Conference on Managing the Change, Developments in Power System Protection (DPSP),.
- Karegar, H. K., & Mohamedi, B. (2009, 6-9 May 2009). *A new method for fault detection during power swing in distance protection*. Paper presented at the 6th International Conference on Electrical Engineering/Electronics, Computer, Telecommunications and Information Technology (ECTI-CON), .
- Khoradshadi-Zadeh, H. (2005, 12-16 June 2005). *Evaluation and performance comparison of power swing detection algorithms*. Paper presented at the IEEE Power Engineering Society General Meeting,.
- Kundur, P. (1994). *Power System Stability Control*. New York: McGraw-Hill.
- Li, W., & Ying-Hao, L. (2000, 2000). *Dynamic stability analyses of a photovoltaic array connected to a large utility grid*. Paper presented at the Power Engineering Society Winter Meeting, 2000. IEEE.
- Lobos, T., et al. (2001, 2001). *Analysis of power system transients using wavelets and Prony method*. Paper presented at the IEEE Porto Power Tech Proceedings,.
- Lotfifard, S., et al. (2010). *Detection of Symmetrical Faults by Distance Relays During Power Swings*. *IEEE Transactions on Power Delivery*, 25(1), 81-87. doi: 10.1109/tpwrd.2009.2035224
- Mahamedi, B. (2010, 27-29 Oct. 2010). *A very fast unblocking scheme for distance protection to detect symmetrical faults during power swings*. Paper presented at the International Power Electronics Conference Proceedings (IPEC),.
- Mahamedi, B. (2011, 15-17 Nov. 2011). *A new power swing blocking function based on wavelet transform*. Paper presented at the 2nd International Conference on Electric Power and Energy Conversion Systems (EPECS),.
- Mahamedi, B., & Jian Guo, Z. (2012). *A Novel Approach to Detect Symmetrical Faults Occurring During Power Swings by Using Frequency Components of Instantaneous Three-Phase Active Power*. *IEEE Transactions on Power Delivery*, 27(3), 1368-1376. doi: 10.1109/tpwrd.2012.2200265
- Martuscello, L., et al. (2009, March 30 2009-April 2 2009). *Tests of distance relay performance on stable and unstable power swings reported using simulated*

data of the August 14 2003 system disturbance. Paper presented at the 62nd Annual Conference for Protective Relay Engineers,.

Mohamad, N. Z., & Abidin, A. F. (2012). A New Technique for High Resistance Fault Detection during Power Swing for Distance Relay. *AASRI Procedia*, 2(0), 50-55. doi: <http://dx.doi.org/10.1016/j.aasri.2012.09.013>

Mohamad, N. Z., & Abidin, A. F. (2012, 23-25 March 2012). *S-Transform based technique to detect high resistance symmetrical fault during power swing.* Paper presented at the IEEE 8th International Colloquium on Signal Processing and its Applications (CSPA),.

Mohamad, N. Z., et al. (2012, 6-7 June 2012). *A new tracking method of symmetrical fault during Power Swing Based on S-Transform.* Paper presented at the IEEE International Power Engineering and Optimization Conference (PEDCO) Melaka, Malaysia,.

Mohamad, N. Z., et al. (2012, 5-6 Dec. 2012). *Symmetrical fault detection technique during power swing based on S-Transform.* Paper presented at the IEEE Student Conference on Research and Development (SCOREd),.

Mohamad, N. Z., et al. (2013, 3-5 Dec. 2013). *The use of S-Transform for distance relay's power swing detection.* Paper presented at the IEEE Jordan Conference on Applied Electrical Engineering and Computing Technologies (AEECT),.

Mooney, J., & Fischer, N. (2006, 0-0 0). *Application guidelines for power swing detection on transmission systems.* Paper presented at the 59th Annual Conference for Protective Relay Engineers, 2006,.

Mozina, C. J. (2012, 7-10 May 2012). *Impact of power system instability on generator protection.* Paper presented at the Transmission and Distribution Conference and Exposition (T&D), 2012 IEEE PES.

Nayak P. K., et al. (2010, 20-23 Dec. 2010). *A comparative assessment of power swing detection techniques.* Paper presented at the Power India Joint International Conference on Power Electronics, Drives and Energy Systems (PEDES).

Parameswariah, C., & Cox, M. (2002). Frequency characteristics of wavelets. *IEEE Transactions on Power Delivery*, , 17(3), 800-804. doi: [10.1109/tpwrdr.2002.1022806](http://dx.doi.org/10.1109/tpwrdr.2002.1022806)

- Pentayya, P., Gartia, A., Saha, S. K., Anumasula, R., & Kumar, C. (2013, 10-13 Nov. 2013). *Synchrophasor based application development in Western India*. Paper presented at the 2013 IEEE Innovative Smart Grid Technologies - Asia (ISGT Asia),.
- Phuttapatimok, S., Sangswang, A., Seapan, M., Chenvidhya, D., & Kirtikara, K. (2008, 11-16 May 2008). *Evaluation of fault contribution in the presence of PV grid-connected systems*. Paper presented at the 33rd IEEE Photovoltaic Specialists Conference, 2008. PVSC '08.
- Rao, J. G., & Pradhan, A. K. (2015). Power-Swing Detection Using Moving Window Averaging of Current Signals. *IEEE Transactions on Power Delivery*,, 30(1), 368-376. doi:10.1109/TPWRD.2014.2342536
- Samantaray, S. R., et al. (2011, 28-30 Dec. 2011). *Spectral energy function for fault detection during power swing*. Paper presented at the International Conference on Energy, Automation, and Signal (ICEAS),.
- Sanaye-Pasand, M., & Jafarian, P. (2011). An Adaptive Decision Logic to Enhance Distance Protection of Transmission Lines. *IEEE Transactions on Power Delivery*, , 26(4), 2134-2144. doi: 10.1109/tpwrD.2011.2159404
- Seethalekshmi, K., et al. (2010, 25-29 July 2010). *SVM based power swing identification scheme for distance relays*. Paper presented at the IEEE Power and Energy Society General Meeting,.
- Seethalekshmi, K., et al. (2012). A Classification Approach Using Support Vector Machines to Prevent Distance Relay Maloperation Under Power Swing and Voltage Instability. *IEEE Transactions on Power Delivery*,, 27(3), 1124-1133. doi: 10.1109/tpwrD.2011.2174808
- Thakallapelli, A., Mehra, R., & Mangalvedekar, H. A. (2013, 6-8 Dec. 2013). *Differentiation of faults from power swings and detection of high impedance faults by distance relays*. Paper presented at the IEEE 1st International Conference on Condition Assessment Techniques in Electrical Systems (CATCON),.
- Trujillo G, L. A., et al. (2013, 5-8 May 2013). *Application of the Prony method for compensation of errors in distance relays*. Paper presented at the 12th International Conference on Environment and Electrical Engineering (EEEIC),.

- Tziouvaras, D. A., & Daqing, H. (2004, 30 Mar-1 Apr 2004). *Out-of-step protection fundamentals and advancements*. Paper presented at the 57th Annual Conference for Protective Relay Engineers,.
- Vaidya, A. P., & Venikar, P. A. (2012, 30-31 March 2012). *ANN based distance protection of long transmission lines by considering the effect of fault resistance*. Paper presented at the 2012 International Conference on Advances in Engineering, Science and Management (ICAESM),.
- Vapnik, V. (1995). The nature of statistical learning theory
- Verzosa, Q. (2013, 8-11 April 2013). *Realistic testing of power swing blocking and out-of-step tripping functions*. Paper presented at the 2013 66th Annual Conference for Protective Relay Engineers,.
- Wall, P., et al. (2010, Aug. 31 2010-Sept. 3 2010). *Demonstration of an inertia constant estimation method through simulation*. Paper presented at the 45th International Universities Power Engineering Conference (UPEC), .
- Wandhare, R. G., & Agarwal, V. (2012, 3-8 June 2012). *A modified control strategy for centralized PV - grid systems for assisting dynamic stability to overcome penetration issues*. Paper presented at the 2012 38th IEEE Photovoltaic Specialists Conference (PVSC),.
- Wandhare, R. G., & Agarwal, V. (2014). Novel Stability Enhancing Control Strategy for Centralized PV-Grid Systems for Smart Grid Applications. *IEEE Transactions on Smart Grid*, 5(3), 1389-1396. doi:10.1109/TSG.2013.2279605
- Xiangning, L., et al. (2008). A Novel Scheme to Identify Symmetrical Faults Occurring During Power Swings. *IEEE Transactions on Power Delivery*, , 23(1), 73-78. doi: 10.1109/tpwrd.2007.911154
- Xiangning, L., et al. (2010). Theoretical Fundamentals and Implementation of Novel Self-Adaptive Distance Protection Resistant to Power Swings. *IEEE Transactions on Power Delivery*, , 25(3), 1372-1383. doi: 10.1109/tpwrd.2010.2043450
- Yusoff, N., & Abidin, A. F. (2013, 19-20 Aug. 2013). *The effect of solar Photovoltaic (PV) system to the characteristic of power swing*. Paper presented at the IEEE 3rd International Conference on System Engineering and Technology (ICSET),.

Yun Tiam, T., & Kirschen, D. S. (2007, 24-28 June 2007). *Impact on the Power System of a Large Penetration of Photovoltaic Generation*. Paper presented at the IEEE Power Engineering Society General Meeting, 2007.

Zadeh, H. K., & Li, Z. (2008, 20-24 July 2008). *Artificial neural network based load blinder for distance protection*. Paper presented at the IEEE Power and Energy Society General Meeting - Conversion and Delivery of Electrical Energy in the 21st Century,.

Zadeh, H. K., & Li, Z. (2008). A novel power swing blocking scheme using adaptive neuro-fuzzy inference system. *Electric Power Systems Research*, 78(7), 1138-1146. doi: <http://dx.doi.org/10.1016/j.epsr.2007.09.007>

Ziegler, G. (July 1999). *Numerical Distance Protection: Principle and Application* (S. Ag Ed. Vol. 1). Germany: Publicis MCD.

University of Malaya

LIST OF PUBLICATIONS AND PAPERS PRESENTED

Published

M.K. Gunasegaran, ChiaKwang Tan, A.H.A. Bakar, H. Mokhlis, H.A. Illias, Progress on power swing blocking schemes and the impact of renewable energy on power swing characteristics: A review, *Renewable and Sustainable Energy Reviews*, Volume 52, December 2015, Pages 280-288, ISSN 1364-0321, <http://dx.doi.org/10.1016/j.rser.2015.07.066>.

(<http://www.sciencedirect.com/science/article/pii/S1364032115007133>)

Proceedings

Gunasegaran M.K.; ChiaKwang Tan; Bakar A.H.A., "Investigation of power swing phenomenon and verification of critical clearing time through theoretical calculations and simulated studies," *3rd IET International Conference on Clean Energy and Technology (CEAT) 2014*, vol., no., pp.1,6, 24-26 Nov. 2014
doi: 10.1049/cp.2014.1478